

# **Airway Smooth Muscle Response to Vibrations**

**Youhua Du**

A thesis submitted to the Auckland University of Technology  
in fulfilment of the degree of  
Doctor of Philosophy



Auckland, New Zealand

© 2006 by Youhua Du

## **Declarations**

I hereby declare that I am the sole author of this thesis.

I authorise the Auckland University of Technology to lend this thesis to other institutions or individuals for the purpose of scholarly research.

---

Youhua Du

I further authorise the Auckland University of Technology to reproduce this thesis by photocopying or by other means, in total or in part, at the request of other institutions or individuals for the purpose of scholarly research.

---

Youhua Du

## **Borrowers Page**

The Auckland University of Technology requires the signatures of all people using or photocopying this thesis. Accordingly, all borrowers are required to fill out this page.

Data	Name	Address	Signature
------	------	---------	-----------

---

## **Acknowledgments**

I have had a large number of friends, family and colleagues who have supported and encouraged me over the past few years of this research and whose input I have greatly valued.

The most significant influence on my research has come from my primary supervisor, Professor Ahmed Al-Jumaily who has been an inspiration, encouragement and direction in this work. Thank you, Ahmed for your support, guidance, advice and patience throughout this research. I also extend my thanks to my colleagues and friends at the DCRC for their friendly and favourable support, in particular, Rob and Prasika for their suggestions, comments and corrections towards this thesis. My heart felt thanks to Gijs, Ingrid and Joe who made themselves available during the experimental stage. Hasmeeta and Maximiano who have always been willing to answer any questions and help me wherever possible. Chris and Yan, from the “6<sup>th</sup> floor chemistry lab”, who enthusiastically provided the equipment and facilities. My thanks go to Jennie and Benneth in managing the resources for this project. Thank you, Pui Ming, Ibtisam, Yasser, Ian, Vera, Fred and Ashis for your honesty and friendship.

Sincere thanks are also extended to all the staff of the faculty and university for their kindness and encouragement during my research period at the Auckland University of Technology.

Finally, I would like to give special thanks to my family (my wife, Jenny and daughter, Lucia) who have been my harbour and sanctuary. I have to give them my thanks for their love, dependence, patience and understanding. Thank you, Jenny and Lucia for loving me!

## Abstract

The main goal of this research was the *in vitro* investigation of the stiffness response of contracted airway smooth muscles under different external oscillations. Living animal airway smooth muscle tissues were dissected from pig tracheas and stimulated by a chemical stimulus (acetylcholine). These tissues were then systematically excited with different external vibrations. The force change was recorded to reflect the muscle stiffness change under vibration. The static and dynamic stiffness of contracted airway smooth muscles in isometric contraction were determined before, during and after vibrations. A continuum cross-bridge dynamic model (the fading memory model) was modified to accommodate smooth muscle behaviour and dynamically describes the cross-bridge kinetics. A two-dimensional finite element model (FEM) was developed to simulate longitudinal and transverse vibrations of the tissue. An empirical equation, derived from the experiments, is incorporated into the FEM.

The results indicate that the stiffness of active smooth muscles can be physically reduced using external vibrations. This reduction is caused by a certain physical position change between actin and myosin. The dynamic stiffness has the tendency of decreasing as the frequency and/or amplitude of external vibration increases. However, the static stiffness decreases with an increase in the frequency and amplitude of excitation until it reaches a critical value of frequency where no variation in stiffness is observed. It is postulated that the tissue elasticity and mass inertia are the main

contributors to the dynamic stiffness while the actin-myosin cross-bridge cycling is the main contributor to the static stiffness.

# Table of Contents

<b>Declarations .....</b>	<b>II</b>
<b>Borrowers Page .....</b>	<b>III</b>
<b>Acknowledgments .....</b>	<b>IV</b>
<b>Abstract.....</b>	<b>VI</b>
<b>Table of Contents .....</b>	<b>VIII</b>
<b>List of Figures.....</b>	<b>XI</b>
<b>List of Tables .....</b>	<b>XIV</b>
<b>Chapter 1 Introduction.....</b>	<b>1</b>
1.1 Lung Structure.....	1
1.2 Structure of Airway Tissue .....	2
1.3 What is Asthma? .....	5
1.4 Airway Smooth Muscle .....	7
1.5 Research Plan.....	12
1.6 Structure of the Thesis .....	15
<b>Chapter 2 Smooth Muscle Mechanics and Literature Survey.....</b>	<b>16</b>
2.1 Introduction.....	16
2.2 Mechanical Properties of Muscle Contraction.....	17
2.2.1 Isometric Contraction.....	17
2.2.2 Isotonic Contraction.....	22
2.2.3 Hill's Equation and Hill's Three-Element Model.....	25
2.2.4 Contracted Smooth Muscle Stiffness-Length Relationship.....	29
2.3 Physiological Procedure of Muscle Contraction.....	31
2.4 Existing Models for Muscle Contraction.....	37
2.5 Available Literature on Muscle Vibrations.....	43
<b>Chapter 3 Experimental Investigation.....</b>	<b>47</b>
3.1 Introduction.....	47
3.2 Experiment Preparations .....	49
3.2.1 Solution Preparation.....	50
3.2.2 Airway Smooth Muscle Tissue Preparation.....	51
3.2.3 Muscle Tissue Contraction.....	54
3.2.4 Replacement of Airway Smooth Muscle Tissue.....	56
3.2.5 Stiffness and Resonance of Setup .....	56
3.3 Longitudinal Vibration.....	57
3.3.1 Setup.....	57
3.3.2 Protocols.....	59
3.4 Transverse Vibration.....	60
3.4.1 Setup.....	60
3.4.2 Protocols.....	61
3.5 Stiffness Normalization.....	62
<b>Chapter 4 Numerical Models .....</b>	<b>65</b>
4.1 Introduction.....	65
4.2 Fading Memory Model .....	67
4.2.1 Fading Memory of Muscle.....	67
4.2.2 Incorporation into Hill's Equation .....	70
4.2.3 Determination of the Constant Parameters from Isometric Quick Release .....	73

4.3	Modification of Fading Memory Model for Airway Smooth Muscle .....	77
4.3.1	Determination of the Constant Parameters for Airway Smooth Muscle.....	78
4.3.2	Finite Duration Length Step.....	81
4.3.3	Development of a Modified Fading Memory Model for Longitudinal Oscillation .....	82
4.4	Finite Element Model.....	84
4.4.1	Physical Laws for the FEM.....	84
4.4.2	Development of Finite Element Formulae.....	86
4.4.3	Assembly of Finite Element Equations.....	93
4.4.4	Longitudinal Vibration.....	94
4.4.5	Transverse Vibration.....	95
<b>Chapter 5</b>	<b>Experimental &amp; Numerical Results.....</b>	<b>96</b>
5.1	Introduction .....	96
5.2	Airway Smooth Muscle Tissue Properties.....	96
5.3	Experimental Results .....	98
5.3.1	Longitudinal Vibration.....	99
5.3.2	Transverse Vibration.....	101
5.4	Numerical Results .....	102
5.4.1	Fading Memory Model .....	102
5.4.2	Finite Element Model.....	104
<b>Chapter 6</b>	<b>Discussion.....</b>	<b>108</b>
6.1	Introduction .....	108
6.2	Longitudinal Vibration Experiments .....	109
6.2.1	Constant Time Duration of Vibration .....	111
6.2.2	Different Time Durations of Vibration .....	117
6.3	Oscillation Cycles Affect Cross-Bridges .....	119
6.4	Empirical Equation of the Stiffness for the Finite Element Model.....	123
6.5	Comparison of Experimental and Numerical Results for the Longitudinal Vibration .....	125
6.6	Compare Experimental and FEM Results for the Transverse Vibration .....	132
6.7	Hysteresivity and Cross-Bridge Cycling Rates.....	138
6.8	Constants $A_i$ for the Fading Memory Model.....	140
6.9	Uncertainties of Airway Smooth Muscle Tissue .....	141
6.10	Other Conditions Affecting the Muscle Response.....	145
<b>Chapter 7</b>	<b>Conclusions &amp; Future Applications .....</b>	<b>148</b>
7.1	Conclusions .....	148
7.2	Future Applications.....	149
<b>References</b>	<b>.....</b>	<b>151</b>
<b>Appendix A</b>	<b>Finite Element Method .....</b>	<b>161</b>
A.1	Linear Basis Function for One-Dimensional Element.....	161
A.2	Basis Function As a Weighting Function .....	163
A.3	Linear Basis Function for Two-Dimensional Elements.....	165
A.3.1	Basis Functions for Rectangular Elements .....	165
A.3.2	Basis Functions for Triangular Elements.....	166
A.4	Finite Element Method.....	168
A.5	Scheme of Assembly.....	172
<b>Appendix B</b>	<b>Strain Tensor and Constitutive Equation for 2D Plane .....</b>	<b>173</b>
<b>Appendix C</b>	<b>Experimental Data .....</b>	<b>179</b>
<b>Appendix D</b>	<b>MATLAB Codes for Numerical Models .....</b>	<b>189</b>
D.1	MATLAB Code for the Finite Duration Length Step (Fading Memory model) .....	189
D.2	MATLAB Code for the Length Oscillation (Fading Memory model) .....	190

D.3	MATLAB Code for the Longitudinal Vibration (FEM).....	191
D.4	MATLAB Code for the Transverse Vibration (FEM).....	195

## List of Figures

Figure 1.1:	Structure of human lung [3].....	2
Figure 1.2:	Schematic representation of the airway wall, in cross-section, from the large bronchi down to the small peripheral bronchioles, SM means the airway smooth muscle [5].....	3
Figure 1.3:	Sketch of the membranous airway wall as viewed in cross-section along the airway axis [5].....	3
Figure 1.4:	Skeletal muscles (a), cardiac muscle (b) and smooth muscle (c), notice the striations in skeletal and cardiac muscle [18].....	8
Figure 1.5:	Sketch of a single-unit and multiunit smooth muscle [19].....	9
Figure 1.6:	Difference in structure between smooth muscle (A) and skeletal muscle (B).....	11
Figure 1.7:	Muscle contraction as caused by cross-bridge attachment.....	11
Figure 1.8:	A follow chart for the research plan.....	14
Figure 2.1:	Isometric force dependence for various modes of stimulation [31].....	18
Figure 2.2:	Isometric force-length relationship [31].....	18
Figure 2.3:	Sarcomere force-length relationships [31].....	19
Figure 2.4:	Length-tension relationships of arterial smooth muscle A active and B passive: (○) determined for 2 min after length change; (●) determined for 27 min after length change [36].....	21
Figure 2.5:	Response of isometric quick release for airway smooth muscle [38].....	22
Figure 2.6:	Isotonic force-length relationship [31].....	23
Figure 2.7:	Response of isotonic quick release [31].....	24
Figure 2.8:	Experiments of force-velocity data. Representative force per mm <sup>2</sup> ( $P$ )/velocity ( $V$ ) curves for Fisher (the dashed line) and Lewis (the solid line) rat tracheal smooth muscle. a) Absolute $P$ and $V$ values. b) Normalised $P$ and $V$ values [9].....	25
Figure 2.9:	Comparison of Hill's equation and Stephens' modified equation to experimental data points [41].....	28
Figure 2.10:	Hill's three-element model [19].....	28
Figure 2.11:	Stiffness-length relationship and fitted by equation (2.7) [26].....	31
Figure 2.12:	Sequence of events in excitation-contraction coupling [4].....	32
Figure 2.13:	Cross-bridge energy cycle [4].....	34
Figure 2.14:	A two-state cross-bridge model for regulation of skeletal muscle.....	35
Figure 2.15:	A four-state cross-bridge model for regulation of smooth muscle.....	36
Figure 2.16:	A scheme of an electrostatic mechanism to represent the contractile mechanism of muscle [58].....	40
Figure 3.1:	A segment of pig trachea, approximately 20 ~ 25 mm in length.....	52
Figure 3.2:	Pig trachea cut open and pinned in dissecting wax dish.....	53
Figure 3.3:	Epithelial and adventitial tissue were peeled off from the smooth muscle of the pig trachea.....	53
Figure 3.4:	A smooth muscle strip was dissected from the pig trachea.....	54
Figure 3.5:	Typical force development of an airway smooth muscle tissue during isometric contraction. 10 <sup>-3</sup> M contraction agent (ACh) was added after approximately 15 seconds. Conditions: $T = 37\text{ }^{\circ}\text{C}$ and $\text{pH} = 7.6$ .....	56
Figure 3.6:	A block diagram of the experimental setup for longitudinal vibration.....	58

Figure 3.7:	A photo of the experimental setup for longitudinal vibration of airway smooth muscle .....	58
Figure 3.8:	A block diagram of the experimental setup for transverse mechanical vibration .....	61
Figure 3.9:	Tissue is vibrated in transverse direction .....	62
Figure 3.10:	Two different stiffness and forces before and after vibration .....	64
Figure 4.1:	A step change in length (transient response) .....	68
Figure 4.2:	Time response of force recovery following a length step (a length step of $\Delta\lambda$ in time $\Delta t$ ) .....	70
Figure 4.3:	Heaviside function (a) and Dirac's delta function (b) .....	73
Figure 4.4:	Hancock's [91] data was fitted by the fading memory model [61] .....	76
Figure 4.5:	Force-velocity relationships for smooth and cardiac muscle .....	79
Figure 4.6:	Typical transient step change in length protocols and terminology, A and B show and length data played back from magnetic (analog) tape as function of time [21] .....	79
Figure 4.7:	Meiss's data is simulated by the fading memory model after using equation (4.15), the force is recovery by a transient step shortening in length, with values of constant parameter $a = 0.35$ , $\alpha_1 = 1.2 \text{ s}^{-1}$ , $\alpha_2 = 8 \text{ s}^{-1}$ , $\alpha_3 = 48 \text{ s}^{-1}$ , $A_1 = 2.5$ , $A_2 = 10$ and $A_3 = 40$ .....	81
Figure 4.8:	Free body diagram of two-dimensional plane element .....	85
Figure 4.9:	Boundary traction in an element .....	92
Figure 4.10:	A strip of smooth muscle tissue is excited with a vibration in the longitudinal direction .....	94
Figure 4.11:	A strip of smooth muscle tissue is excited with a vibration in the transverse direction .....	95
Figure 6.1:	Longitudinal vibrations reduce force and stiffness during isometric contraction. Forces (A and B) and amplitudes of length (C and D) were recorded during isometric contraction. The smooth muscle tissue excited with 15 Hz is shown on the left hand side (A and C), the tissue excited with 65 Hz is shown on the right hand side (B and D). The amplitude of both excitations was 3.8% of the reference length $L_r$ . Conditions: $T = 37 \text{ }^\circ\text{C}$ and $\text{pH} = 7.7$ .....	110
Figure 6.2:	Longitudinal vibrations reduce force during isometric contraction under different durations of vibration: 1 second (A), 2 seconds (B), 3 seconds (C) and 5 seconds (D). All of the vibrations are at a frequency of 35 Hz and with amplitude of the vibration of 3.8% of $L_r$ .....	111
Figure 6.3:	Dynamic stiffness versus vibration frequencies, mean values $\pm 95\%$ confidence interval ( $n = 11$ ) .....	113
Figure 6.4:	Static stiffness versus vibration frequencies, mean values $\pm 95\%$ confidence interval ( $n = 11$ ) .....	113
Figure 6.5:	Dynamic stiffness versus amplitude of vibration .....	116
Figure 6.6:	Static stiffness versus amplitude of vibration .....	117
Figure 6.7:	Dynamic stiffness versus durations of vibration, mean values $\pm 95\%$ confidence interval ( $n = 6$ ), the amplitude is 3.8% of $L_r$ .....	118
Figure 6.8:	Static stiffness versus durations of vibration, mean values $\pm 95\%$ confidence interval ( $n = 6$ ), the amplitude is 3.8% of $L_r$ .....	119
Figure 6.9:	Effects of the initial force response ( $T_1/T_0$ ) to different shortening times ( $\Delta t$ ) and length shortening ratios ( $\Delta\lambda$ ) .....	122
Figure 6.10:	FEM model simulates the longitudinal vibration with frequency 45 Hz and amplitude 3.8% .....	124
Figure 6.11:	Experimental (top) and FEM (bottom) dynamic stiffness versus frequencies for the longitudinal vibration .....	126

Figure 6.12: Experimental (top) and FEM (bottom) static stiffness versus frequencies for the longitudinal vibration .....	127
Figure 6.13: Stiffness from the fading memory model versus frequencies for the longitudinal vibration.....	128
Figure 6.14: Experimental (top) and FEM (bottom) dynamic stiffness versus durations for the longitudinal vibration .....	130
Figure 6.15: Experimental (top) and FEM (bottom) static stiffness versus durations for the longitudinal vibration.....	131
Figure 6.16: Mechanical transverse vibrations reduce force and stiffness during isometric contraction. Forces (A and B) and amplitudes of oscillation (C and D) were recorded duration isometric contraction. The smooth muscle tissue excited with 5 Hz is shown on the left hand side (A and C), the tissue excited with 25 Hz is shown on the right hand side (B and D). The length change ratio of both excitations was 4.8% of the reference length $L_r$ .....	133
Figure 6.17: Experimental dynamic stiffness versus vibration frequencies, mean values $\pm$ 95% confidence interval ( $n = 6$ ) .....	134
Figure 6.18: FEM dynamic stiffness versus vibration frequencies.....	135
Figure 6.19: Experimental static stiffness versus vibration frequencies, mean values $\pm$ 95% confidence interval ( $n = 6$ ) .....	136
Figure 6.20: FEM static stiffness versus vibration frequencies .....	136
Figure 6.21: Experimental dynamic stiffness versus tissue length change ratio.....	137
Figure 6.22: Experimental static stiffness versus tissue length change ratio.....	138
Figure 6.23: Length-force loops during the oscillation for 5 Hz and 2.2% of $L_r$ .....	139
Figure 6.24: Phase-frequency relationship for the fading memory model.....	140
Figure 6.25: Illustration of method used to calculate angle of orientation of airway smooth muscle ( $\theta$ ). Specimen was aligned with long axis of (ASM) airway vertical, and $\theta$ was measured relative to transverse axis [105]....	142
Figure 6.26: Cutting the tissue along the long axis and transverse axis .....	144
Figure 6.27: Schematic illustrations of muscle adaptation and resulting shifts in both the active and passive length-force curve. This indicates the reference length for smooth muscle is very unstable [37].....	144
Figure 7.1: A proposal of acoustic vibration setup for future application .....	150
Figure A.1: Relationship between global nodes and element nodes for one-dimensional problem.....	161
Figure A.2: Linear basis functions $\varphi_1(\xi)$ and $\varphi_2(\xi)$ .....	163
Figure A.3: Weighting functions $w_n$ are associated with the global nodes $n$ .....	164
Figure A.4: A two-dimensional rectangular element.....	166
Figure A.5: Area coordinates for a triangular element .....	167
Figure A.6: Assembling three unit sized elements into a global stiffness matrix.....	172
Figure B.1: Schematic illustration of a material body in two configurations: $\beta_0$ (undeformed state) and $\beta$ (deformed state). The position of a material particle, relative to a common origin, is given by $X$ and $x$ in these two configurations. $X_i$ and $x_j$ are orthogonal.....	174

## List of Tables

Table 3.1	Ingredients used in the preparation of <i>Kreb's</i> solution.....	51
Table 5.1	Measure properties of original tissue.....	98
Table 5.2	Average of eleven tissues dynamic stiffness ( $K_d$ ) with 95% confidence interval to different frequencies and amplitudes.....	99
Table 5.3	Average of eleven tissues static stiffness ( $K_s$ ) with 95% confidence interval to different frequencies and amplitudes.....	100
Table 5.4	Average of six tissues dynamic stiffness ( $K_d$ ) with 95% confidence interval to different frequencies and time durations.....	100
Table 5.5	Average of six tissues static stiffness ( $K_s$ ) with 95% confidence interval to different frequencies and time durations.....	100
Table 5.6	Average of six tissues dynamic stiffness ( $K_d$ ) with 95% confidence interval to different frequencies and length change ratios.....	101
Table 5.7	Average of six tissues static stiffness ( $K_s$ ) with 95% confidence interval to different frequencies and length change ratios.....	102
Table 5.8	Results of the initial force response ( $T_1/T_0$ ) to different finite time durations ( $\Delta t$ ) and length shortening ratios ( $\Delta l/l_0$ ).....	103
Table 5.9	Results of the force response ( $T_1/T_0$ ) to different frequencies and amplitudes.....	104
Table 5.10	Results of the phase degree to different frequencies and amplitudes.....	104
Table 5.11	Results of dynamic stiffness ( $K_d$ ) for the longitudinal vibration to different frequencies and amplitudes.....	105
Table 5.12	Results of static stiffness ( $K_s$ ) for the longitudinal vibration to different frequencies and amplitudes.....	106
Table 5.13	Results of dynamic stiffness ( $K_d$ ) for the longitudinal vibration to different frequencies and time durations.....	106
Table 5.14	Results of static stiffness ( $K_s$ ) for the longitudinal vibration to different frequencies and time durations.....	106
Table 5.15	Results of dynamic stiffness ( $K_d$ ) for the transverse vibration to different frequencies and length change ratios.....	107
Table 5.16	Results of static stiffness ( $K_s$ ) for the transverse vibration to different frequencies and length change ratios.....	107
Table A.1	Relation of global nodal values and local nodal values.....	162
Table A.2	Value $u(\zeta)$ is weighted by the basis functions on the nodal parameters.....	163
Table C.1	Dynamic stiffness ( $K_d$ ) of eleven tissues to different frequencies and amplitudes for the longitudinal vibration.....	179
Table C.2	Static stiffness ( $K_s$ ) of eleven tissues to different frequencies and amplitudes for the longitudinal vibration.....	181
Table C.3	Dynamic stiffness ( $K_d$ ) of six tissues to different frequencies and time durations for the longitudinal vibration.....	184
Table C.4	Static stiffness ( $K_s$ ) of six tissues to different frequencies and time durations for the longitudinal vibration.....	185
Table C.5	Dynamic stiffness ( $K_d$ ) of six tissues to different frequencies and length change ratios for the transverse vibration.....	185
Table C.6	Static stiffness ( $K_s$ ) of six tissues to different frequencies and length change ratios for the transverse vibration.....	187

# **Chapter 1**

## **Introduction**

### **1.1 Lung Structure**

The main function of the human lung is to provide oxygen to body tissues for the metabolism of all living cells for growth and to remove carbon dioxide from the body. The respiratory system can be likened to an inverted tree-like structure with the trunk representing the trachea and the leaves representing the alveolar sacs and the alveoli. The trachea divides into two bronchi to supply the right and left lungs. The right lung has three lobes (right upper, right middle and right lower), while the left lung has two lobes (left upper and left lower). The remaining room on the left hand side is reserved for the heart (see Figure 1.1). Furthermore, each lobe consists of the bronchi, bronchioles, alveolar ducts, alveolar sacs and alveoli.

The lung's material properties play an essential role in determining the various biological and physiological functions of the lung and are important key parameters in lung biomechanical models. The gross structure of the lung tissue is a nonlinear elastic structure that will collapse like a balloon and expel all of its air through the trachea whenever there is no force to keep it inflated [1]. All of the airway walls contain smooth muscle, elastin and collagen fibres. While cartilage rings exist in the trachea to keep it

from collapsing under normal conditions. In the walls of the bronchi, less extensive cartilage plates also maintain the stiffness of the walls. These cartilage plates become progressively less extensive in later generations of bronchi and are not present in the bronchioles. In these airways, it is not the rigidity of the walls that prevent airway collapse but the expansion of the airways due to transpulmonary pressure [2]. Furthermore, a living lung tissue not only has a passive force which is due to the diaphragm movement but also an active force which is due to smooth muscle shortening.

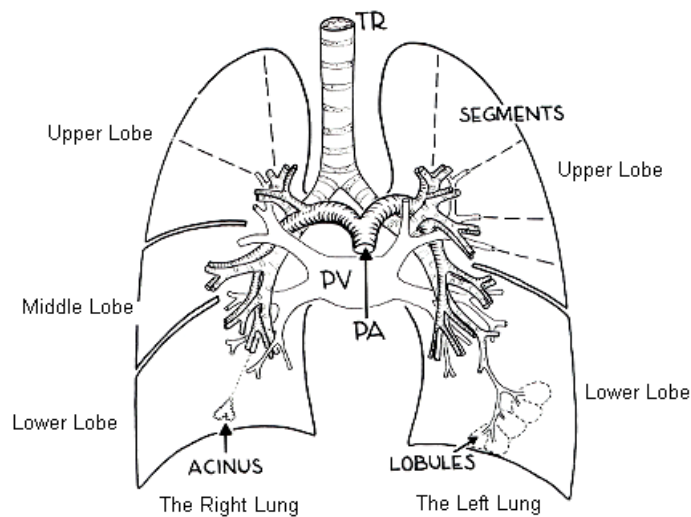


**Figure 1.1 Structure of human lung [3].**

## **1.2 Structure of Airway Tissue**

Airway tissue is the most important factor in determining the overall lung function. It is different from most other organ tissues in that it undergoes large amplitude deformation even during normal breathing. Consequently, this tissue must be highly compliant and capable of large amplitude changes in length and circumference [4]. Relative to most vessels in the circulatory system, the airways are highly dynamic and can actively contract (to almost total occlusion) when the smooth muscle is stimulated. Allergen

exposure can cause a rapid constriction of airway smooth muscle (as in the case of severe asthma) that can severely reduce normal ventilation within a period of minutes to hours [5].

A histological view, as shown in Figure 1.2, describes the airway wall structure and its variation with distance along the tree. In a cross-section, the membranous airway wall appears as shown in Figure 1.3. Airways are covered with the epithelium (EP), over the inner surface as its first defence from external intruders, similar to the lumens of other human organs. This lining of pseudo-stratified ciliated columnar cells sits on top of a basement membrane (BM) that separates smooth muscles (SM) of the lamina propria layer. Just behind the basement membrane is a subepithelial collagen layer.

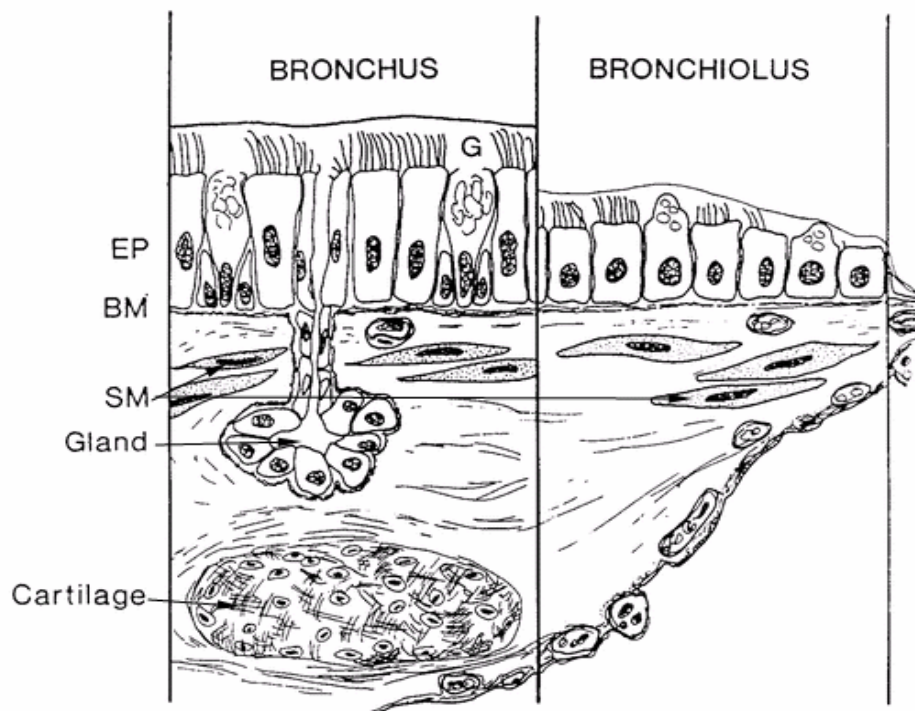


**Figure 1.2** Schematic representation of the airway wall, in cross-section, from the large bronchi down to the small peripheral bronchioles, SM means the airway smooth muscle [5].

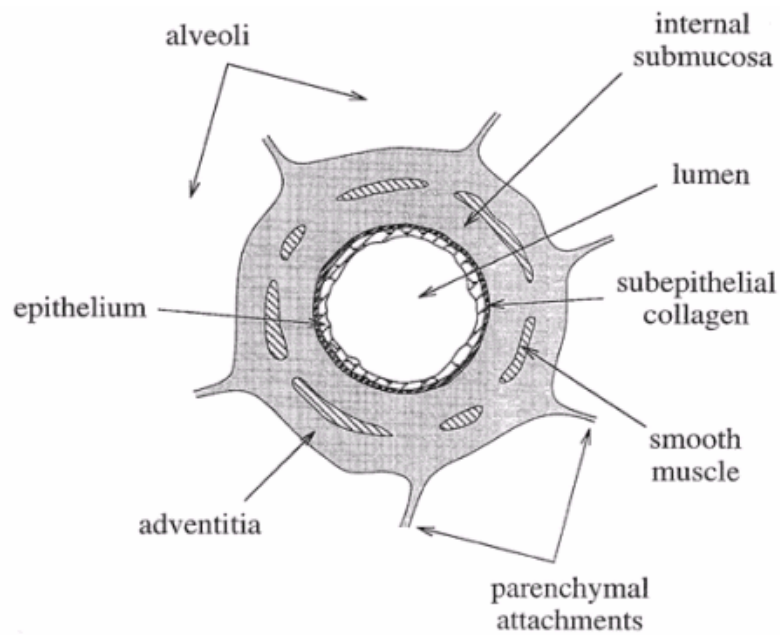


**Figure 1.3** Sketch of the membranous airway wall as viewed in cross-section along the airway axis [5].

On top of the cilia is a sol and a gel layer that forms a mucous blanket for trapping particulates from further invasion into the alveoli where diffusion occurs. These collected particulate debris move toward the trachea, where it can be eliminated by coughing. Supporting the epithelium is a basement membrane that is composed of type-IV collagen, laminin, entactin/nidogen, and heparin sulphate. The subepithelial collagen layer is more important from a structural viewpoint and is considerably thicker than the basement membrane. This layer is composed of type-III and type-V collagen, laminin, and elastin [5]. The main role of the smooth muscles layer is to cause to airway contraction (e.g. asthmatic attack). Beyond the smooth muscle is the adventitia, a layer that is dispersed and highly variable in thickness, whose outer margin is connected to the lung parenchyma.

### **1.3 What is Asthma?**

Asthma is one of the most common pulmonary diseases in the respiratory system. It mostly leads to a common result that causes extremely difficult breathing. Gas exchange is no longer effective as in normal lungs and cellular tissues are either starved of oxygen refreshment or killed completely. More than 25% of the New Zealand population [6] and 3% to 5% of the U. S. population [7] suffer from asthma-related syndromes. A definition of asthma from the Merriam-Webster Dictionary is given as “a condition often of allergic origin that is marked by continuous or paroxysmal laboured breathing accompanied by wheezing, by a sense of constriction in the chest, and often by attacks of coughing or gasping”[8], and bronchial asthma is defined as “asthma resulting from spasmodic constriction of bronchial muscle”.

The main roleplayer in an asthmatic attack is the airway smooth muscle. Asthma is characterised by chronic inflammatory disorders of the airways associated with increased airway responsiveness (known as the airway hyperresponsiveness) to various stimuli [9]. Fredberg [10] suggested that this airway hyperresponsiveness may increase the cross-bridge cycling rates and shorten the airway smooth muscle. The shortening of the airway smooth muscles regulates the airway luminal diameter and narrows the airway. Since cartilage rings exist in the upper airways to keep them from collapsing, asthma mainly results from the occlusion or obstruction in the middle part of airways (lower bronchi and bronchioles). Airway smooth muscle area is pathologically increased when inflammatory conditions of the airway such as chronic pulmonary disease in relation to asthma, which increase heterogeneity of airway smooth muscle function [11 and 12]. Evidence shows that an increase in airway smooth muscle mass,

which is due to hyperplasia and hypertrophy, appears to occur in chronic severe asthma [13-15].

Overall, the contraction of smooth muscle is the main driving mechanism during an asthmatic attack and mainly contributes to airway obstruction. Other factors of airway obstruction in asthma include edema of mucosa, increased mucous secretion, cellular (especially eosinophilic and lymphocytic) infiltration of the airway walls, and injury and desquamation of the airway epithelium.

Asthma is usually linked to environmental or genetic factors, although these relationships are not well understood. Typically, all asthmatics with active disease have hyperresponsive (hyperreactive) airways which manifest as an exaggerated bronchoconstrictive response to many different stimuli. The trigger may be an allergen (allergic hypersensitivity) such as plant pollen, house dust mites, molds, or a particular food. Other common triggers of asthma attacks are nonallergenic types that include emotional upset, aspirin, sulfiting agents (used in wine, beer, and to keep greens fresh in salad bars), exercise, and breathing cold air or smog. In the early phase (acute) response, smooth muscle shortening (contraction) is accompanied by excessive secretion of mucus that may clog the bronchi and bronchioles and worsen the attack. The late phase (chronic response) is characterized by inflammation, fibrosis, edema, and necrosis of the epithelia cells [1, 7 and 16].

Although asthma is not completely curable at this time, it can be controlled by controlling environmental factors and by using medical treatments. Controlling environmental factors aim to avoid or minimize the triggers of asthma attacks that precipitate symptoms or exacerbations. An acute attack is treated by using a medical

inhaler, such as a beta<sub>2</sub>-adrenergic agonist to help relax smooth muscle in the airways and reopen the airways. However, long-term therapy of asthma strives to suppress the underlying inflammation. Anti-inflammatory drugs such as inhaled corticosteroids, cromolyn sodium, nedocromil, and leukotriene blockers are frequently used for this purpose [17].

## **1.4 Airway Smooth Muscle**

There are three main kinds of muscles found in the body (shown in Figure 1.4): skeletal muscle, cardiac (heart) muscle and smooth muscle. Skeletal muscles produce movement by exerting force on tendons, which are around bones or other structures (e.g. skin). The principal tissue in the heart wall is called the cardiac muscle. Smooth muscles are found mainly in the walls of hollow organs (digestive and urinary tract organs, respiratory system, uterus, and blood vessels). Both skeletal and cardiac muscle exhibit striped patterns (visible bands) under a microscope, and hence are known as striated (striped) muscles. The other muscle has fibers with no externally visible striations and is known as smooth muscle. Skeletal muscle can be contracted under conscious control and is often called voluntary muscle. While cardiac and smooth muscles are called involuntary muscles as it can not be contracted under conscious control.

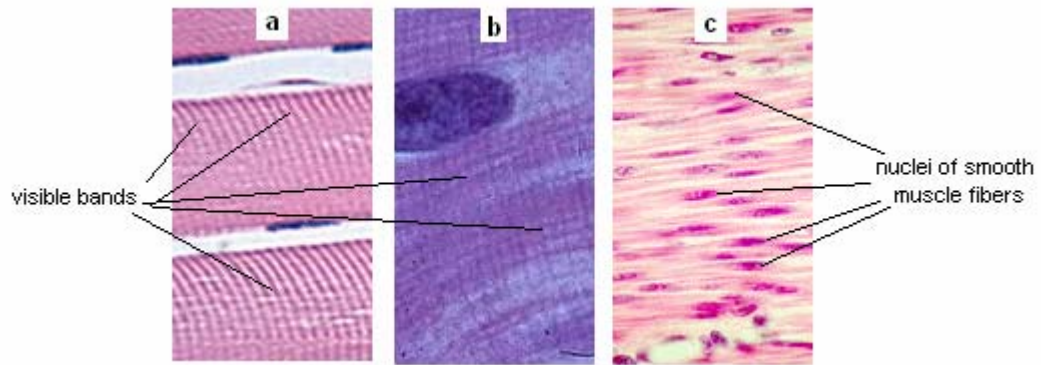


**Figure 1.4** Skeletal muscles (a), cardiac muscle (b) and smooth muscle (c), notice the striations in skeletal and cardiac muscle [18].

The two main characteristics of smooth muscles are: 1) its contraction and relaxation periods are slower than skeletal and cardiac muscle and; 2) its action is rhythmical. Smooth muscle fibers (cells) are small (2 to 5  $\mu\text{m}$  in diameter, and 100 to 300  $\mu\text{m}$  in length), spindle-shaped and slender. Each fiber contains one centrally located nucleus (the dark-pink dots in Figure 1.4c). They are subdivided into two groups: single-unit (also called visceral muscle) and multiunit (see Figure 1.5). The single-unit smooth muscle cells are crowded together and behave somewhat like those of the cardiac muscle. Electrical stimulation of one cell is followed by stimulation of adjacent smooth muscle cells. These muscles are usually stimulated and act rhythmically as a unit. In contrast, multiunit smooth muscles, like skeletal muscle, consist of muscle fibers that are structurally independent of each other, often innervated by single nerve endings and respond to neural stimulation with graded contractions. The multiunit smooth muscles are in the large airways of the lung and in large arteries [4 and 19].

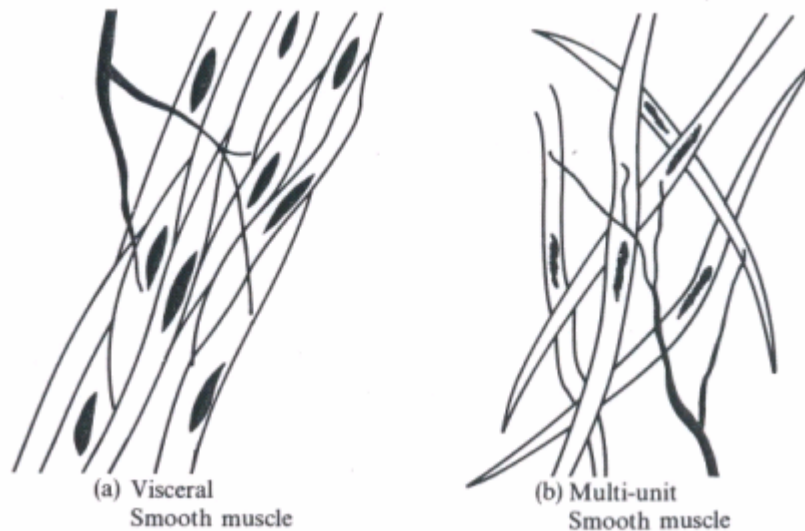


**Figure 1.5 Sketch of a single-unit and multiunit smooth muscle [19].**

A muscle's contractile elements provide its active force through the actin and myosin "ratcheting" mechanism. Actin and myosin are two different proteins, and actin is thinner than myosin. Actin is commonly referred to as "thin filaments" and myosin as "thick filaments". Myosin is made up of a number of myosin molecules. Each myosin molecule consists of a long "tail" and a large "head". Groups of myosin molecules arrange themselves such that the molecules in the longitudinal direction of the thick filament are tail to tail and the heads in the radial direction are in a helical pattern.

Actin is more complicated than myosin in that it contains other proteins. The main protein is actin that forms a double stranded helix. Within the groove defined by the double stranded actin helix runs the second protein of the thin filament, called tropomyosin. A thin filament of skeletal and cardiac muscle has a third protein called troponin complex (or troponin). This complex is attached along the tropomyosin molecule at regular intervals. The difference with smooth muscle is that troponin is absent in the thin filaments.

The actin and myosin myofilaments within the myofibrils in skeletal and cardiac muscle cells are arranged in a regular fashion both longitudinally and radially throughout the myofibril, as seen in Figure 1.6. In the longitudinal direction these myofilaments overlap in a regular fashion, and viewed under a microscope this regular overlap generates a series of light and dark bands (see Figure 1.4 and 1.6). For smooth muscle, the actin and myosin myofilaments within the myofibrils are very thin and arranged more randomly than in skeletal and cardiac muscle cells. As a result, smooth muscle fibers lack striations. Figure 1.6 shows the difference in structure between smooth and skeletal muscle. In skeletal and cardiac muscle, there is an important length unit, called a sarcomere, which is defined as the length between two consecutive Z-lines. Obviously, there is no sarcomere in smooth muscle. The Z-line, in skeletal and cardiac muscle, is a coin-shaped protein sheet that anchors the actin filaments and also connects each myofibril to the next throughout the width of the muscle cell. However, in smooth muscle, the dense body, which acts as anchoring point for groups of actin filaments, corresponds to the Z-line of skeletal and cardiac muscle. Some of these dense bodies in turn are attached to the cell membrane whereas others are located throughout the cell but are held in place by a scaffold of structural protein cross-attachments from one dense body to another.

When the heads of myosin attach to the thin filaments, the muscle generates an active force (see Figure 1.7). Muscle shortening occurs by allowing the relative sliding of the thick and thin filaments and the myofilaments (thin and thick filaments) are found not to shorten. This theory is generally known as the sliding filament theory [20].

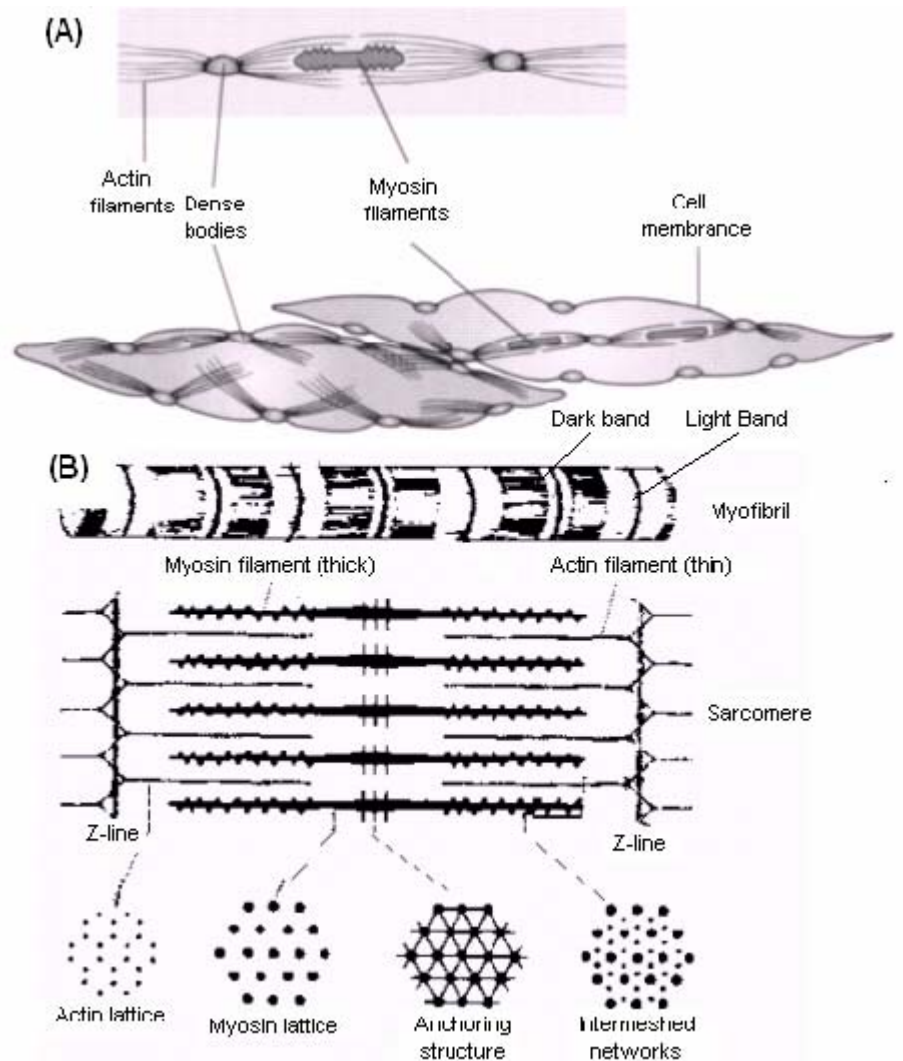


**Figure 1.6** Difference in structure between smooth muscle (A) and skeletal muscle (B).

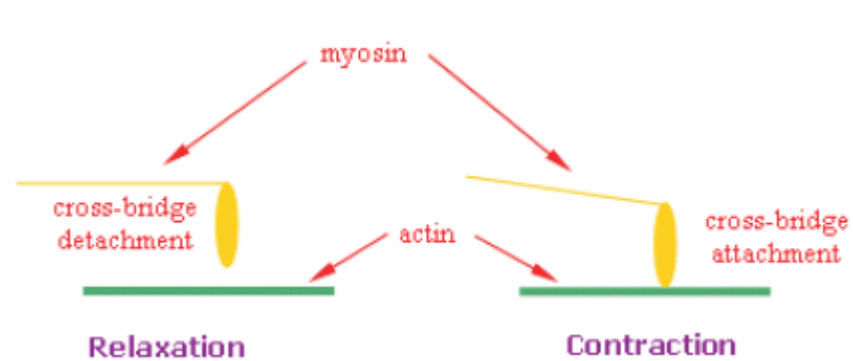


**Figure 1.7** Muscle contraction as caused by cross-bridge attachment.

Although smooth muscles have a different structure when compared to skeletal and cardiac muscle, the fundamental mechanical processes of contraction in smooth muscle (force-length relationship, force-velocity relationship, etc.) have a qualitative similarity to those processes occurring in skeletal and cardiac muscle. Furthermore, the results of research on smooth muscles in the last three decades have revealed that the presence of all the components is apparently necessary for the function of a sliding-filament-crossbridge contraction mechanism [21].

## **1.5 Research Plan**

Since the driving mechanism for any asthmatic attack is the shortening of airway smooth muscle, the main objective of this research is to determine whether airway smooth muscle contraction can be relaxed by vibrations. To achieve this, two types of vibration will be tested: longitudinal and transverse. The former has been attempted by other authors [6, 22-30] who proved that stiffness variation does exist with longitudinal oscillations. However, no attempts have been made using the latter method. It is believed if oscillation does relax contracted airway smooth muscle, it could be incorporated in a bronchodilation process to relief airway passages. Since any bronchodilation can be introduced as pressure waves, this will introduce transverse rather than longitudinal vibration. Therefore, the main objectives of this work are:

1. Develop a test rig suitable for testing the effect of longitudinal and transverse oscillation on contracted airway smooth muscle.
2. Test several live airway smooth muscle tissues extracted from the pig tracheas and subjected to longitudinal and transverse vibration and measured the resulting change in the stiffness of the airway smooth muscle.

3. Develop a distribution (fading memory model) and a finite element model for the above two tests for generalization as well as to extend the study on a further range of excitation.

The specific objectives may be summarised in Figure 1.8.

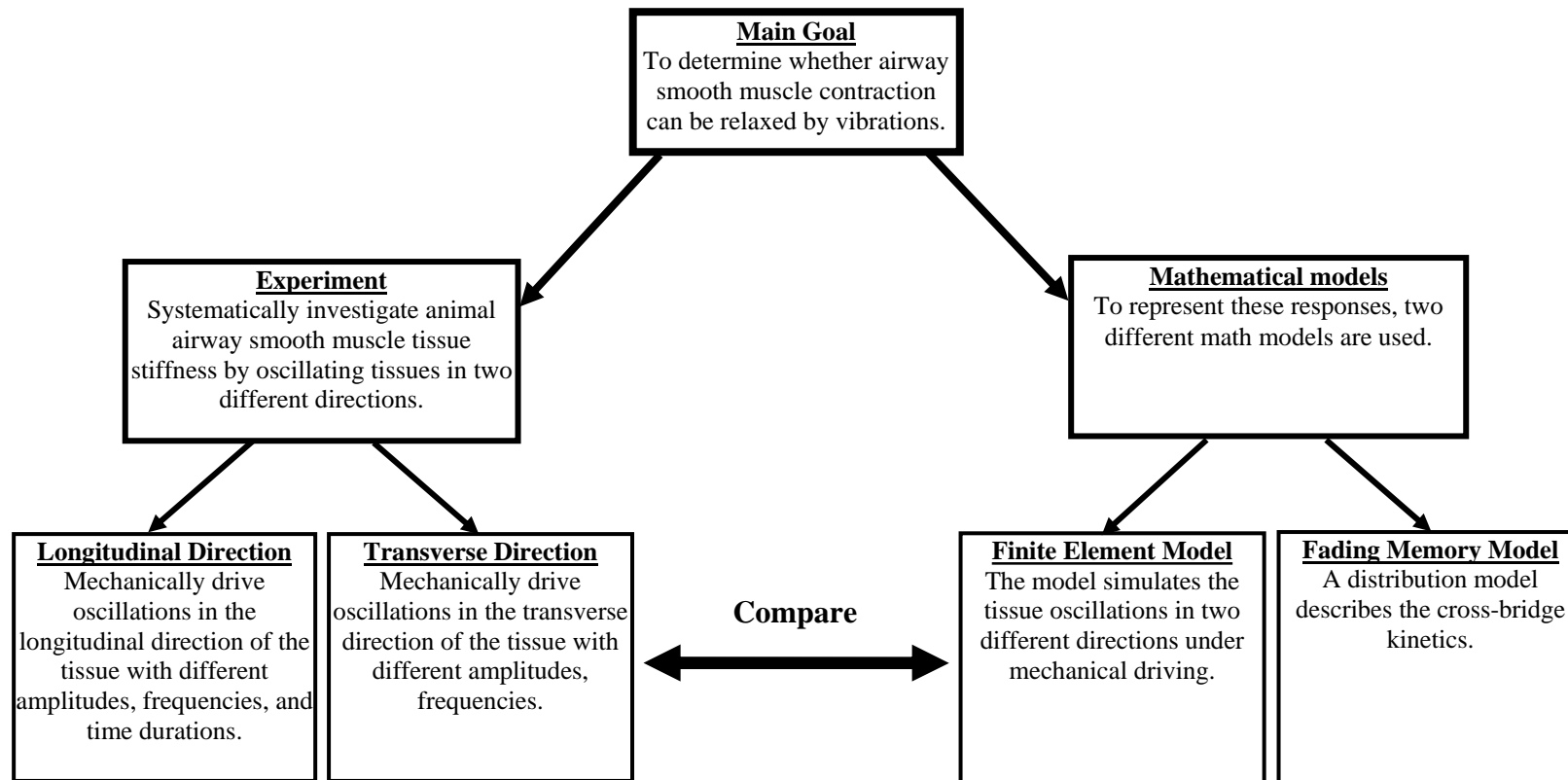


**Figure 1.8** A follow chart for the research plan.

## **1.6 Structure of the Thesis**

This chapter has described the general background of airway smooth muscles as related to asthma. The chapter has also presented the research plan. Chapter 2 presents the fundamental knowledge for smooth muscle and the relevant results from other researchers. Chapter 3 details all the experiments performed during the research. Chapter 4 introduces the fading memory and FEM model. Chapter 5 lists all the results from the experiments and mathematical models. Chapter 6 rationally and physically discusses the behaviours observed in both experimental and theoretical investigations. Chapter 7 concludes this research and looks to the future.

## **Chapter 2**

### **Smooth Muscle Mechanics and Literature Survey**

#### **2.1 Introduction**

The three main structural elements that exist in respiratory tissues are elastin, collagen and smooth muscles. The latter plays a major role in an asthmatic attack. The airway smooth muscle is different from other connective tissues in that it combines both active and passive forces. During the normal lung breath cycles, the airway smooth muscles display passive and viscoelastic properties in the resting state. Once the airway smooth muscles are contracted by some stimuli [9], as in an asthmatic attack, the contractile mechanism of these muscles will generate an active force which causes a shortening in the muscle length and dominate their properties.

This work focuses on the active behaviour of airway smooth muscles. To understand the foundation of the research, a fundamental knowledge of smooth muscles contraction and related work from the literature are introduced in the following sections.

First, the contracted smooth muscle properties will be discussed from a mechanical perspective in Section 2.2. Second, the physiological procedure of muscle contraction will be presented at a molecular level in Section 2.3. Third, available models related to

muscles contraction are summarized in Section 2.4. Finally, available literature on muscle vibrations are reviewed in Section 2.5.

## **2.2 Mechanical Properties of Muscle Contraction**

Muscle tissues can contract and generate a force when it is stimulated. In most cases, two kinds of muscle contraction modes are considered. If the muscle is fixed in such a way so that the ends cannot move (at a constant length), this contraction is known as an isometric contraction. In contrast, another mode of contraction, called isotonic contraction, occurs when the muscle is allowed to contract or shorten against a constant loading.

### **2.2.1 Isometric Contraction**

For an isometric contraction, the development of the generated force depends on the mode of stimulation (see Figure 2.1). A single stimulus generates a twitch, in which the force increases rapidly and then decreases. If a second stimulus is applied before the first twitch has fallen to zero, the peak force of the second twitch is higher than that of the first. If the stimulus is maintained at a certain frequency, the generated force rises smoothly and this muscle is said to be in tetanus. The plateau force is called the isometric force for the muscle length [19 and 31].

An isometric contraction experiment can be performed where the amount of isometric force generated by a muscle is measured for a number of different muscle lengths. The result of this experiment is called the isometric force-length relationship. The ideal result of such a relationship for skeletal muscles is shown in Figure 2.2.

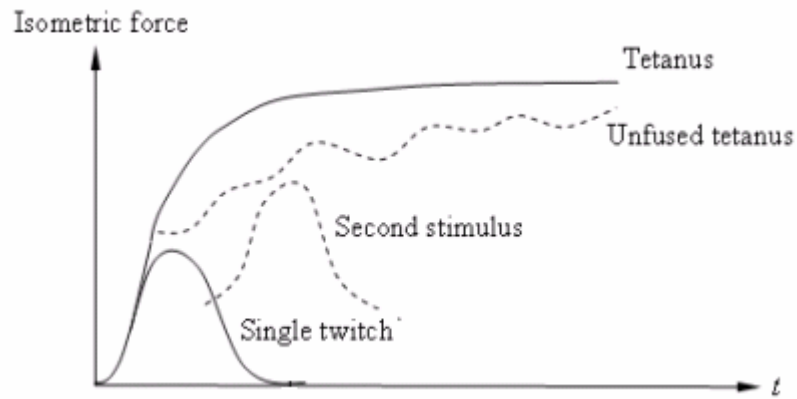


**Figure 2.1** Isometric force dependence for various modes of stimulation [31].

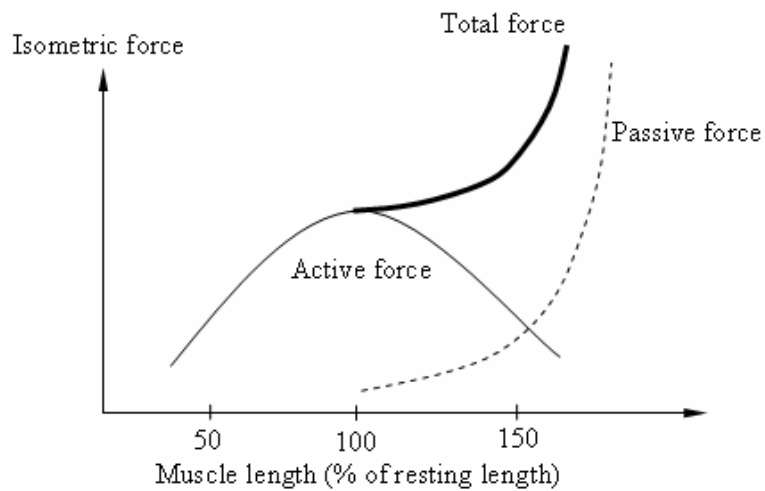


**Figure 2.2** Isometric force-length relationship for skeletal muscle [31].

In terms of theory, a passive muscle (muscle which is not contracting) resists extension beyond its normal resting length (see the dashed line in Figure 2.2). It is possible to measure the passive force-length behaviour when the muscle is in the passive state. By subtracting the passive force from the total force, we can obtain the amount of active force generated in the muscle through contraction (see the thin solid line in Figure 2.2). As can be seen, this active force is maximal when the length is close to the resting length, and decreases if the muscle length is both increased or decreased. The parabolic behaviour of the isometric force-length relationship is determined by the contractile mechanism of the muscle, and can be explained by different degrees of interaction

between the actin and myosin. The following explanation comes from striated muscles and details the isometric force relationship to the sarcomere (the unit length of striated muscle). However, this explanation is also appropriate for the smooth muscle.

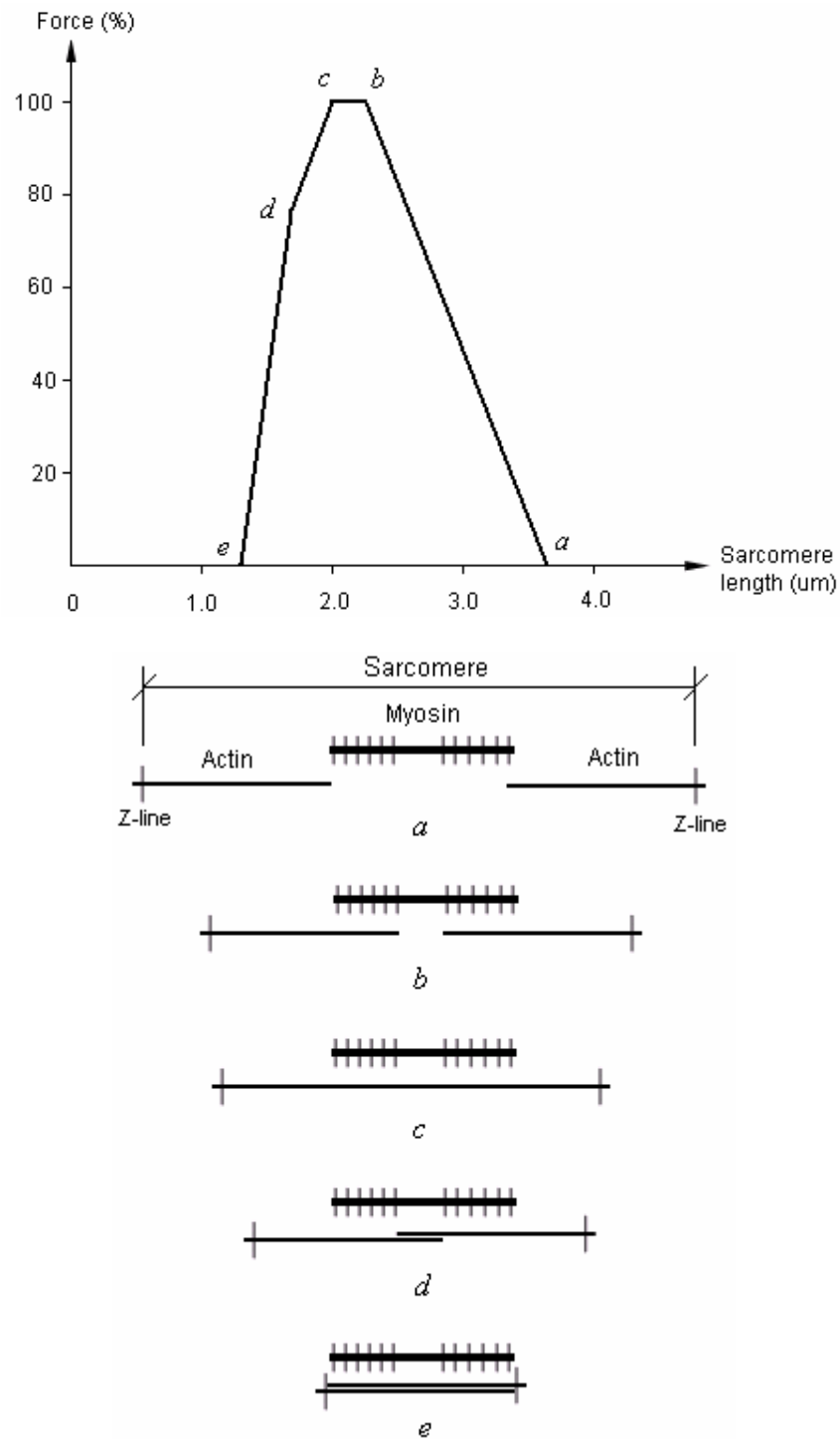


**Figure 2.3 Sarcomere force-length relationships [31].**

At point *a* (Figure 2.3), no force is generated in the sarcomere as there is no interaction between the actin and myosin. At point *b* there exists a maximum force as there is a maximum interaction between the actin and myosin. The maximum force continues up to point *c* when the actin filaments start to interfere. At point *d*, there is a steric interference of the actin filaments limiting the interaction between them and the myosin. At point *e*, there is interference between both the actin and myosin, resulting in no force production. Since no “sarcomere” (unit length) can be found in smooth muscles, some researchers [32-35] have suggested that the average distance between the successive dense bodies might represent an estimate of the contractile unit length in smooth muscles. An isometric force-length relationship for smooth muscle was measured by Seow [36] and is shown in Figure 2.4.

Two facts can be noticed from Figure 2.4. Firstly, the history of muscle loading is an important factor in generating an active force. Different settling times are required to develop different isometric forces, see Figure 2.4 (A). Secondly, the passive force exists for the entire length range and not only when the tissue length is beyond the normal resting length (see Figure 2.4 (B)). This may be attributed to the random arrangement of actin and myosin and the lack of identifiable “sarcomere” in smooth muscles. From another point of view, the resting length (where there is no passive force) and the length that correlates with maximal force generation are not unique in smooth muscles. Bai *et al.* [37] suggested that the terminology in smooth muscle where the length that correlates with maximal force generation should be called the “reference length” ( $L_{ref}$ ) rather than “optimal length” as used in striated muscles (see Figure 2.4). An appropriate approach for adjusting the reference length will be introduced in Chapter 3.

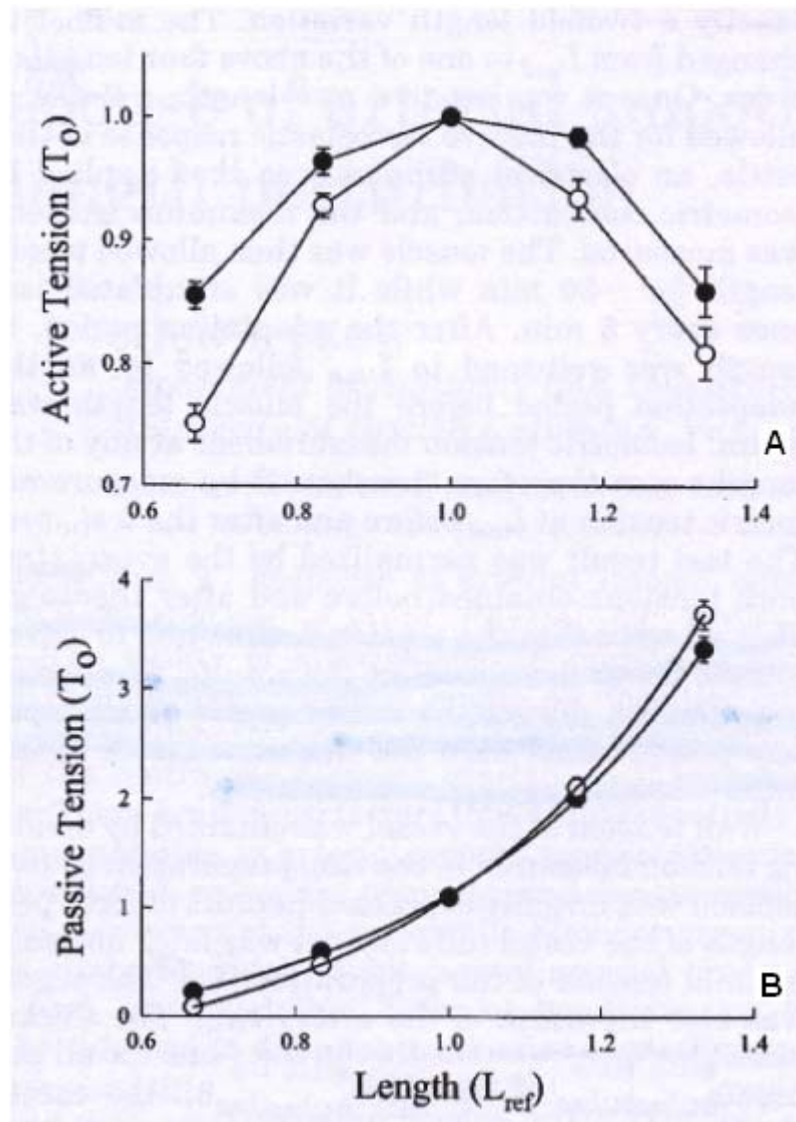


**Figure 2.4** Length-tension relationships of arterial smooth muscle A active and B passive: (○) determined for 2 min after length change; (●) determined for 27 min after length change [36].

When a muscle in isometric contraction is suddenly shortened and clamped at a new fixed length (transient change in length), this is called an isometric quick release. These kinds of experiments have been conducted on smooth muscles [21 and 38]. Gunst *et al.* [38] tested dog airway smooth muscles, and the result is shown in Figure 2.5. The muscle tissue was initially stimulated at zero time by acetylcholine (ACh), and the isometric force then developed to a maximum value. After approximately 1 minute, a transient shortening in length occurred and the muscle tissue was clamped at a new fixed length (70% of  $L_0$ ). The results show that the force changes abruptly to an

extremely low level (lower than the force before stimulation), and the force subsequently recovers to a new plateau force through the time course (a slow recovery follows the initial recovery). The extent of shortening (length step) determines the extent of the extreme force (the initial fall in the force) and the new plateau force is determined by the isometric force-length relationship (see Figure 2.2 and 2.4). The experimental data also shows that the initial recovery time is typically less than 10 seconds [38].

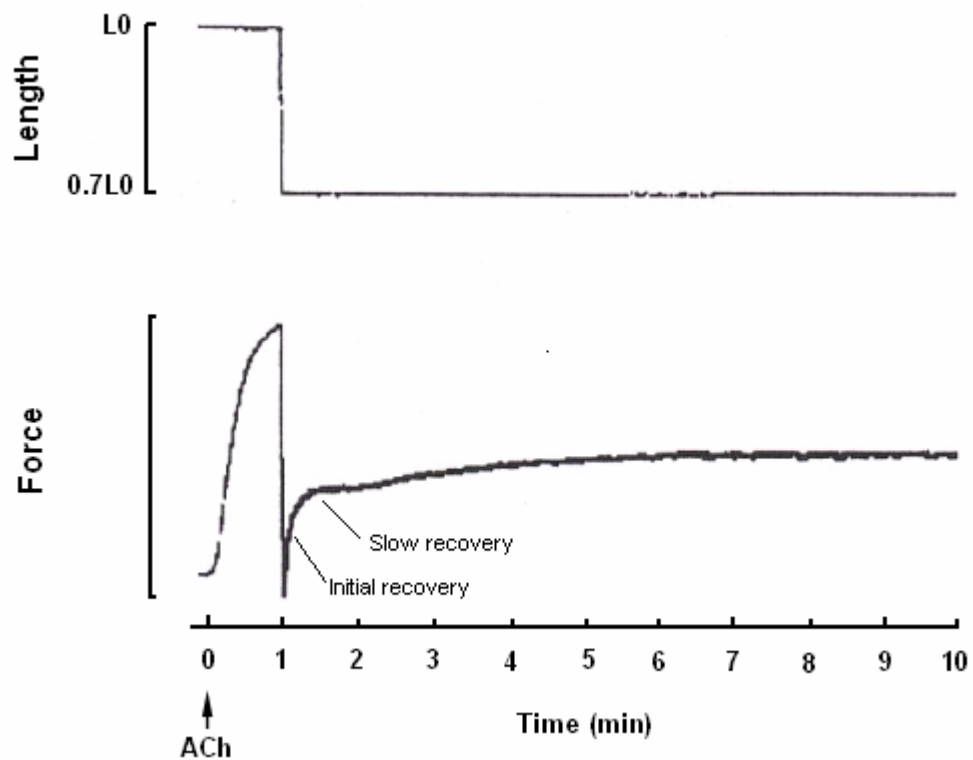


**Figure 2.5** Response of isometric quick release for airway smooth muscle [38].

### 2.2.2 Isotonic Contraction

In an isotonic contraction, the muscle is allowed to shorten against a constant loading. The experiment is normally performed with the muscle attached to one end of a lever with a fixed amount of weight. Initially, the muscle is contracted at a constant length

(i.e. initially isometric contraction) to generate a force. When the value of the generated force reaches that of the applied weight (known as the afterload), the muscle starts to shorten. It has been found that the velocity of the shortening is constant for a given afterload (see Figure 2.6). A higher loading gives a slower shortening velocity and a lower loading produces a higher shortening velocity. This is the reason our muscles are able to lift small loads quickly or large loads slowly.

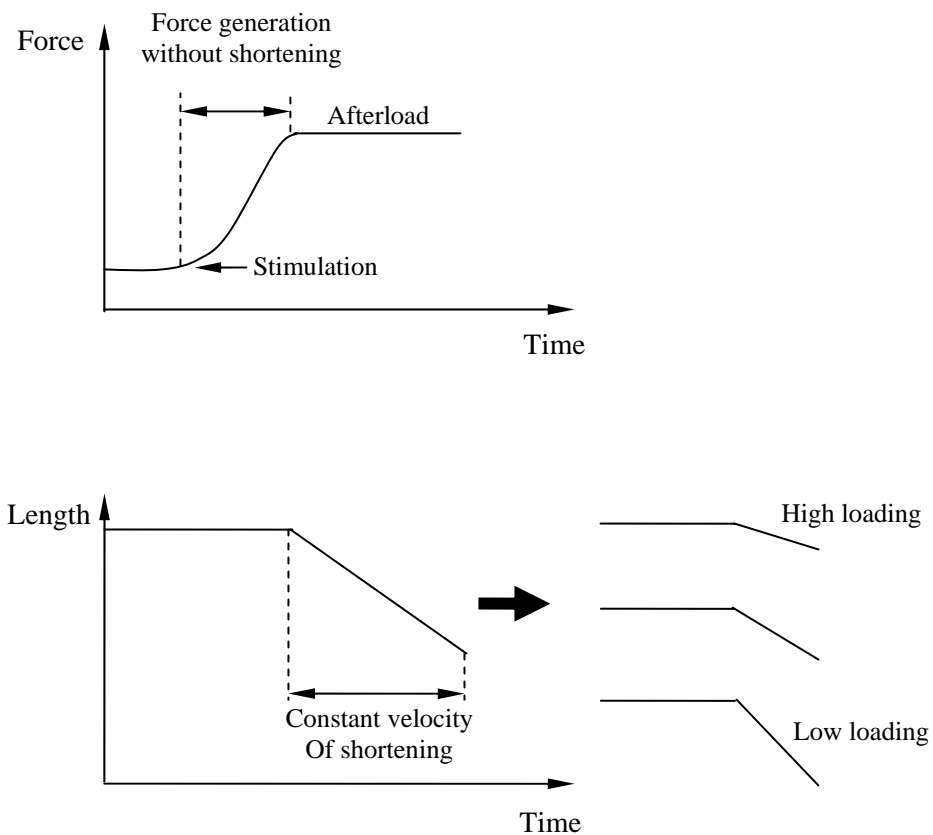


**Figure 2.6** Isotonic force-length relationship [31].

If the experiment is designed such that the muscle first contracts isometrically and then is abruptly released to shorten against a constant afterload, this is known as an isotonic quick release. Once release occurs, the force falls rapidly to the level of the new afterload. Initially, there is an abrupt shortening that coincides with the transient change

in force. Subsequently, a slower isotonic shortening occurs at a velocity that corresponds to the new afterload (see Figure 2.7).

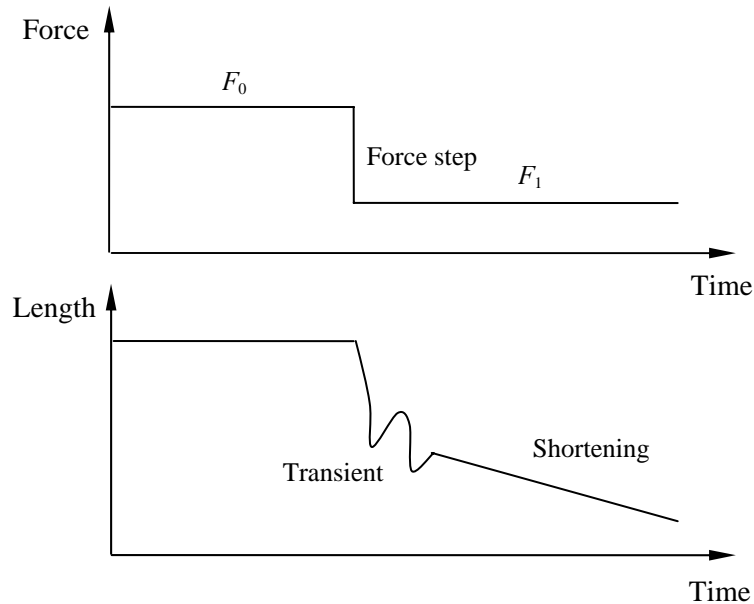


**Figure 2.7** Response of isotonic quick release [31].

An isotonic contraction experiment can be performed by measuring the velocity of shortening by varying the amount of afterloads. The result of this experiment is called the isotonic force-velocity relationship which has a characteristic hyperbolic shape. Furthermore, different types of muscles have different velocity responses. Blanc *et al.* [9] measured airway smooth muscles from Fisher and Lewis rats (see Figure 2.8), and found that under the same afterload, the muscle shortening velocity of the Fisher rats was higher than the velocity of Lewis rats, (see Figure 2.8 (a)). Therefore, one can conclude that the airway smooth muscle of the Fisher rats is more active than the airway smooth muscle from Lewis rats. However, both curves are nearly identical after normalization (see Figure 2.8 (b)). Figure 2.8 (b) shows that the maximum force is generated when the muscle is contracting isometrically (at zero velocity). The maximum velocity occurs when there is no afterload (experimentally this is found from extrapolating the curve from low values of afterload).

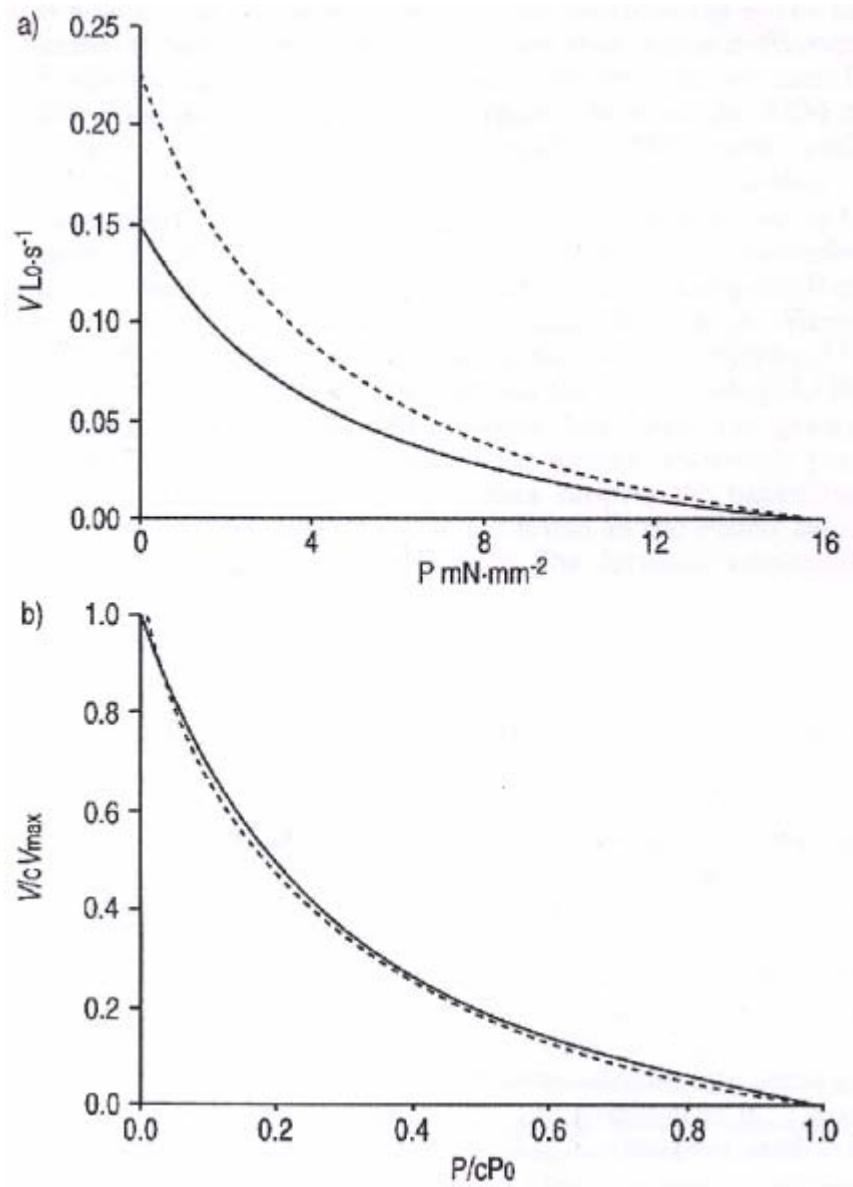


**Figure 2.8** Experiments of force-velocity data. Representative force per  $\text{mm}^2$  ( $P$ )/velocity ( $V$ ) curves for Fisher (the dashed line) and Lewis (the solid line) rat tracheal smooth muscle. a) Absolute  $P$  and  $V$  values. B) Normalised  $P$  and  $V$  values [9].

### 2.2.3 Hill's Equation and Hill's Three-Element Model

Hill's equation [39] is one of the most famous equation in muscle mechanics. This equation can be written as:

$$(v + b)(F + a) = b(F_0 + a) \quad (2.1)$$

where  $F$  is the force in a muscle,  $v$  is the velocity of shortening,  $F_0$  is the maximum force at zero velocity (isometric force), and  $a$  and  $b$  are constants. If the constants  $a$  and  $b$  are ignored on the left-hand side of the equation, then equation (2.1) shows that the energy of work done by the muscle is equivalent to the energy conversion from the chemical reaction in the muscle, and that this energy is conserved. Hill's equation referred to the ability of a tetanized skeletal muscle and the empirical equations based on experimental data from frog sartorius muscle [39]. The original derivation of this equation was from a thermo-mechanical expression [39]. First of all, Hill proposed the equation for a balance of energy:

$$E = A + H + W \quad (2.2)$$

where  $E$  is the rate of energy release,  $A$  is the activation or maintenance heat,  $W$  is the rate of work done ( $W = F \cdot v$ ), and  $H$  is the shortening heat. If the muscle is in an isometric condition (no shortening and no velocity), then equation (2.2) is reduced to:

$$E = A \quad (2.3)$$

Equation (2.3) shows that the rate of energy release is equal to the activation energy. When the muscle shortens, an additional chemical reaction takes place. This amount of "extra energy" should be equal to the sum of the shortening heat and the work done ( $H + W$ ). From experimental data, Hill proposed two empirical equations as follows:

$$H + W = b(F_0 - F) \quad \text{and} \quad H = a \cdot v \quad (2.4)$$

From equation (2.4) one can obtain:

$$H + W = a \cdot v + F \cdot v = b(F_0 - F) \quad (2.5)$$

Rewriting equation (2.5), one obtains equation (2.1). This equation also represents the characteristic hyperbolic curve of a force-velocity relationship. Many years later, Hill admitted that it is better to consider equation (2.1) directly from the force-velocity relationship [40]. Stephens *et al.* [41] modified the Hill's equation as follows:

$$v = \frac{\beta(F_0 - F)}{(\alpha + F)(\gamma - F)} \quad (2.6)$$

where  $\gamma$  is a new constant,  $\alpha$  and  $\beta/\gamma$  are approximations of  $a$  and  $b$  in the Hill's equation (equation (2.1)), and  $\gamma > F_0$ . When  $F_0$  approaches  $\gamma$ , the velocity  $v$  is calculated as an infinite value from this modified equation, which suggests that  $\gamma$  can be interpreted as the maximum force a cross-bridge can bear. Stephens *et al.* used the modified equation to fit the experimental data from airway smooth muscle. The result is shown in Figure 2.9. A better fit was achieved by using the modified force-velocity equation, especially at the high loading end of the curve

Hill's equation cannot describe a single twitch or the mechanical behavior of an unstimulated muscle (passive state). For these reasons, previous authors used mechanical elements to develop a better model known as the Hill's three-element model which is shown in Figure 2.10. Two elements, namely the contractile component and the series elastic component, are arranged in series and another element called the parallel elastic component is arranged in parallel.

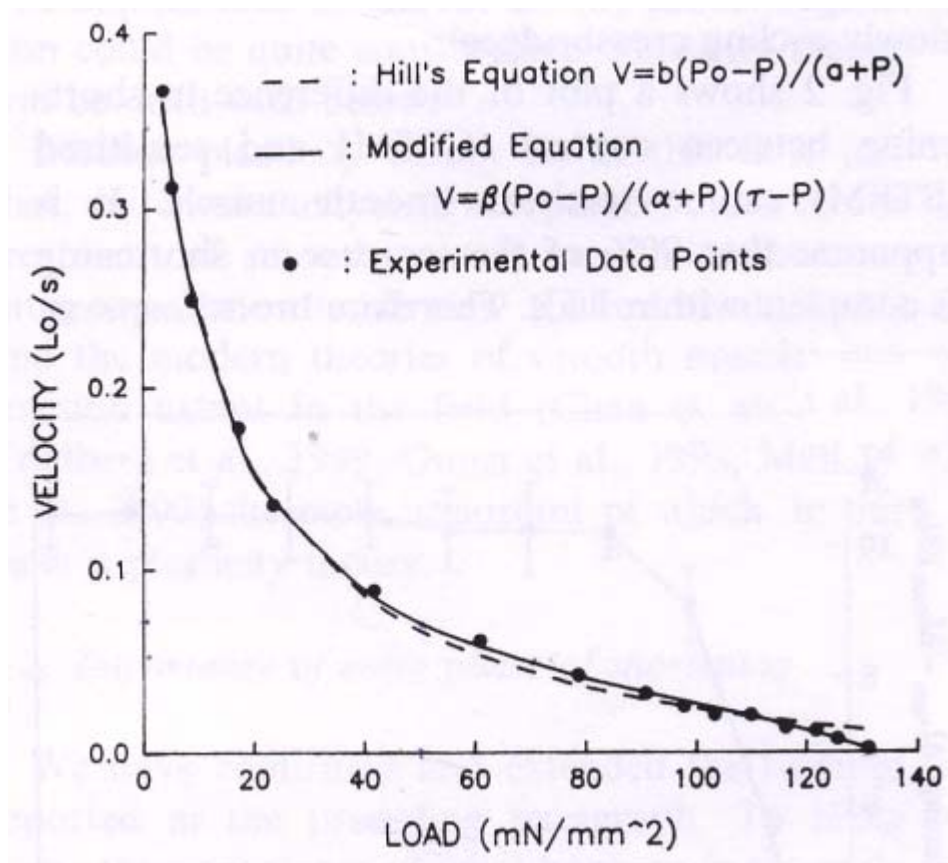


Figure 2.9 Comparison of Hill's equation and Stephens' modified equation to experimental data points [41].

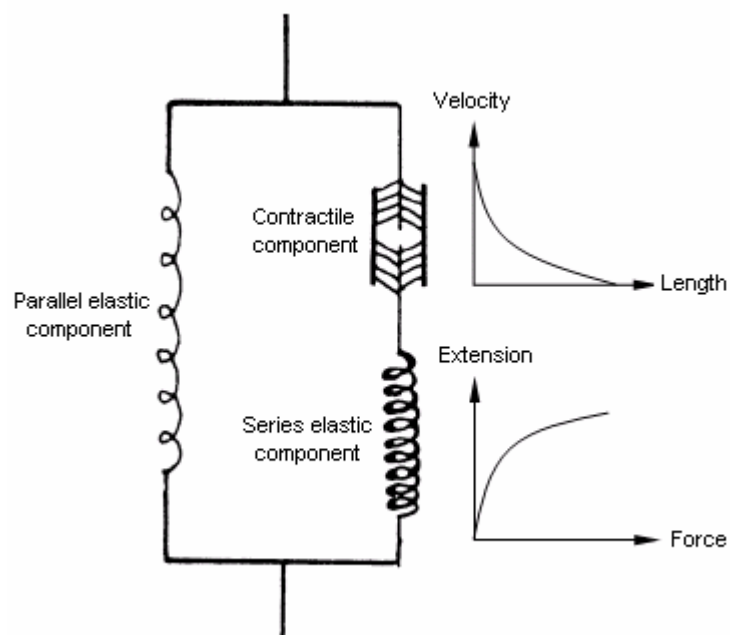


Figure 2.10 Hill's three-element model [19].

The contractile component is designed as a “black-box” to lump all of the active features of contraction. It is assumed that this component is freely extensible in its resting state, and is capable of shortening when activated. Once fully activated, the force generated by this contractile component is assumed to be dependent only on its instantaneous length and velocity and independent of time.

The series elastic component is represented by an undamped spring, which accounts for the muscle elasticity in isometric conditions. Therefore, the length of this element is dependent only on the force in the muscle and is independent of the kinetics of contraction. The series elasticity may be due to the intrinsic elasticity of the actin, myosin molecules and cross-bridges.

The parallel component represents the potential energy stored in a relaxed muscle (the elasticity of the muscle at rest) when it is stretched beyond its resting length. It is assumed that the element represents the passive elastic structures such as connective tissue and muscle cell membranes.

#### **2.2.4 Contracted Smooth Muscle Stiffness-Length Relationship**

The stiffness of a contracted muscle is determined by the active force. From this point of view, the muscle stiffness is a rough reflection of the number of active cross-bridge interactions [23]. Furthermore, the muscle length determines the number of active cross-bridge interactions (see Figures 2.2 and 2.3). Thus, the stiffness-length relationship of contracted muscle is more closely related to the force-length relationship. However, in reality this conclusion is not completely valid as the number of active cross-bridges is not the only factor that determines the muscle stiffness at different muscle lengths. For

smooth muscle, the contractile mechanism in a cell is embedded in the tissue attached to the surrounding cells and connective tissue at numerous points via membrane-associated dense bodies along its entire length, rather than just at its ends [42 and 43]. Meiss and Pidaparti [26, 27, 43 and 44] worked on airway smooth muscle from dogs and ovarian smooth muscle from rabbits for a variety of muscle lengths under isometric and isotonic contractions and proposed a “radial constraint hypothesis”. This hypothesis states that an activated smooth muscle tissue, under a very light (or zero) isotonic load, will shorten at constant volume until it reaches an equilibrium length. As the extremities of shortening are approached, the tissue must expand significantly in the radial direction to preserve the constant-volume condition. This expansion would be counter-acted by forces developed in connective tissue that are arranged in a radial direction. The strained connective tissue would serve as a load on the contractile apparatus (the force being transferred by the incompressible cells and extracellular matrix) and this would cause the shortening to be limited. It would also cause the axial stiffness of the muscle tissue to rise as more cross-bridges were recruited in response to the reduced internal shortening velocity [27]. Meiss [26] proposed a set of empirical equations as follows, and used this equation to fit the experimental data (Figure 2.11):

$$\begin{aligned}
 S_A &= \alpha \pi K_c L^{-3/2} V^{1/2} \exp \left[ 2K_c \left( \frac{(\pi V)}{L} \right)^{1/2} \right] \\
 S_T &= K_T F_A + S_0 \\
 S_L &= 1 / \left[ (1/S_A) + (1/S_T) \right]
 \end{aligned}
 \tag{2.7}$$

where  $L$  is the length of tissue,  $V$  is the volume of the tissue,  $F_A$  is axial force,  $\alpha$ ,  $K_c$ ,  $K_T$  and  $S_0$  are constants. The resultant longitudinal stiffness ( $S_L$ ) is calculated by the axial stiffness ( $S_A$ ) and transverse stiffness ( $S_T$ ) in series. Equation (2.7) shows that the muscle stiffness is very high at extremely short lengths. The stiffness then declines with

increasing muscle lengths. Pidaparti *et al.* [45] developed a three-dimensional FEM model with viscoelastic material properties to stimulate this relationship.

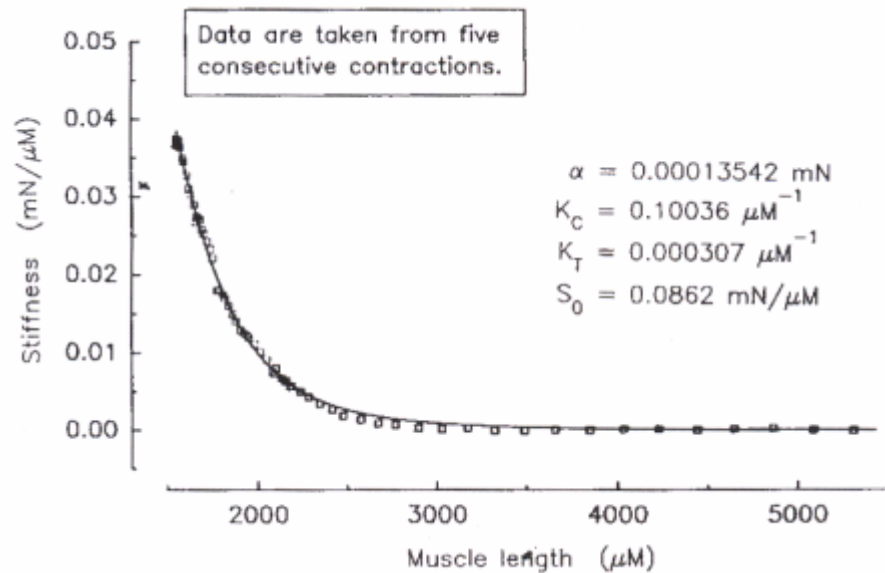


**Figure 2.11** Stiffness-length relationship and fitted by equation (2.7) [26].

### 2.3 Physiological Procedure of Muscle Contraction

Section 2.2 introduces the mechanical properties of muscle contraction and discusses the force-length and velocity-length relationships. In this section, the muscle contraction will be explained from a physiological point of view. More physiological details are provided to show how muscle contracts in response to stimulation. The muscle shown in Figure 2.12 is skeletal muscle, but the principle of muscle contraction by stimuli is the same for all types of muscles.

An action potential propagates from the terminal of the nerve and along the muscle cell membrane to raise the potential of the membrane. The high membrane potential opens voltage dependent gates and allows a small amount of calcium ions ( $\text{Ca}^{2+}$ ) to enter the sarcoplasmic reticulum (RS) (see Figure 2.12). This event triggers a much greater

release of calcium ions into the cell. These calcium ions act as a trigger to interact with actin, and cause the actin to expose itself to cross-bridge attachment, which results in muscle contraction. When the potential of the membrane drops, the calcium ions drain from the cell and back into the sarcoplasmic reticulum. No interacted actin is blocked from the cross-bridges, and the muscle relaxes.

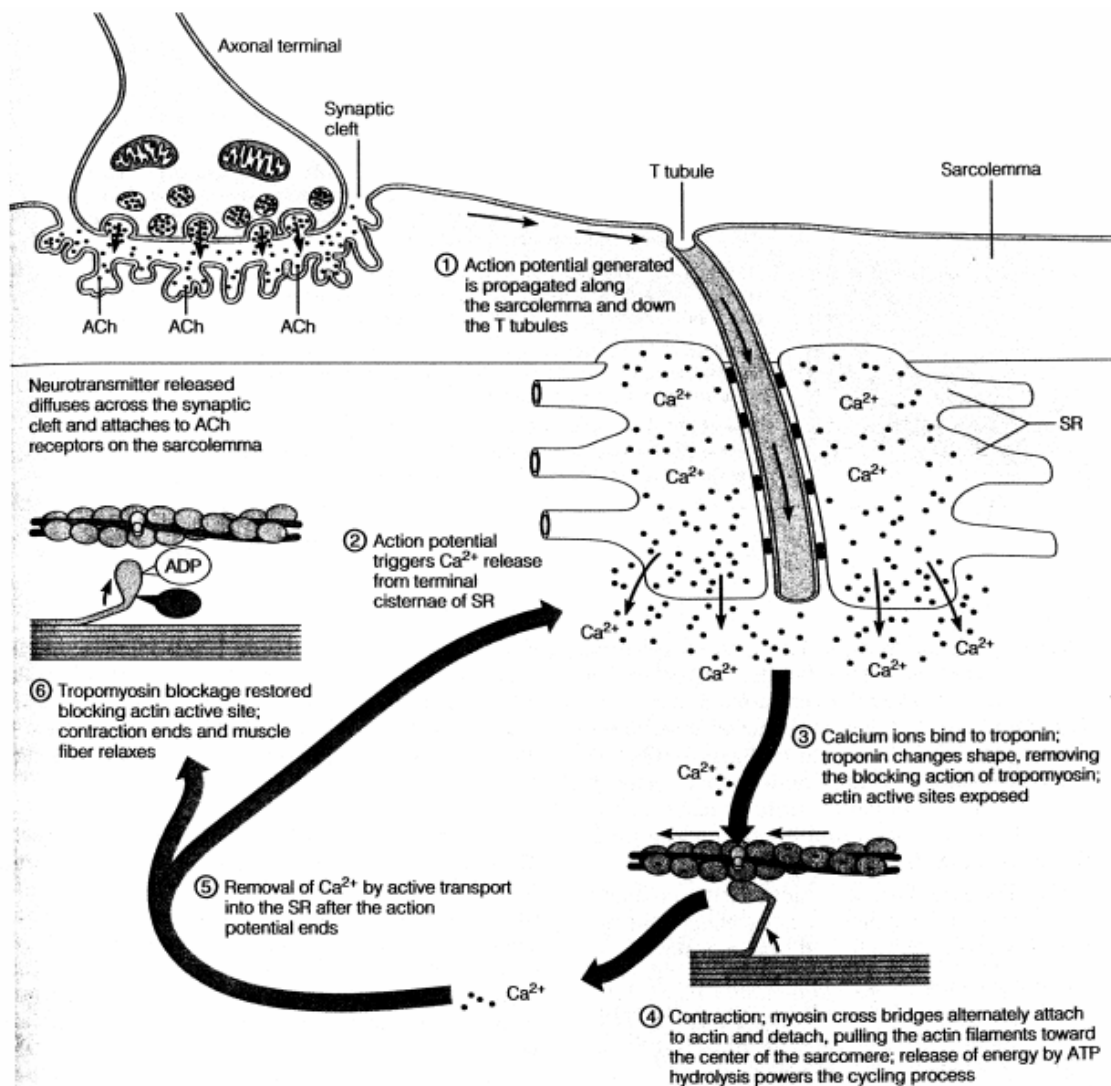


Figure 2.12 Sequence of events in excitation-contraction coupling [4].

Figure 2.12 describes the action of the calcium ions that trigger the actin to unblock or block themselves to the cross-bridges. The next process presents cross-bridge attachment and detachment (cycling).

Once actin is exposed to the cross-bridges, the cross-bridges can attach and detach to the actin. Cross-bridge cycling occurs through a different mechanism. The energy causing cross-bridge cycling in the muscle cell is called adenosine tri-phosphate (ATP). The chemical equation by which ATP generates energy is:



where P is free phosphate and ADP is adenosine di-phosphate. The process of cross-bridge cycle is shown in Figure 2.13, and explained as follows:

1. Cross-bridge attachment: The activated myosin head is strongly attracted to the exposed binding site on actin and cross-bridge binding occurs. At this point the myosin head is in its high-energy configuration.
2. The working stroke: A myosin head binds to the actin to slide resulting in contraction of the muscle. As the myosin head rotates, the myosin tail is stretched thereby generating a force. ADP and P are released from the myosin head during this process. The myosin molecule is now at its low-energy configuration.
3. Cross-bridge detachment: As a new ATP molecule binds to the myosin head, myosin's hold on actin loosens and the cross-bridge releases from the actin.
4. “Cocking” of the myosin head: ATP is split into ADP and P to provide the energy needed to return the myosin head to its high-energy configuration and to cock the myosin head. This provides the potential energy needed for its next sequence of attachment and working stroke. From the above process, the ratio between the duration of the working stroke phase and the total time of the cross-bridge cycle is called the duty ratio.

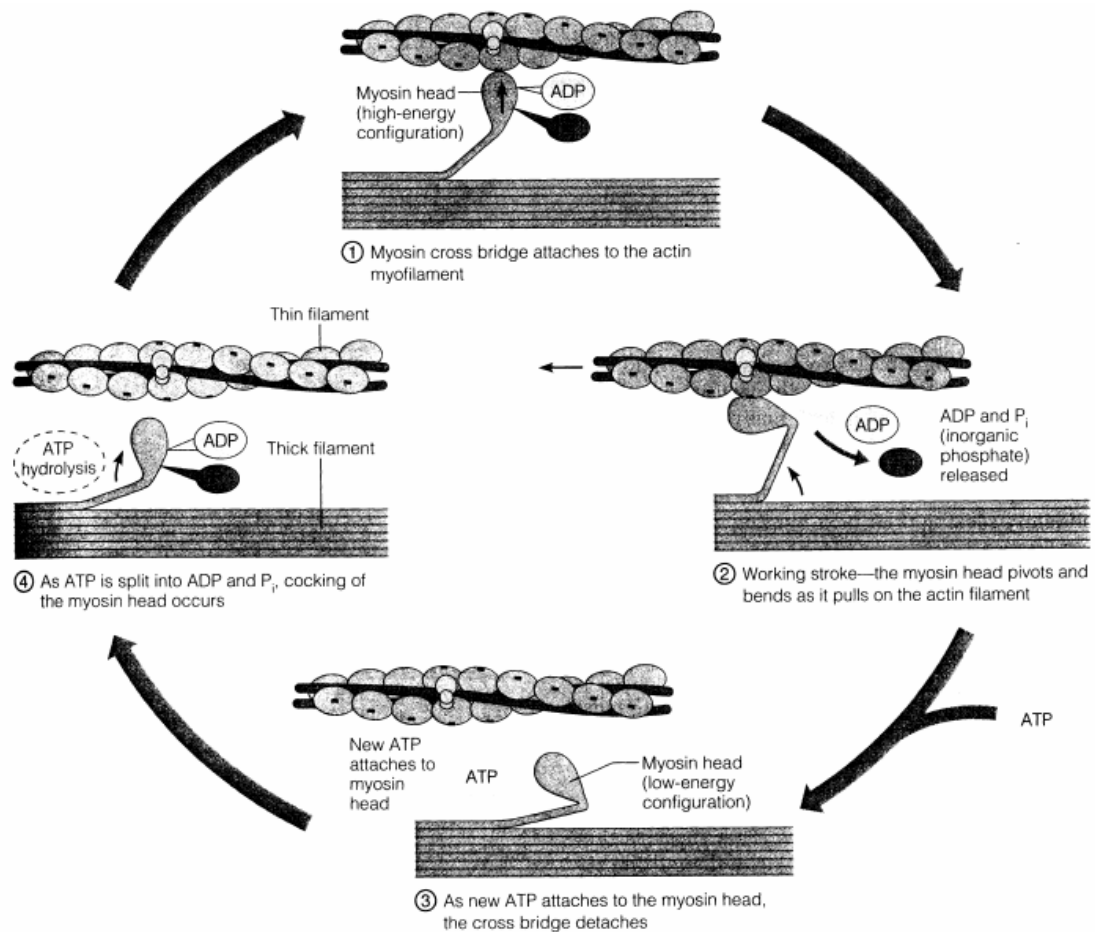


**Figure 2.13** Cross-bridge energy cycle [4].

One phenomenon related with death is *rigor mortis*, where contracted muscle can not be relaxed from its contracted state. The reason for this is that the dead body ceases the manufacture of ATP which is required for cross-bridge detachment and relaxation of the contacted muscle.

The scenarios of the cross-bridge regulation for tetanised skeletal muscle and smooth muscle are different. During skeletal muscle tetanus, the cross-bridges are continually and dynamically attaching, detaching and then re-attaching (see Figure 2.13). This process was proposed using a two-state cross-bridge model by Huxley [20] and Murphy [46] (see Figure 2.14). In Figure 2.14, **A** is actin, **M** is myosin, **A<sub>off</sub>** means that the actin

is blocked to myosin when the calcium ions flow out the muscle cell, and  $A_{on}$  means that the actin is unblocked to myosin when the calcium ions flow into the cell. The loop on the right side in Figure 2.14 represents the cross-bridge cycling during continuous muscle contraction, ATP and ADP + P alternate to control cross-bridge attachment and detachment. Thus, the rate of ATP consumption is maintained at a high level in skeletal muscle contraction. Also, the rate of ATP consumption by cross-bridge cycling is proportional to the power output and can be extremely high in the contracting skeletal muscle.

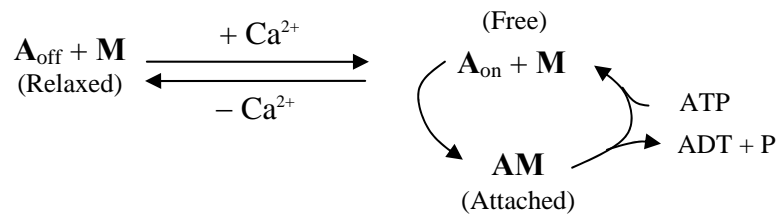


**Figure 2.14** A two-state cross-bridge model for regulation of skeletal muscle.

The cross-bridge regulation for smooth muscle is more complicated than skeletal muscle. With the onset of smooth muscle isometric contraction (tetanus), cross-bridge cycling begins and the number of cross-bridge interactions increases and approaches a plateau, as previously shown in Figure 2.1. During this process, rapidly cycling cross-bridges convert progressively to slow cycling latch bridges. This regulatory process finally approaches to a steady state, and dynamic cross-bridge cycling then can be said to have attained the latch state (or latch bridges). In the meanwhile, the rate of ATP consumption and the phosphorylation falls and is maintained at a low level [47]. Phosphorylation is the addition of the third phosphate group to a molecule. The phosphate bond that forms as a result contains the energy stored in this reaction [7]. In this latch state, the rate of cross-bridge cycling is decreased to its smallest value

attainable and the active force has increased to its maximum attainable value. The low rate of ATP consumption causes almost no energy consumption for the body. For this kind of cross-bridge regulation, Chi and Murphy [32 and 48] proposed a four-state model rather than a two-state model to compare skeletal muscle in 1988. A scheme of a four-state cross-bridge model is shown in Figure 2.15.

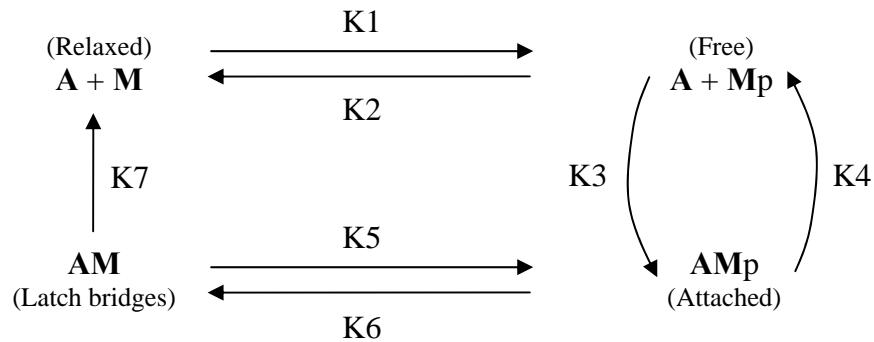


**Figure 2.15** A four-state cross-bridge model for regulation of smooth muscle.

The four states of cross-bridges in the model are: free unphosphorylated ( $M$ ), phosphorylated ( $Mp$ ), attached cross-bridges under phosphorylated ( $AMp$ ), and attached cross-bridges under dephosphorylated (latch bridges,  $AM$ ). The detached cross-bridges probably have bound ATP, whereas the attached cross-bridges may have bound ADP. In the regulation of smooth muscle, most of the cross-bridges occur in the latch state, and a small portion of the cross-bridges dynamically attaches and detaches under the fast cycling phosphorylated cross-bridges (the loop on the right side in Figure 2.15). Additionally, a few cross-bridges are also relaxed. These four states can convert to each other, except that the conversion between free unphosphorylated ( $M$ ) and latch bridges ( $AM$ ) (see Figure 2.15) is not permitted. The latch bridges can be converted to free unphosphorylated bridges, but the free unphosphorylated bridges cannot directly convert to latch bridges. The seven rate constants ( $K$ ) reflect the possibility of these conversions.

K1 and K2 are the rate constants representing the phosphorylation of **M** to **Mp** and **AM** to **AMp** by the active myosin light-chain kinase (MLCK),  $\text{Ca}_4^{2+}$ -calmodulin complex. K2 and K5 are the rate constants for the dephosphorylation of **Mp** to **M** and **AMp** to **AM** by myosin light-chain phosphatase (MLCP) [49-51]. K3 and K4 are the rate constants representing the attachment and detachment of the fast cycling phosphorylated cross-bridges. Hai *et al.* assumed that the ratio of K3/K4 is 4:1 [48]. K7 is the rate constant for latch-bridge detachment. This value is very small when compared to the other rate constants. An assumption for relaxed muscle is that all cross-bridge are in the detached unphosphorylated state (i.e., the initial conditions for a relaxed smooth muscle are  $[\mathbf{M}] = 1.0$ ,  $[\mathbf{Mp}] = [\mathbf{AMp}] = [\mathbf{AM}] = 0$  ( $\text{K1} = \text{K6} = 0$ )).

## 2.4 Existing Models for Muscle Contraction

Limited models are available on smooth muscle mechanics. Also with the limited experimental facilities available for this research; it is very difficult to establish a new postulation. Therefore, it is felt a quick review of available models on other types of muscles will give a good foundation for this research.

Huxley [20] investigated striated muscles and observed that the light band diminishes during contractions (see Figure 1.4 and 1.6). He proposed that this could be explained by allowing the relative sliding between the thick and thin filaments. The thin and thick filaments themselves were found not to shorten. This process also explains the sarcomere force-length relationship shown in Figure 2.3. This proposal is known as the sliding filament theory. A numerical model for the sliding filament theory was developed by Huxley for the striated muscle [20]. This model is based on the sarcomere (unit length) and idealized as elastic springs which form links between the thick and

thin filaments. The following equilibrium equation establishes the relation between the numbers of attached cross-bridges:

$$\frac{\partial n(x,t)}{\partial t} = (1-n)f(x) - n \cdot g(x) \quad \text{or} \quad -v \frac{\partial n}{\partial x} = f - (f+g)n \quad (2.9)$$

where  $n$  is the number of attached cross-bridges,  $f$  is the rate parameter of cross-bridge attaching (bonding),  $g$  the rate parameter of cross-bridge detaching (unbonding), and  $x$  is the displacement that is the distance from the stress-free configuration of the cross-bridge to the nearest actin site. Also  $n$ ,  $f$  and  $g$  are determined by the parameter  $x$ .

The active force generated is proportional to the number of attached cross-bridges ( $n$ ). Huxley used the equation to simulate the variation of partial muscle activations and the unique quasi-hyperbolic relationship between shortening and force. This classical equation was modified by other researchers.

Huxley's model contains the internal variable  $x$  in the equations (see equation (2.9)) which introduces considerable difficulty in numerical computations. Zahalak [52] recognized the importance of eliminating  $x$  from the constitutive equations and proposed that the number of the attached cross-bridges,  $n$ , at any time is to approximately a Gaussian distribution. Tozeren [53] eliminated the internal variable  $x$  in the final equations by the method of integration described in the section entitled 'Mathematical Formulation'.

During isometric force development, growing cross-bridge traction transfers loading locally between both filaments (actin and myosin). This causes them to extend and slide locally relative to each other. Mijailovich *et al.* [54] considered that the effects of

filament extensibility of actin and myosin filaments on actin-myosin interaction which evolve from temporally and spatially distributed strains (filament strain). They suggested that these strains will affect the final results from Huxley's model. After reformulating Huxley's model [20], the result was a better fit to the experimental data for isometric force development.

Later, Huxley and Simmons [55] proposed two states of attachment for a cross-bridge to explain the initial rapid change in muscle length. The time rate of attachment was assumed to be slow as in Huxley's original model, but the transition between attached states was assumed to occur very rapidly. The rapid recovery of force observed in transient tension data is associated with the transients between attached states.

Redaelli *et al.* [56] geometrically developed a three-dimensional model of the sliding mechanism, which was able to identify the architectures that accomplish the continuous sliding for shortening. Almost 200 different configurations have been simulated by changing the cross-bridge binding range in this model. Redaelli *et al.* used the model to calculate the attached cross-bridges (in percentage), sliding velocity and duty ratio for different working stroke distances.

Some researchers plausibly imagined the actin-myosin sliding mechanism as electrostatic mechanisms [57-59]. The principle of force generation from the sliding mechanism is that of a dielectric rod suspended in the electric field between the plates of a capacitor (Figure 2.16). The charge induced on the rod is asymmetrically distributed, and there is always an attractive force tending to draw the rod further into the field of the capacitor. The dielectric rod is assumed to represent an actin filament, and the capacitor field is assumed to represent the cross-bridges. The energy required to

sustain muscle contraction is supplied through the hydrolysis of ATP and has been shown to be of reasonable magnitude. However, this model can only model isometric force development.

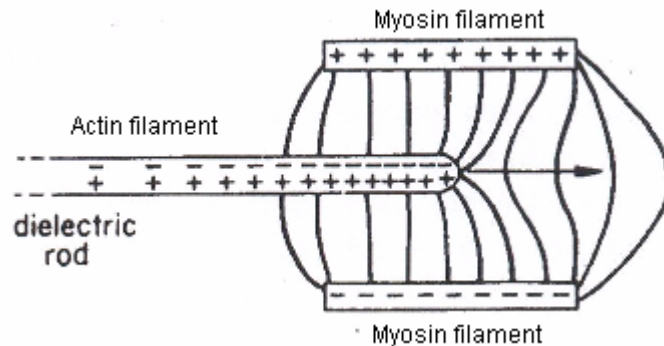


**Figure 2.16** A scheme of an electrostatic mechanism to represent the contractile mechanism of muscle [58].

Shadmehr and Wise [60] developed a simple muscle model by using a viscous shock absorber (damper) element in parallel with the contractile element. They used the model to simulate muscle transient forces by a length stretch, a twitch mode, and an unfused tetanus.

Finally, we introduce a cross-bridge kinetic model known as the “fading memory model”, which was developed by Hunter *et al.* [61]. The benefit of the model is that it is very simple and describes cross-bridge kinetics integrally rather than consider the detail of the structure. It is also not designed for a specific type of muscle making it useful for this work. The model is not intended to accurately model the biophysical events underlying muscle contraction. The model can however be interpreted in terms of certain biophysical processes. The main advantage of the model is that it gives the dynamic force response with muscle length changes. The model was originally used to simulate cardiac muscle by using the experimental data from cardiac muscle. This model will be further discussed and modified to fit airway smooth muscle in this research.

The above models describe striated muscle, especially skeletal muscle. Since the structure of smooth muscle is slightly different from the structure of striated muscle, these models are not directly suited to smooth muscles. However, their postulations and ideas are helpful in creating a new model for smooth muscle.

An important model for smooth muscle is the four-state model of Hai and Murphy [48] which describes four kinetic states by four time differential equations. The model combines the four-state model with Huxley's [20] model and uses the rate constants (K) instead of the internal variable  $x$  [32]. The average distance of dense bodies was used instead of a sarcomere. The model successfully predicts the isotonic force-velocity curves for smooth muscle. Yu *et al.* [62] used the same method as Hai and Murphy [48] to model the nonisometric contraction of smooth muscle. The calculation of the cross-bridge length distribution was simplified by assuming a Gaussian distribution as first done by Zahalak [52] for skeletal muscle. The model is used to simulate transient changes in muscle length. Further, Mijailovich *et al.* [63] used a four-state model integrated with Huxley's [20] model to simulate a length perturbation under isometric contraction.

Hai and Kim [64] improved the four-state model by adding an ultra slow latch-bridge cycle. The new model was called the thin-filament-regulated latch-bridge model, which provided better fits to the experimental data than the four-state model [48]. But the new model provides more challenges for numerical computation.

Some researchers have used other approaches to model smooth muscle contraction. Blanc and Lecarpentier [9 and 35] directly modified Huxley's model to airway smooth muscles to compare experimental data from rabbits, rats and humans.

Anafi and Wilson [65] proposed an empirical model for the dynamic force-length behavior of airway smooth muscle. The model predicted the experimental data for force-length loops of airway smooth muscle under length oscillation. Similar work has been done by Bates and Lauzon [66], who improved Hill's equation (equation (2.1)) by adding another nonlinear elastic term to account for tissue rheology. This is believed to play a significant role in the dynamics of the mechanical behaviours. This model represented the experimental data for force-length loops of airway smooth muscle under length oscillation.

The principle of electrostatic mechanisms have also been used for smooth muscles. Lambert *et al.* [34] used Hill's three element model for smooth muscles. The contractile element was described as a side-polar structure, where the cross-bridges are arranged on both sides of a myosin filament to form two side-polar structures that interact with actin filaments, the polarities of both sides being opposite. The force generated in the muscle is proportional to the number of myosin filaments and the length of the overlap between actin and myosin filaments. This reference assumes that, under steady-state conditions, the geometric arrangement of the contractile units and filaments within these units determines the kinematic characteristics of smooth muscles. The model predicts the force-length relationship of the muscle under isometric contraction.

At a cellular level, researchers recently hypothesized that the airway smooth muscle cell behaves as a glassy material [67 and 68]. A glass is a material that has the disordered molecular state of a liquid and, at times, the rigidity of a solid. The factor that affects the molecular state of glassy material is the thermodynamic temperature. But instead of changing the thermodynamic temperature, the cell is proposed to modulate an effective temperature known as the "noise" temperature. The hypothesis is based on three

assumptions: 1) soft glassy materials are soft, 2) soft glassy materials are “scale-free”, meaning that when the matrix stiffness is measured over a wide range of frequencies, no resonant frequency stands out. In other words, the stiffness follows a weak power law, and 3) the dominant frictional stress in soft glassy materials is not of viscous origin or attributable to a viscous-like stress (proportional to the elastic stress). To confirm this hypothesis, Laudadio *et al.* [68] cultured rat airway smooth muscle cells, and then measured the elastic and frictional moduli. They found that the stiffness increased with frequency as a weak power law, and changes of friction paralleled those of stiffness until they approached a Newtonian viscous limit. These findings indicate that airway smooth muscle cells could act as a glassy material. However, this hypothesis has yet to be fully proved and researchers have not established any mathematical models for this hypothesis.

## **2.5 Available Literature on Muscle Vibrations**

Many experiments have been performed on smooth muscles. These experiments investigated smooth muscles from different perspectives: biomechanical, biochemical or biomedical. But, only experimental data of interest will be given in this section, i.e. experiments that are based on biomechanical principles.

Ljung and Sivertsson [24, 25 and 29] applied oscillation tests on smooth muscle tissues (veins from rats and thoracic aorta from rabbits) in the longitudinal direction to find the inhibition of the active force. Unfortunately, their apparatus was crude, which resulted in resonance within the setup. For this reason, their results were not completely accurate as they were unable to filter the effects of resonance. Also, only the dynamic force responses during the oscillations were investigated.

Sjoqvist and Ljung [30] oscillated vein smooth muscle from rats in the longitudinal direction at 40 Hz and the amplitude of oscillations was from 2.5% to 3.0% of the tissue length. The results showed the prompt and reversible reduction of the active force but that neither the pattern of the phasic contractions nor the electrical cell membrane discharge was altered. The degree of reduction also increased with increasing vibration amplitude.

Fredberg *et al.* [23 and 69] conducted experiments on bovine trachea airway smooth muscle tissues at a breathing frequency of 0.33 Hz. The amplitude of imposed tidal stretch was from 0.25% to 8% of the tissue length. Shen *et al.* [28] also conducted similar tests on airway smooth muscles from Mongrel dogs. Both groups investigated the response of muscle tissues resulting from the dynamic force and hysteresivity. All the results indicated both a degree of reduction of dynamic force and a hysteresivity increase with increasing amplitude.

Dhanaraj *et al.* [22] applied longitudinal vibrations on canine tracheal smooth muscle tissues following isotonic shortening. The response of an activated smooth muscle tissue to force length oscillations at 33 Hz for 1 second was obtained. The result showed that the decreasing force response to successive length cycles may be fitted by an exponential curve. The same result has been obtained by Meiss and Pidaparti [27].

Gunst and Russell [70] conducted experiments that applied a continuous stretch on canine tracheal smooth muscle tissues. The results showed that total force increased during the stretch, but that the active force decreased. They concluded that the contractile element length established during isometric contraction would affect the muscle force obtained during subsequent stretching of the muscle.

A micro-experiment was applied by Shue and Brozovich [71]. They conducted length perturbations on a smooth muscle cell. A length perturbation sequence that combines multiple sine waves with increasing frequency was developed. The results suggested that a fixed distribution of cross-bridge state was reached after 40 seconds of  $\text{Ca}^{2+}$  activation and that the cross-bridge cycling rate did not change during the period of force maintenance.

Rembold and Murphy [72] investigated  $\text{Ca}^{2+}$  concentration  $\text{Ca}^{2+}$ -dependent cross-bridge phosphorylation by myosin light-chain kinase (MLCK). This is postulated to be the primary regulator of force development in smooth muscle. They found that the changes in aequorin-estimated myoplasmic  $\text{Ca}^{2+}$  can reasonably predict the time course of phosphorylation and isometric force in agonist-stimulated pig carotid smooth muscle, if  $\text{Ca}^{2+}$  is not changing rapidly. The results suggested that  $\text{Ca}^{2+}$ -dependent cross-bridge phosphorylation is the primary determinant of cross-bridge function. These results also support the latch-bridge hypothesis as an explanation for the economy of force maintenance in smooth muscle.

Ohhashi *et al.* [73] investigated microvibrations (1 – 80 Hz and amplitudes less than 2% of the tissue length) imposed upon isolated quiescent ureter and portal venous smooth muscle tissues from dogs. The results from their research showed that the microvibrations increased the rate of spontaneous contractions after a latency of about 1 minute. They also found that the stimulating action of microvibration increased the calcium ions ( $\text{Ca}^{2+}$ ) influx through the membranes of smooth muscles.

Some researches have reported that chest-wall vibration can modify the drive to breathe and the sensation of dyspnoea, or treat an asthmatic attack [74 and 75]. Chest-wall

vibrations can also be used to produce oscillations of the lung tissue. As the lung is vibrated, it is conceivable that vibration stimulates intrapulmonary receptors and such afferent activity may contribute to the effects of vibration upon respiratory control and sensation [74]. The chest-wall vibration can restore the natural chest mobility as the main breathing mechanism in the respiratory function of the lung. The detail of the whole process for chest-wall vibration treatment is not clear. The prevalent hypothesis is based on the physiological mechanisms behind the effects of vibration on respiratory sensation and ventilatory control centered on the afferent activity from the chest-wall [76].

However, an *in vivo* study to investigate the effects of whole-body vibration on the mechanical behaviour of human muscle was done by Bosco's research group [77]. The results showed remarkable and statistical enhancement in average velocity, average force and average power in the leg skeletal muscle. Other *in vivo* experiments [78] investigated the effect of vibration on muscular contraction. The results showed that there was a significant improvement in muscular strength and activation for concentric isotonic contraction performed during an applied vibration.

None of the above references however have successfully studied the effect of various oscillation parameters on the length and force response of airway smooth muscle in high frequencies range. In this research, a thorough and comprehensive experimental program is developed and designed to investigate the effects of oscillation duration time, amplitude and frequency on two types of experimental parameters proposed in this work, namely the static and dynamic stiffness.

## Chapter 3

### Experimental Investigation

#### 3.1 Introduction

Since there is only a limited theoretical understanding of airway smooth muscles, experimental investigations are the most common method for studying their biological behaviour. Normally, the property behaviours of various tissues are derived from experimentation. This lays the foundation for many of the available mathematical models, which are normally developed to extend our knowledge of tissue behaviour and properties.

In this investigation, it is anticipated that experimentation will give insight into the contracted smooth muscle response under external excitations. The experimental results will also be used to validate the numerical model being developed in this work. Ideally *in vivo* tests would be used to give the exact response to excitation, but there are risks and ethical requirements involved in conducting such experiments. Thus, *in vitro* experimentation is used in this research. Samples of animal tissues are used as they are deemed to be sufficient for this stage of the investigation.

A sample of prior *in vitro* experiments conducted by other researchers [22-25, 27-30, 69 and 70] was given in Chapter 2. These experiments investigated smooth muscle responses under muscle length changes and all indicated that the smooth muscle contractile mechanism was a function of muscle length. They also showed that oscillating length changes can reduce the active muscle force. However, all of the previous experiments did not systematically describe the relationship between the muscle responses and the characteristics of oscillations (such as the frequencies, amplitudes and time durations). This work focuses on these variables and on the relationships between them and the muscle response.

The purpose of this study is to systematically determine the response of contracted airway smooth muscles under different external excitations. To achieve this, excitations were applied to active airway smooth muscles and the contracted forces were recorded. It is anticipated that the results will reflect changes in the muscle stiffness in response to excitation.

Two testing scenarios are adopted in this work. Firstly, to understand the axial response of smooth muscle, longitudinal excitation was implemented. However, direct axial *in vivo* excitation does not occur naturally (since the orientation of airway smooth muscle is along the circumference of airways) and so transverse excitation by pressure waves is a more realistic excitation. Therefore, the second scenario determines the active muscle response to excitation perpendicular (transverse) to the tissue axis.

Mechanical vibration was attempted to determine the vibration response in both directions. In all cases, static and dynamic forces were recorded, representing the dynamic and static stiffnesses for the muscle tissue during and after vibrations.

In real airways, the force generated statically by airway smooth muscle is taken to be in mechanical equilibrium with the passive reaction force developed by the elastic load against which the muscle has shortened. Since both forces depend upon muscle length, the airway is presumed to adjust itself to the muscle length at which these opposing forces are in a static equilibrium balance [23]. It is reasonable to regard this static force-length characteristic of the activated muscle as an isometric contraction (see Figure 2.2). Thus, an isometric contraction mode was used in this work for all muscle tests.

The experimental preparations for each experiment will be given individually in the following sections of this chapter. The stiffness calculations of the muscle for these experiments will be introduced at the end of the chapter.

## **3.2 Experiment Preparations**

The experimental investigation in this research focuses on active smooth muscle cells. To keep the tissues alive after removal from an animal, they are kept in a special solution (Kreb's solution) normally used for such investigations. The tissues used in this work are from pigs.

During the experimentation, all the generated and recorded signals were processed by computer data-acquisition software using NI-DAQ7/LabVIEW6. The results observed during the experiments are presented and discussed in Chapter 5 and 6, respectively.

### 3.2.1 Solution Preparation

A physiological solution is necessary for two reasons:

1. To form an artificial environment that supports the prolonged life of the smooth muscle tissue after dissection.
2. Act as a medium for the delivery of chemicals or electricity that activates the smooth muscle cells.

A commonly used saline solution is Krebs's solution [25, 27, 28, 70, 79-82], which was used for both the tissue bath and to preserve the pig lungs. It is prepared by mixing the following chemicals (in mM): 125.48 (NaCl), 4.99 (KCl), 1.82 (CaCl<sub>2</sub>·2H<sub>2</sub>O), 15.08 (NaHCO<sub>3</sub>), 1.05 (MgCl<sub>2</sub>·6H<sub>2</sub>O), 0.98 (NaH<sub>2</sub>PO<sub>4</sub>), and 11.10 (glucose).

Each experiment required at least 15 L of the solution, which was prepared one day before the experiment to ensure that the solution reached the correct temperature (4 °C) [6 and 82]. Two containers were filled with 11.175 litres and 2.775 litres of distilled water. Another three containers were filled with solution 1, solution 2 and glucose solution as shown in Table 3.1.

Krebs's solution was prepared immediately before the experiment by pouring 11.175 L of distilled water in to a 20 L container. Then, 600 ml of solution 1, 300ml of solution 2, and 150 ml of glucose solution were added. After mixing, the rest of the 2.775 L of distilled water was used to wash these three containers (solution 1, solution 2 and glucose solution) and to make up 15 litres of the solution.

**Table 3.1**      **Ingredients used in the preparation of *Kreb's* solution**

<b>Solution 1</b>	
NaCl	110.0 g
KCl	5.65 g
CaCl <sub>2</sub> ·2H <sub>2</sub> O	4.02 g
MgCl <sub>2</sub> ·6H <sub>2</sub> O	3.20 g
Fill distilled water up to	600 ml
<b>Solution 2</b>	
NaHCO <sub>3</sub>	19.0 g
NaH <sub>2</sub> PO <sub>4</sub>	2.30 g
Fill distilled water up to	300 ml
<b>Glucose solution</b>	
Glucose	30.0 g
Fill distilled water up to	150 ml

### **3.2.2 Airway Smooth Muscle Tissue Preparation**

Pig tracheas were obtained from a local abattoir. Whole pig lungs were removed from adult pigs (with an approximate weight of 60 – 70 kg) immediately after they were butchered. The pig lungs were then completely immersed in the chilled *Kreb's* solution.

A 20 – 25 mm long segment of trachea was dissected from the lung (see Figure 3.1) in the laboratory. The cartilaginous rings were cut along the longitudinal direction of the trachea, and the trachea was pinned in a dissecting wax dish. Figure 3.2 shows the pinned trachea, with the inner side of trachea facing upwards. The tip of the pin indicates the gap between two ends of cartilaginous rings where the airway smooth muscle exists. Under a magnifying glass, the smooth muscle area was cleaned of epithelial and adventitial tissue layers (Figure 3.3). Small strips of smooth muscle tissue (approx. 2.5 mm wide and 18 mm long) were gently cut from the muscle sheet. Special

care was taken to follow the natural division of the tissue in discrete fiber bundles [27 and 44] (Figure 3.4). Two very small pieces of cartilaginous rings were left at the two ends of the tissue strip to protect the tissue sample from damage during the experiment when it was mounted on hooks. The tissue was submerged in a bath of Kerb's solution held at 37 °C. The bath was constantly aerated with a 95% O<sub>2</sub> and 5% CO<sub>2</sub> mixture to maintain the pH at 7.4 to 7.6 [28, 35, 70, 79, 82 and 83]. The tissue was also allowed to accommodate for 45 min – 1 hour [24, 25 and 70] before the experiment was begun.



**Figure 3.1** A segment of pig trachea, approximately 20 ~ 25 mm in length.

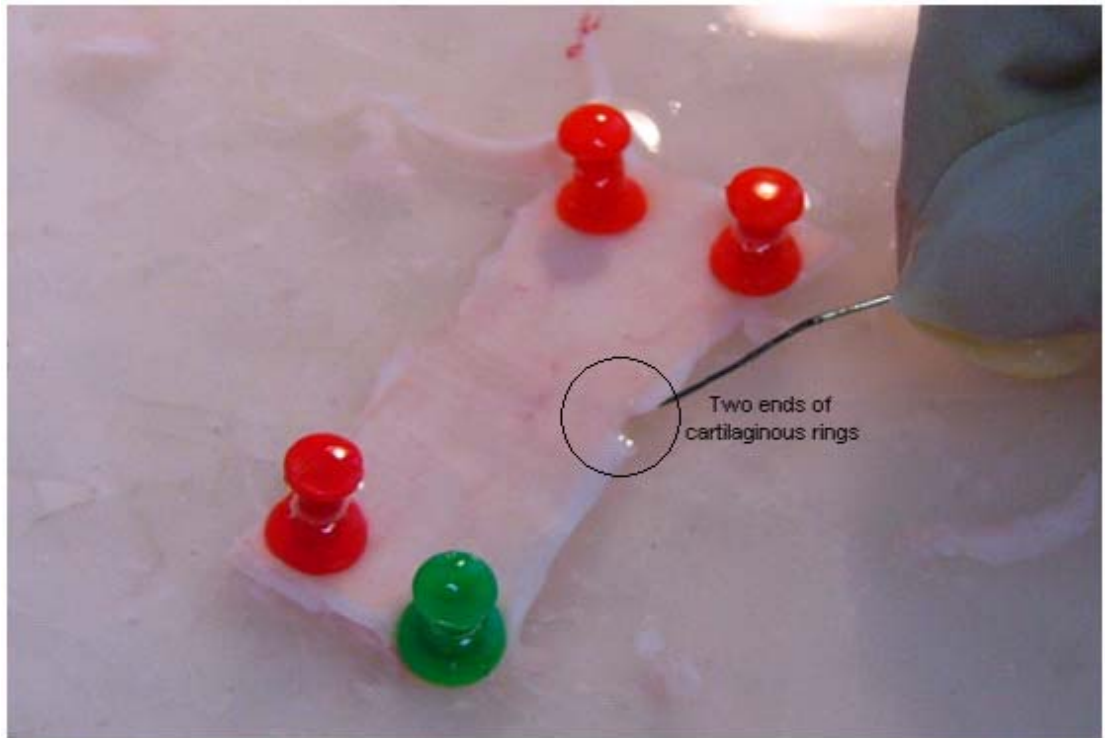


**Figure 3.2** Pig trachea cut open and pinned in dissecting wax dish.

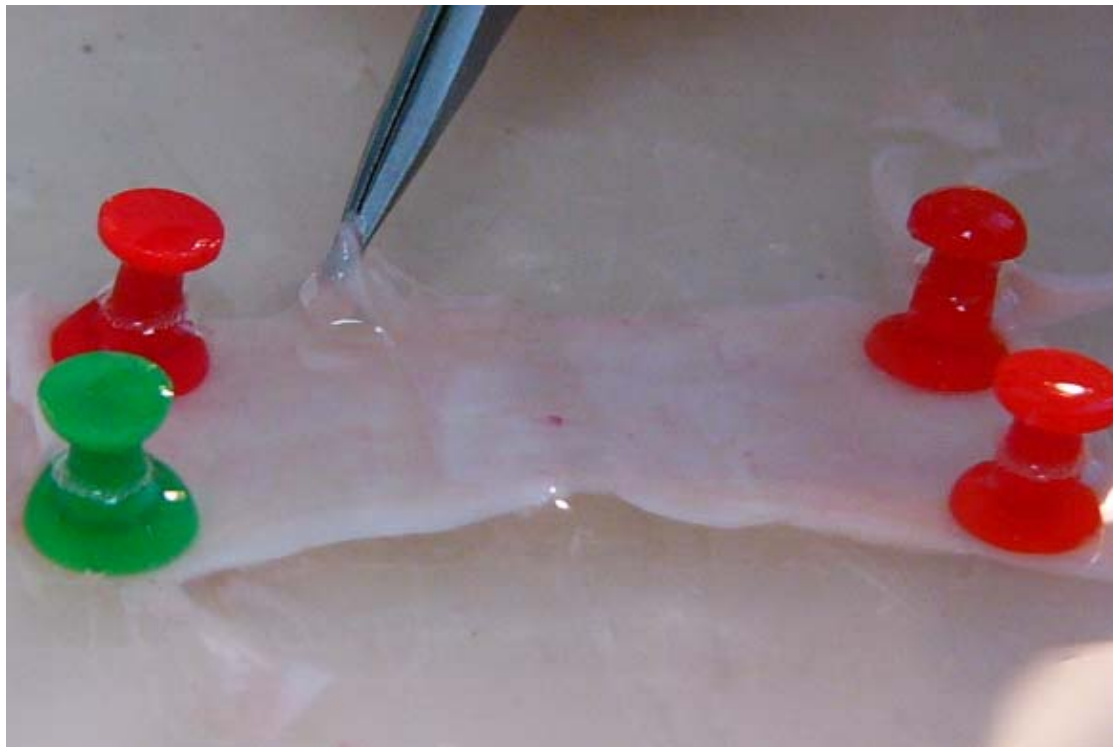


**Figure 3.3** Epithelial and adventitial tissue were peeled off from the smooth muscle of the pig trachea.

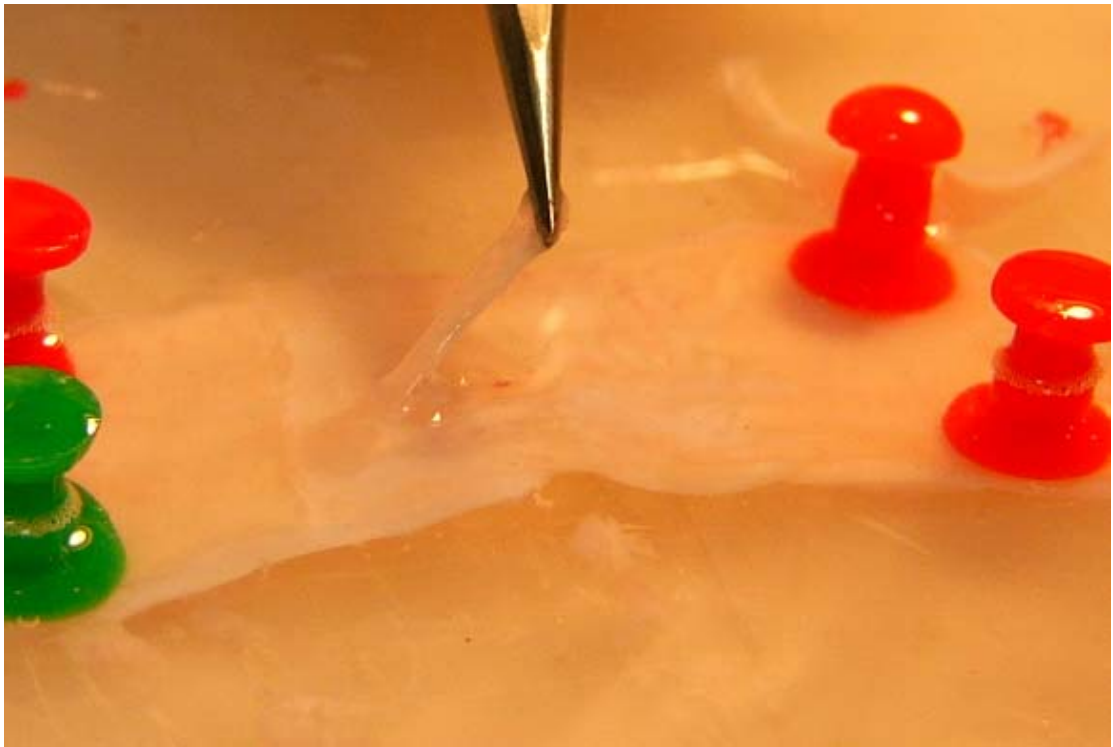


**Figure 3.4** A smooth muscle strip was dissected from the pig trachea.

Before the start of each experiment, the length of the smooth muscle tissue was adjusted to a reference length ( $L_r$ ), to ensure that the passive force in the muscle tissue was minimal. For reference length adjustment, the tissue was stretched slightly and placed on the hooks. The length of the tissue was adjusted (shortened) until minimal force was recorded. This reference length was considered to reflect the optimal length (where  $L/L_0 = 1$ ) correlating to maximal force generation. The smallest passive force was called the initial force ( $F_{ini}$ ).

### **3.2.3 Muscle Tissue Contraction**

Three different stimulations can be used to contract muscle tissues when conducting *in vitro* experiments: electrical stimulation; chemical stimulation; or a combination of both electrical and chemical stimulations [21-23, 26, 27, 44 and 81].

The process of muscle contraction was introduced in the previous chapter, and the scheme of the contraction is as shown in Figure 2.12. Electrical stimulation is normally induced by applying an electrical excitation to the muscle directly. This process generates an action potential that propagates along the cell membrane to raise the potential of the membrane. This causes changes in the membrane potential which opens voltage dependent gates and allows calcium ions ( $\text{Ca}^{2+}$ ) to enter the muscle cell to contract the muscle (as discussed in Chapter 2).

Chemical stimulation is induced due to the fact that chemical stimulus acts at the axon terminal of a motor neuron and releases acetylcholine (ACh) (see Figure 2.12). The latter diffuses across the synaptic cleft and attaches to ACh receptors on the sarcolemma. This creates an action potential and again allows calcium ions to enter the muscle cell to contract the muscle. It is important to note that irrespective of the mechanism that generates the contraction, the final contraction of the muscle is identical.

In the present experiments, airway smooth muscle tissues were contracted chemically by adding acetylcholine chloride (ACh) [23, 28 and 81]. At a pharmacological level, the concentration of ACh used is from  $10^{-5}$  to  $10^{-2}$  M [28, 70, 79, 81, 84-86]. For this reason, a concentration of  $10^{-3}$  M of ACh was used for all experiments.

Due to chemical stimulation, an isometric force was developed and typically follows the behaviour shown in Figure 3.5. After the contracted force reaches a plateau (completely contracted), it is called the original contracted force ( $F_0$ ). External oscillations are then applied as detailed in the following section.

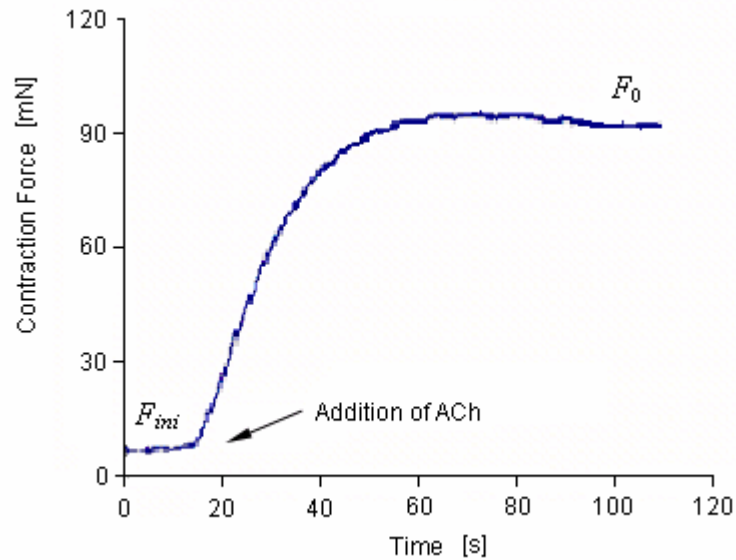


**Figure 3.5** Typical force development of an airway smooth muscle tissue during isometric contraction.  $10^{-3}$  M contraction agent (ACh) was added after approximately 15 seconds. Conditions:  $T = 37\text{ }^{\circ}\text{C}$  and  $\text{pH} = 7.6$ .

### 3.2.4 Replacement of Airway Smooth Muscle Tissue

During experimentation, the airway smooth muscle tissues were constantly monitored for degradation. The condition used to determine whether the reuse of the muscle tissue was possible was whether the force (without any excitation) was within 10% of  $F_0$  ( $F_0 \pm 10\%$ ). Between any two consecutive excitations, the muscle tissue was allowed to recover. If the muscle recovery force was lower than 90% of  $F_0$ , the tissue was considered degraded and was replaced by a new piece of tissue [36].

### 3.2.5 Stiffness and Resonance of Setup

To check the rigidity of the experimental setup, direct measurement of total system stiffness of the setups (including that of the force transducer, hooks and all other mechanical components), gave a value of more than  $1.74 \times 10^3$  mN/mm. This is much larger than the stiffness of the muscle tissues, and so the stiffness of the setup can be

neglected during experimentation. The lowest resonant frequency of the system was predicted to be 132 Hz, which was above the frequency of oscillations being studied during the experiments, and therefore experimental resonances were not observed during the experiment

### **3.3 Longitudinal Vibration**

For this type of experiment, contracted smooth muscle tissues were oscillated in the longitudinal direction. Oscillations were applied at different frequencies, amplitudes and time durations with data relating to the forces and amplitudes being acquired and processed by a computer.

#### **3.3.1 Setup**

The response of the smooth muscle to longitudinal vibrations was investigated using the experimental setup shown in Figure 3.6 and Figure 3.7. A strip of smooth muscle was mounted on two hooks. One was fixed to a force transducer (WPI, FORT100), while the other was connected to a speaker (Soundwel, HX1688) which was used to generate length oscillations for the airway smooth muscle tissue. The length adjuster was on the force transducer side for adjustment of tissue reference length. The force transducer was connected to a signal conditioner (WPI, TBM4M). This was recalibrated to the zero reading for the transducer before experimentation, and also pre-amplified the transducer output signals. The frequency and the amplitude of the oscillations were controlled by a computer through a power amplifier (LDS, PA25E).

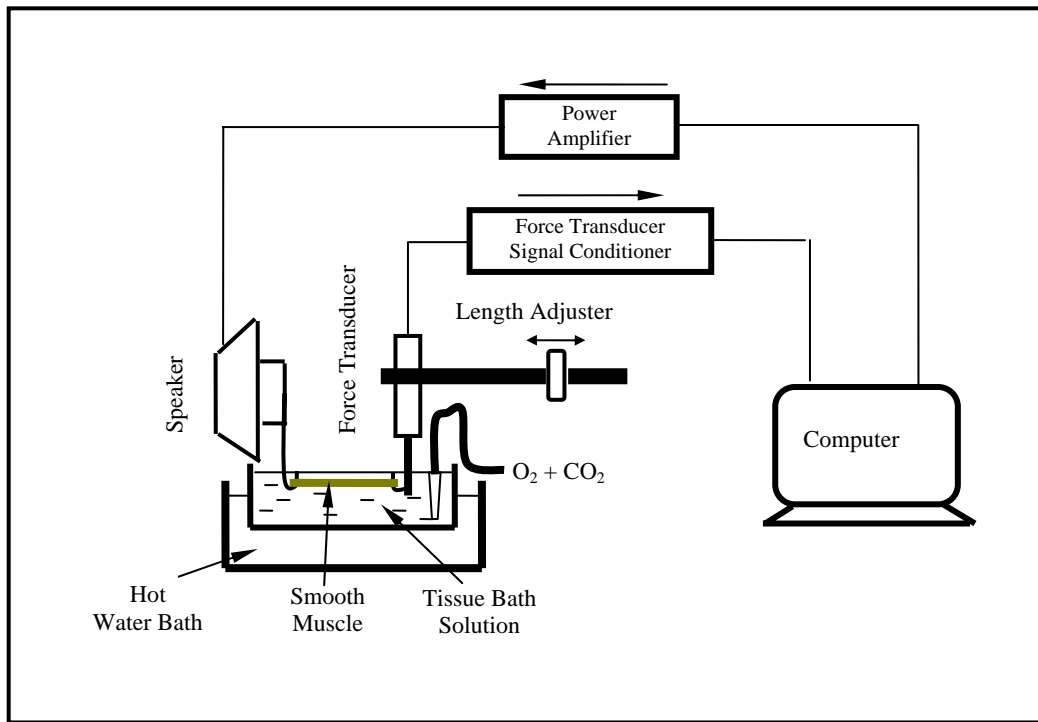


**Figure 3.6** A block diagram of the experimental setup for longitudinal vibration.

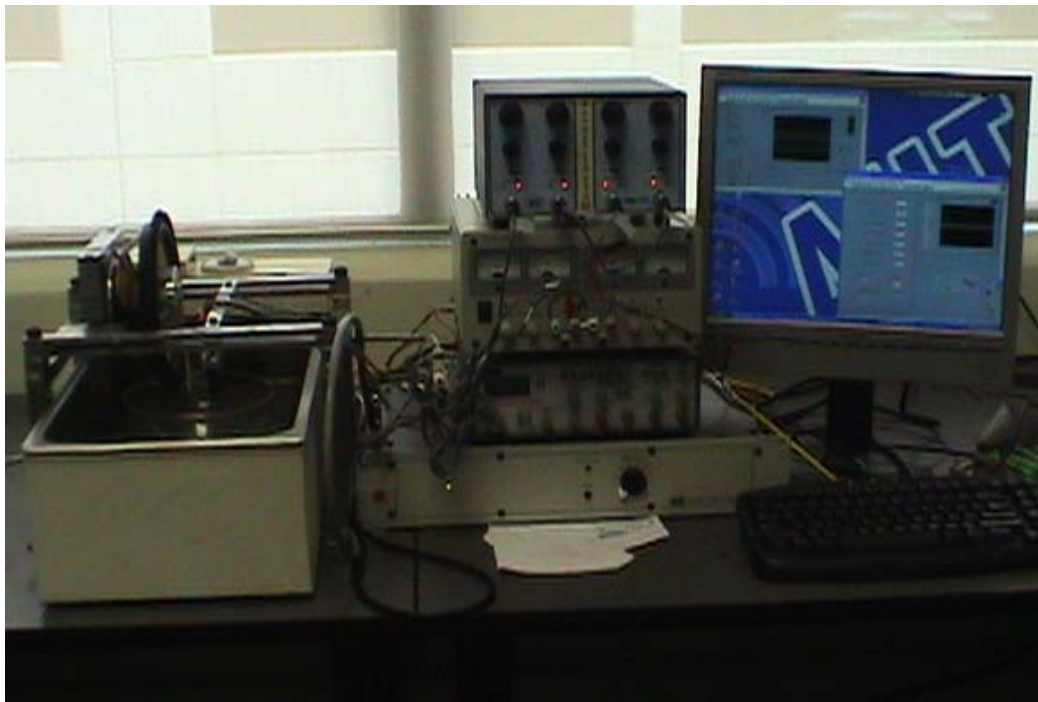


**Figure 3.7** A photo of the experimental setup for longitudinal vibration of airway smooth muscle.

### 3.3.2 Protocols

Each set of experiments was started by stabilizing the original contracted force  $F_0$  (Figure 3.5). In order to obtain an initial value for the original tissue stiffness, the original force exerted by the contracted smooth muscle was measured before the main experiment and then a very small oscillation was applied to the tissue (with an amplitude of  $< 1\%$  of  $L_r$ , frequency 5 Hz and time duration of 1 second). This oscillation was kept small enough so that it had no observable effect on the contractile events. From the data captured during this measurement, the stiffness was calculated as the ratio of force change to the length change ( $K = \Delta F/\Delta l$ ). This value is considered to be the original stiffness correlating with the original force  $F_0$  of the contracted smooth muscle. These initial values are also used in the numerical model as an initial parameter.

The main purpose of the experiments was to determine the variation of the active smooth muscle stiffness in response to oscillations of different frequencies and amplitudes. This investigation was conducted in two parts. First, for a constant time duration of oscillation, the frequencies and amplitudes of the longitudinal oscillation were changed. The frequencies were changed from 5 to 75 Hz in steps of 10 Hz, and the amplitudes were 1.2%, 2.5%, 3.8%, 4.5%, and 6.0% of  $L_r$  respectively. The time duration of the oscillations was restricted to 1 second in this part of the investigation.

The second part of the investigation was to inspect the response of the active smooth muscle stiffness over different time durations with oscillations. The muscle tissues were oscillated at frequencies of 5 Hz, 35 Hz and 65 Hz, for a time duration of 1, 2, 3 and 5 seconds respectively. The amplitude of these oscillations was maintained at 3.8% of  $L_r$ .

## **3.4 Transverse Vibration**

The experimental setup for the transverse vibration is similar to that used for longitudinal vibration. However, in this part of the experimentation, oscillations were applied in the transverse direction at different frequencies and amplitudes with the time duration limited to 1 – 2 seconds (the optimal time bases on the analysis of previous experiments).

### **3.4.1 Setup**

The equipment setup used for this part of the experimentation is shown in Figure 3.8. A strip of smooth muscle was mounted on two hooks, with one fixed to a force transducer (WPI, FORT100), while the other was fixed to the setup. A length adjuster was placed on the force transducer side for the tissue reference length adjustment. The force transducer was connected to a signal conditioner (WPI, TBM4M) that was recalibrated to the zero reading of the force transducer, and also pre-amplified the transducer output signals. The centre of the tissue sample was held in position by a small transverse oscillator — a high-speed length controller (ASI, 322C). The length controller consisted of a high performance moving magnet rotary motor and a control panel. This transverse oscillator was connected to a sweep/function generator (TTI, TG230 2MHz) through a power amplifier (LDS, PA25E).

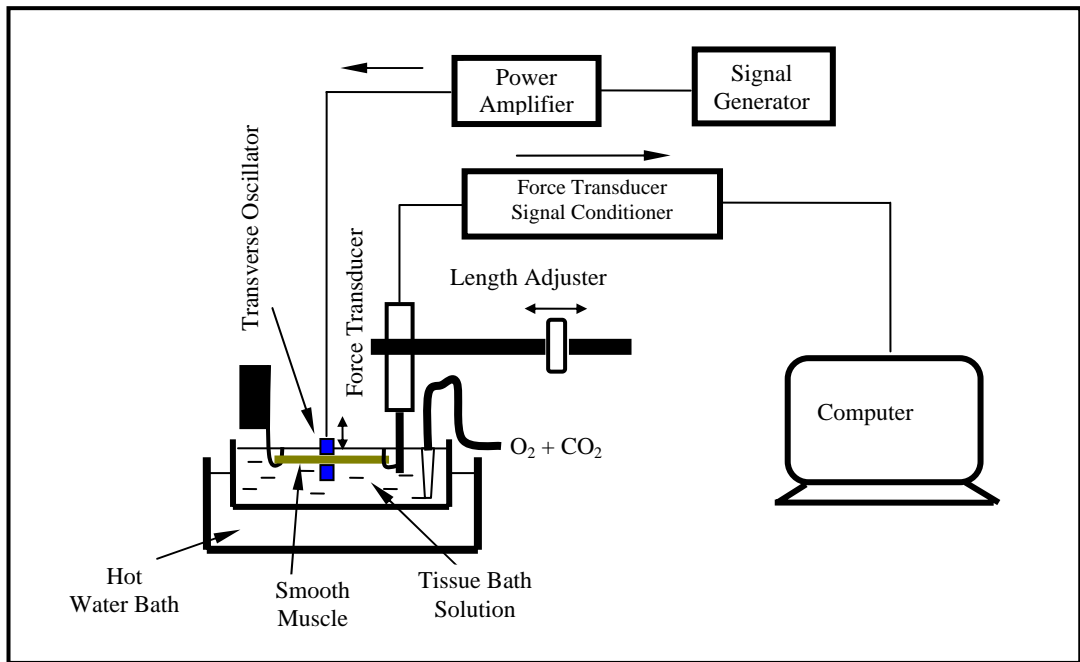


**Figure 3.8** A block diagram of the experimental setup for transverse mechanical vibration.

### 3.4.2 Protocols

Each set of experimentation was initialized by stabilizing the original contracted force  $F_0$  (Figure 3.5). As before, the main purpose of the experiments was to determine the variation of the active smooth muscle stiffness by varying the frequencies and amplitudes of the oscillations. The extent of the tissue fluctuation is the same as the amplitude of oscillation and this extent can finally be converted to a length change ratio of the tissue (percent of  $L_r$ ) as shown in Figure 3.9. The displacement OC is the same as the amplitude of oscillation. If the amplitude OC is much smaller than the initial length, AB (considered as the reference length,  $L_r$ ), the arc AC can be approximated as a straight line, AC. Thus, the relationship between the amplitude and length change ratio is calculated using the geometrical relation:

$$\Delta l = \frac{2\sqrt{A_a^2 + (0.5L_r)^2} - L_r}{L_r} \times 100\% \quad (3.1)$$

where  $\Delta l$  is the percent length change ratio,  $A_a$  is the amplitude of oscillation and  $L_r$  is the reference length.

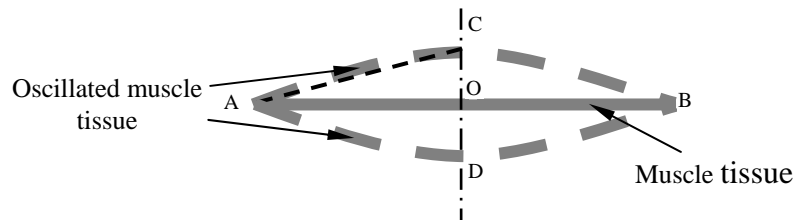


**Figure 3.9** Tissue is vibrated in transverse direction.

The frequencies were changed from 5 to 55 Hz at steps of 10 Hz, with length change ratios of 2.2%, 3.5% and 4.8% of  $L_r$  respectively. The time duration of the oscillations was maintained at levels between 1 – 2 seconds for this investigation.

### 3.5 Stiffness Normalization

To obtain a quantitative and normalized measurement of the effects of vibration, the ratio of stiffness changes was calculated during the experiments. In this work, both dynamic and static stiffnesses were normalized.

If muscle tissue is excited with an oscillation, both the length and force changes are functions of time. The dynamic stiffness of this tissue is then defined as:

$$S = \frac{dF(t)}{dl(t)} \quad (3.2)$$

where  $F(t)$  is the tissue force and  $l(t)$  is the tissue length. Since both force and length are waveforms, the dynamic stiffness can be defined as the ratio of the change in peak force to the change in peak length [22 and 28]:

$$S = \frac{\Delta F}{\Delta l} \quad (3.3)$$

During vibrations, the amplitude of length is constant, and so the stiffness varies with the variation of force.

In this research, the dynamic stiffness was normalized by dividing the stiffness at the end of vibration ( $S_e$ ) by the stiffness at the beginning of the vibration ( $S_b$ ):

$$K_d = \frac{S_e}{S_b} = \frac{\Delta F_e}{\Delta F_b} \quad (3.4)$$

where  $\Delta F_e$  and  $\Delta F_b$  are the peak force excursion at the end and beginning of the vibration, respectively, and  $K_d$  is the dynamic stiffness. This stiffness describes the muscle tissue stiffness changes during the episode of the vibration. This value has to reflect the dynamic behavior of the muscle including active contraction, viscoelasticity and inertia of the tissue mass.

The static stiffness was normalized as follows: a muscle tissue is at a certain length ( $l$ ) with a certain force ( $F_1$ ), and has a stiffness in this state of  $S_1$ . After a vibrational excitation, the force changes to  $F_2$ , but the length of the tissue is kept constant. For this new state, the correlated stiffness is  $S_2$  (Figure 3.10).

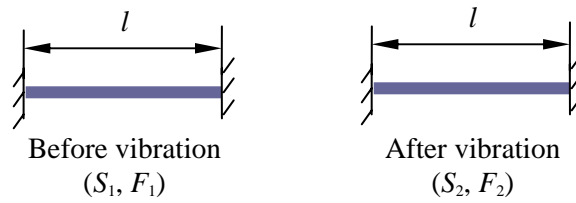


**Figure 3.10** Two different stiffness and forces before and after vibration.

The relationship of the stiffness and forces is then given by:

$$K_s = \frac{S_2}{S_1} = \frac{F_2}{F_1} \quad (3.4)$$

where  $K_s$  is static stiffness [27]. For calculating the active stiffness only, all the forces ( $F_1$  and  $F_2$ ) are subtracted by the small passive initial force ( $F_{ini}$ ), and equation (3.4) becomes:

$$K_s = \frac{S_2}{S_1} = \frac{F_2 - F_{ini}}{F_1 - F_{ini}} \quad (3.5)$$

This passive initial force ( $F_{ini}$ ) can be neglected, if it is small compared to  $F_1$  and  $F_2$ . In this case, the static stiffness change can be approximated by equation (3.4).

The static stiffness does not deal with changes in the episode of vibration and only represents the effect of the episode, since the inertia of the tissue is only considered during vibration and the viscoelasticity of the tissue is unchanged before and after the vibration [88]. Therefore, the  $K_s$  is able to realistically reflect the muscle active stiffness change from vibration.

## Chapter 4

### Numerical Models

#### 4.1 Introduction

The mechanical behaviour of contracted smooth muscle is more complicated than other airway tissues due to the fact that both active and passive forces are involved. Furthermore, the regulation of cross-bridges in smooth muscle has four states, which is more complicated than the two-state model for skeletal muscle. This complexity will be reflected in the following mathematical model. Existing mathematical models for muscle contraction have already been surveyed in Chapter 2. The backbone of these models is the sliding filament theory and Huxley's model [20].

In brief, Huxley established a balance for cross-bridge regulation, where the time rate of activated cross-bridges is equal to the rate of forward attachment subtracted by the rate of forward detachment, see equation (2.9). All of the rates are described by the relative position of actin-myosin from static force-length or quasi-static force-velocity relationships [20, 52-54]. For smooth muscle, the balance for cross-bridge regulation is still important, but this balance is contributed by the four states of cross-bridge process, and the force-length and force-velocity relationships still need to determine the rates of state [32, 48, 62-64]. In summary, these numerical models can accurately predict the

muscle force development, and the shortcoming of these models is the difficulty in numerical computations and the reliance on static or quasi-static simulations.

The fading memory model [61] is a model which does not consider the structure of muscle and describes cross-bridge kinetics integrally. It looks for the time response of the dynamic events and can not quantitatively simulate the biophysical events underlying muscle contraction, but can qualitatively interpret certain biophysical processes. The main advantage of this model is that it gives dynamic force responses with muscle length changes. Although this theory was developed for cardiac muscle [61], in this research the fading memory model will be modified to address the behaviour of airway smooth muscles.

The fading memory model describes the cross-bridge kinetics for the muscle contractile mechanism only. However, for an entire muscle tissue under external excitations, the muscle response is not only determined by the contractile mechanism, but also by the tissue rheology (viscoelasticity). Furthermore, in this research we hypothesize that tissue mass inertia plays a significant role in the dynamic behaviour if the tissue strips are under high oscillating frequencies (compared to normal breathing frequencies). For this kind of dynamic simulation, the finite element method (FEM) is an efficient tool that can be used. It is worth mentioning that commercially available FEM software is good at determining the eigenvalues and eigenfunctions for a specific problem with predetermined mechanical and physical properties. In this research, however, the process is reversed. The eigenfrequencies are known and the properties, such as the stiffness modulus are needed to be determined. This is the main reason why it was felt that it would be easier to develop a new FEM code rather than use an available commercial package.

The following sections of this chapter will firstly introduce the fading memory model. Necessary modifications are then introduced to modify this model to address the behaviour of airway smooth muscle. Finally, a two-dimensional FEM model will be developed to simulate oscillating events of airway smooth muscle tissue. All the numerical results are presented and discussed in Chapter 5 and 6, respectively.

## **4.2 Fading Memory Model**

As mentioned above, this is not an appropriate model to describe the dynamic behaviour of smooth muscle, however, it can be modified to accommodate smooth muscle behaviour. Initially, some details of this theory are presented to help the reader understand the basic principles as well as to understand the modifications presented in this work.

### **4.2.1 Fading Memory of Muscle**

A continuum cross-bridge dynamic model was developed by Hunter *et al.* [61], and is usually called the fading memory model. This model is initially assumed to have a constant level of bound calcium and steady state tropomyosin kinetics. The model is based on a macroscopic viewpoint where the dynamic response of the model only considers the total population of the activated cross-bridges. In the model, the input is the muscle length change and the output is the muscle force response. This model is established by an isometric quick release, accommodated by Hill's equation, and the constant parameters determined by muscle properties from experimental data [31 and 61].

First, a length ratio ( $\lambda$ ) is defined as the actual muscle length divided by the resting length, (i.e.  $\lambda = 1.0$  is the muscle resting length that contributes to the maximum isometric force). The advantage of using  $\lambda$  to give a normalized dimension is the fact that the absolute size of the muscle tissue is disregarded. Also, the force is normalized as  $T/T_0$ , where  $T$  is a responding force and  $T_0$  is an isometric force from the force-length relationship (see Figure 2.2 and 2.4). The fading memory model considers an isometric quick release as a transient step change (shortening) in length of  $\Delta l$ . See Figure 4.1.

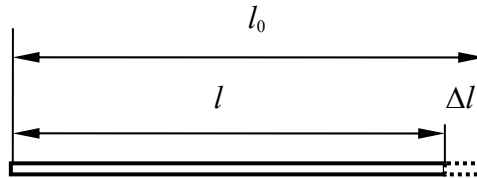


**Figure 4.1** A step change in length (transient response).

Let an unspecified function,  $Q(T, T_0)$  (this function will be determined later), be a nonlinear function of  $T$  and  $T_0$ , and assume that this function is zero when  $T$  is equal to  $T_0$ , i.e.  $Q(T_0, T_0) = 0$  (this means that there is no response). Consider now the effect of a change in length ( $\Delta\lambda$ ) at a time  $\tau$  ( $\tau < t$ ) on the current response at time  $t$ . The change in  $Q(T, T_0)$  (at time  $t$ ) resulting from this length step change (at time  $\tau$ ) can be determined from:

$$\Delta Q = \Phi(t - \tau) \cdot \Delta\lambda = \Phi(t - \tau) \frac{d\lambda(\tau)}{d\tau} d\tau = \Phi(t - \tau) \dot{\lambda} d\tau \quad (4.1)$$

where  $\Phi(t)$  is the material response function, and  $\Phi(t - \tau)$  is the response at time  $t$  to a stimulus at time  $\tau$  ( $\tau < t$ ). Integrating equation (4.1) one obtains:

$$Q(t) = \int_{-\infty}^t \Phi(t-\tau) \dot{\lambda} d\tau \quad (4.2)$$

This type of integral is known as a hereditary integral. Equation (4.2) assumes that the overall response of the muscle depends more upon recent events than on earlier events as the material has a “fading memory”. Furthermore, the material response function  $\Phi(t-\tau)$  can be assumed to be a superposition of these events. This gives:

$$\Phi(t-\tau) = \sum_{i=1}^N A_i \exp[-\alpha_i(t-\tau)] \quad (4.3)$$

where  $A_i$  and  $\alpha_i$  are constant parameters for the material. These constants will be determined using experimental data. Substituting equation (4.3) into equation (4.2) gives:

$$Q(T(t), T_0) = \sum_{i=1}^N A_i \int_{-\infty}^t \exp[-\alpha_i(t-\tau)] \dot{\lambda}(\tau) d\tau \quad (4.4)$$

After an isometric quick release, the force falls abruptly and then rises to a new force level (Figure 4.2).  $T_1/T_0$  is the initial fall in the force. In fact, the force recovery curve in Figure 4.2 shows evidence of three distinct physical processes:

1. an initial fast recovery,
2. a slight oscillation (critically damped) which is indicative of a second order process,
3. a subsequent slow recovery phase (evidence of a first order process).

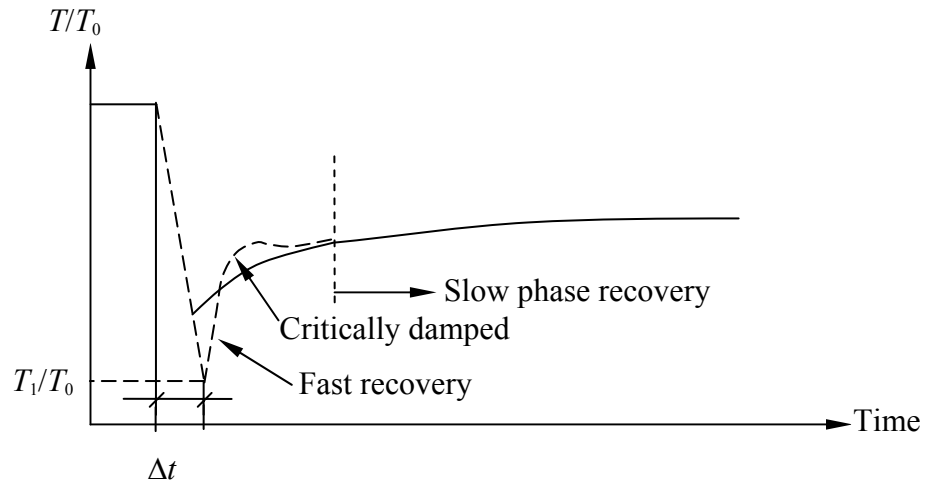


**Figure 4.2** Time response of force recovery following a length step (a length step of  $\Delta\lambda$  in time  $\Delta t$ ).

The force recovers to a new level that depends on the isometric force-length relationship (see Figure 2.2 and 2.4). Based on this, equation (4.4) is limited to three events of this superposition (i.e.  $N = 3$ ) and can be written as:

$$Q(T(t), T_0) = \sum_{i=1}^3 A_i \int_{-\infty}^t \exp[-\alpha_i(t-\tau)] \dot{\lambda}(\tau) d\tau \quad (4.5)$$

#### 4.2.2 Incorporation into Hill's Equation

A parameterised form of the nonlinear function  $Q(T, T_0)$  can be determined from constant velocity experiments (isotonic contraction). In these experiments, the muscle length is shortened at a constant rate (isotonic contraction) in response to a reduction in force to a constant value less than  $T_0$ . A plot of the force versus velocity is called the isotonic force-velocity relationship, (Figure 2.8(b)).

The curve is typically hyperbolic and the equation was first proposed by Hill [39] as:

$$-V = \frac{b\left(\frac{T}{T_0} - 1\right)}{\frac{T}{T_0} + a} \quad (4.6)$$

where  $a$  and  $b$  are constants and  $V$  is the shortening velocity. This relationship shows that the maximum force generated occurs when the muscle is contracting isometrically (zero velocity) and that the maximum velocity occurs when there is no afterload. Experimentally, this is found by extrapolating the curve from very low values of afterload. From equation (4.6), the “no afterload” condition can be expressed as:

$$V_{\max} = V_0 = \frac{b}{a}$$

or

$$b = a \cdot V_0 \quad (4.7)$$

Substituting equation (4.7) in to equation (4.6) gives:

$$\frac{-V}{aV_0} = \frac{\frac{T}{T_0} - 1}{\frac{T}{T_0} + a} \quad (4.8)$$

For a constant velocity, equation (4.5) can be considered to only have one constant ( $N = 1$ ) and can be written as:

$$\begin{aligned}
Q(T, T_0) &= A_1 \int_{-\infty}^t \exp[-\alpha_1(t-\tau)] \dot{\lambda} d\tau \\
&= A_1 \dot{\lambda} \cdot \exp(-\alpha_1 t) \int_{-\infty}^t \exp(\alpha_1 \tau) d\tau \\
&= \frac{A_1 \dot{\lambda} \cdot \exp(-\alpha_1 t)}{\alpha_1} [\exp(\alpha_1 \tau)]_{-\infty}^t \\
&= \frac{A_1 \dot{\lambda}}{\alpha_1}
\end{aligned} \tag{4.9}$$

Since the length has shortened by the time, and  $\dot{\lambda}$  is substituted with  $-V$ , equation (4.9) can then be written as:

$$Q(T, T_0) = -\frac{A_1 V}{\alpha_1} \tag{4.10}$$

Under the same conditions, equation (4.8) and (4.10) match exactly. Therefore:

$$Q(T, T_0) = \frac{\frac{T}{T_0} - 1}{\frac{T}{T_0} + a} \quad \text{and} \quad V_0 = \frac{\alpha_1}{A_1 a} \tag{4.11}$$

From equation (4.11),  $Q$  is zero when  $T$  and  $T_0$  are equal. This agrees with the assumption at the beginning of section 4.2.1. Finally, equation (4.5) can be rewritten as:

$$\frac{\frac{T}{T_0} - 1}{\frac{T}{T_0} + a} = \sum_{i=1}^3 A_i \int_{-\infty}^t \exp[-\alpha_i(t-\tau)] \dot{\lambda}(\tau) d\tau \tag{4.12}$$

### 4.2.3 Determination of the Constant Parameters from Isometric Quick Release

Referring to equation (4.12), the constants,  $A_i$ ,  $\alpha_i$  and  $a$ , are determined from muscle experimental data. A typical experiment is a transient step change in length. In this section, equation (4.12) will be derived for a transient step change in length, and then compared with the experimental results to determine the values of the constants. Before discussing a transient step change in length, two useful functions, the Heaviside and Dirac's delta functions, will be introduced, (see Figure 4.3).

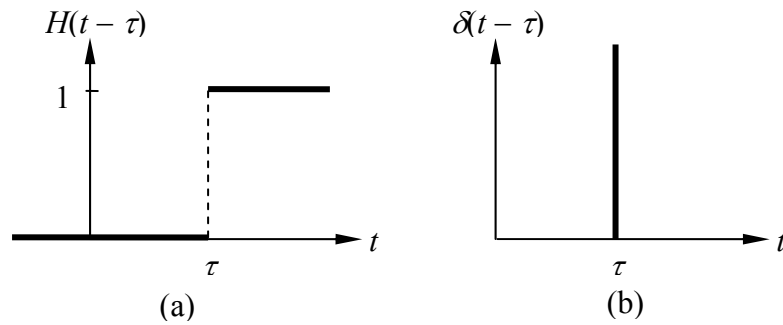


**Figure 4.3** Heaviside function (a) and Dirac's delta function (b).

The Heaviside function is a unit step function and defined as below, which has the unit step jump at an arbitrary positive value  $\tau$ .

$$H(t - \tau) = \begin{cases} 0 & \text{if } t < \tau \\ 1 & \text{if } t > \tau \end{cases} \quad (\tau \geq 0) \quad (4.13)$$

The use of the Heaviside function is apparent when it is convolved with a continuous time function  $f(t)$  [87]:

$$f(t)H(t-\tau) = \begin{cases} 0 & \text{if } t < \tau \\ f(t) & \text{if } t > \tau \end{cases} \quad (4.14)$$

Phenomena of an impulsive nature, such as the action of very large values over very short intervals of time (for instance at instantaneous time  $\tau$ ), can be represented by the Dirac's delta function:

$$\delta(t-\tau) = \begin{cases} \infty & \text{if } t = \tau \\ 0 & \text{otherwise} \end{cases}$$

and (4.15)

$$\int_0^{\infty} \delta(t-\tau) dt = 1$$

The Dirac's delta function also has an important characteristic for any continuous time function  $f(t)$  [87]. The convolution of  $f(t)$  with the Dirac's delta function maps:

$$\int_{-\infty}^{\infty} f(t)\delta(t-\tau) dt = f(\tau) \quad (4.16)$$

The Heaviside and Dirac's delta functions are related through the time derivative [87]:

$$\frac{d}{dt} H(t-\tau) = \delta(t-\tau) \quad (4.17)$$

Consider a transient step change in length (isometric quick release as seen in Figure 2.5). The length change (at time  $\tau$ ) and velocity can be expressed by using Heaviside and Dirac's Delta functions as:

$$\begin{aligned}\lambda &= \Delta\lambda \cdot H(\tau) + \lambda_0 \\ \dot{\lambda} &= \Delta\lambda \cdot \frac{dH(\tau)}{d\tau} = \Delta\lambda \cdot \delta(\tau)\end{aligned}\tag{4.18}$$

Substituting equation (4.18) into equation (4.12) gives:

$$\frac{\frac{T}{T_0} - 1}{\frac{T}{T_0} + a} = \Delta\lambda \sum_{i=1}^3 A_i \int_{-\infty}^t \exp[-\alpha_i(t - \tau)] \delta(\tau) d\tau\tag{4.19}$$

Defining zero time as the instance of the length step, after using equation (4.16), equation (4.19) can be written as:

$$\frac{\frac{T}{T_0} - 1}{\frac{T}{T_0} + a} = \Delta\lambda \sum_{i=1}^3 A_i \exp(-\alpha_i t)\tag{4.20}$$

$T_1$  is the initial fall in the force (see Figure 4.2), and represents the minimum force which can be obtained from equation (4.20) at  $t = 0$

$$\frac{\frac{T_1}{T_0} - 1}{\frac{T_1}{T_0} + a} = \Delta\lambda \sum_{i=1}^3 A_i\tag{4.21}$$

The constants  $A_i$  and  $\alpha_i$  are the material parameters that depend on muscle properties. The constants  $A_i$  are dimensionless. Equation (4.21) utilizes these three constants in determining the lowest force reached (labelled  $T_1$ ) immediately after a transient step. In

other words, these constants determine the degree of cross-bridge detachment that is disrupted by a transient step change in a length. The other constants ( $\alpha_i$ ) have units of  $s^{-1}$  to determine the muscle response time (recovery rate), which represents the time for reattachment of the disrupted cross-bridges. The constant ( $a$ ) is from Hill's equation, which is determined from the isotonic force-velocity relationships (Figure 2.8(b)). All these constant parameters are determined from the muscle properties. The amount of superposition (number of rate constants,  $N$ ) depends on the dynamic events of the muscle. Hunter *et al.* [61] used cardiac muscle experimental data in the model to address the behaviours of cardiac muscle. The details of their modification are presented as follows.

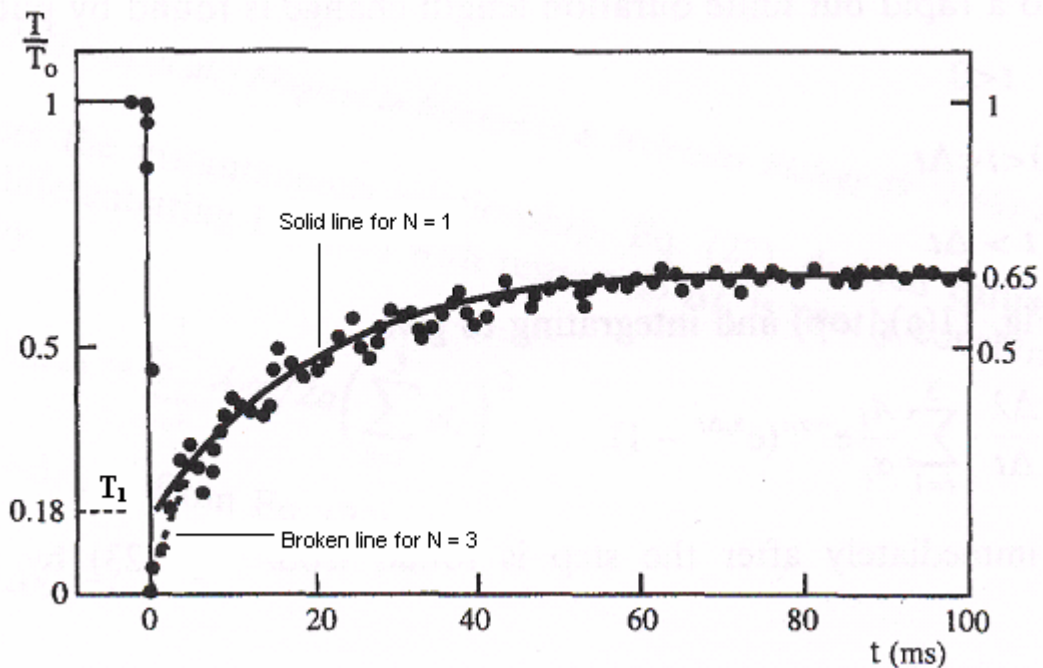


**Figure 4.4** Hancock's [92] data was fitted by the fading memory model [61].

The constant parameter  $a$ , is from Hill's equation, which is determined by the force-velocity relationship. Experimental data for the isotonic force-velocity relationship from cardiac muscle [89-91] gives a relative velocity ( $V/V_0$ ) of approximately 25% at a

relative force ( $T/T_0$ ) of 50%. Setting  $T/T_0 = 0.5$  and  $V/V_0 = 0.25$  in equation (4.8) gives  $a = 0.5$ .

The transient step change in length experiments required to evaluate the rate constants from equation (4.20) have been performed for ferret cardiac muscle at 27 °C by Hancock *et al.* [92]. In these experiments, the force response followed a 2% length step accomplished in 2 ms. Hunter *et al.* [61] fitted the experimental result using equation (4.20) (Figure 4.4) and got good agreement. The solid line in Figure 4.4 is from equation (4.20) with one rate constant ( $N = 1$ ) and parameters  $a = 0.5$ ,  $\alpha_1 = 75 \text{ s}^{-1}$  and  $A_1 = 50$ . The broken line in the figure is from equation (4.20) with all three rate constants ( $N = 3$ ,  $\alpha_2 = \alpha_3 = 2850 \text{ s}^{-1}$ , and  $A_2 = A_3 = 175$ ). The horizontal broken line in the figure (at  $T/T_0 = 0.18$ ) marks the immediate post-step force for the single rate constant relation, which is useful for determining the parameter  $A_1$ . The figure shows that using the three rate constants ( $N = 3$ ) provided better fits to the experimental data than using one rate constant.

### **4.3 Modification of Fading Memory Model for Airway Smooth Muscle**

It is worth emphasizing here that the fading memory theory was originally developed for cardiac muscle only. However, in this work some modifications are introduced to make it suitable for airway smooth muscles. Recall from Chapter 3 that the fading memory model disregards muscle structure itself and only considers the time response after a biophysical event. Furthermore, the different constant parameters ( $\alpha_i$ ) can determine different time responses in the model. Comparing Figure 2.5 for smooth muscle and 4.4 for cardiac muscles, it can be observed that isometric quick release is

identical irrespective of the type of muscle. The behavior is such that the force falls abruptly and subsequently rises to a new maximum level determined by the isometric force-length relationships. The only difference between the two types of muscle is the recovery time. From the both figures (Figure 2.5 and 4.4), we find that the time response of cardiac muscle is much faster than that for smooth muscle. This means that the cross-bridge cycling rate of cardiac muscle is much faster than the cycling rate of smooth muscle. Based on this, the fading memory model can be reasonably modified for smooth muscles.

#### **4.3.1 Determination of the Constant Parameters for Airway Smooth Muscle**

In equation (4.20), the parameter  $a$ , is a non-dimensional parameter. The experimental data from smooth muscle [41, 93 and 94] gives a relative velocity ( $V/V_0$ ) of approximately 16 – 19% at a relative tension ( $T/T_0$ ) of 50%. Setting  $T/T_0 = 0.5$  and  $V/V_0 = 0.16 - 0.19$  in equation (4.8) gives  $a$  to be between 0.32 – 0.38. Therefore, in this work, the value of  $a$  is assumed to be 0.35 for airway smooth muscle. To compare both smooth and cardiac muscles, the force-velocity relationships are presented in Figure 4.5 by using equation (4.8). The figure shows that, under the same loading condition, the smooth muscle has a slower shorting velocity than cardiac muscle. This is in agreement with the fact that the cross-bridge cycling rate in smooth muscle is slower than in cardiac muscle.

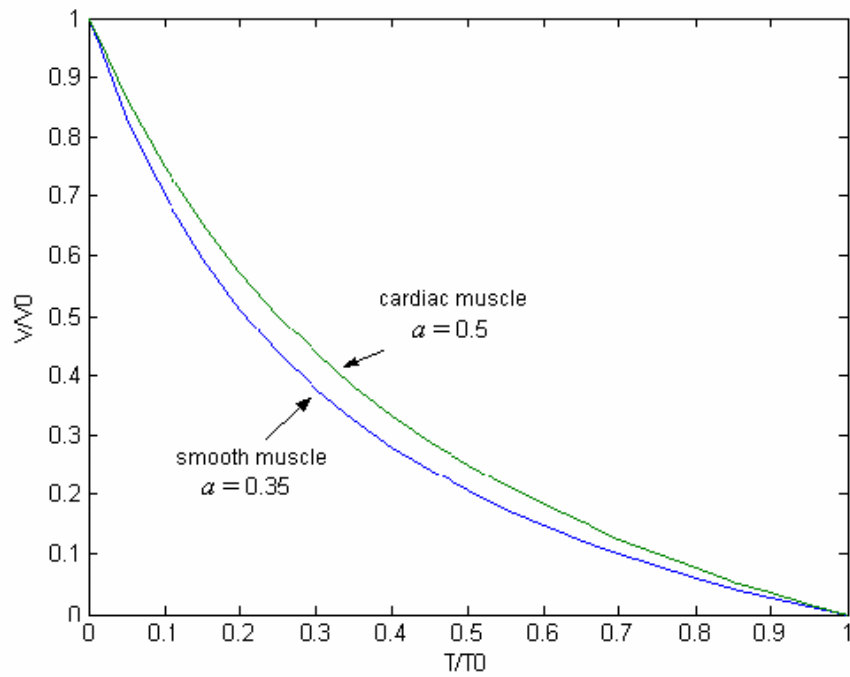


**Figure 4.5** Force-velocity relationships for smooth and cardiac muscle.

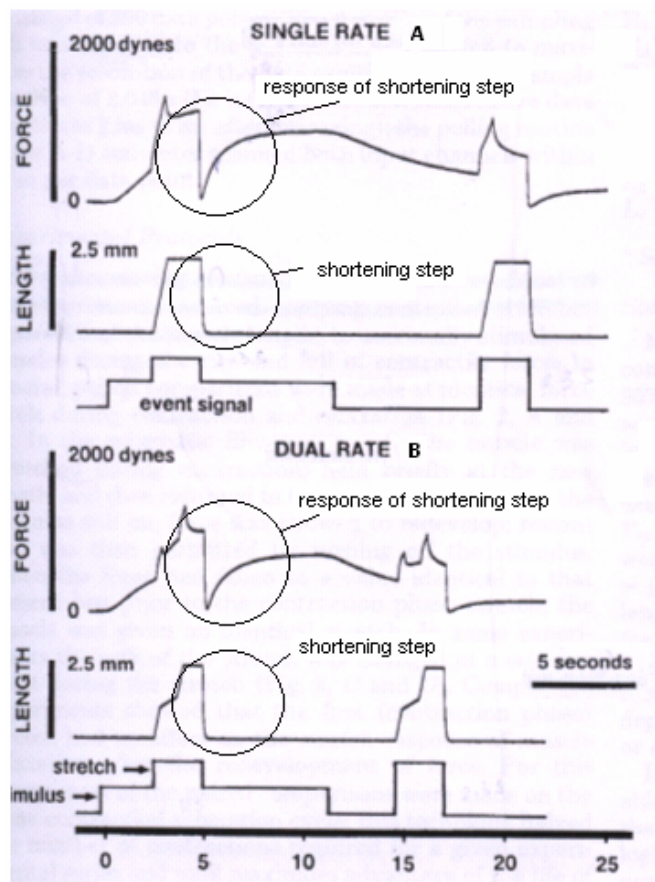


**Figure 4.6** Typical transient step change in length protocols and terminology, A and B show and length data played back from magnetic (analog) tape as function of time [21].

The parameters  $\alpha_i$  and  $A_i$ , in equation (4.20) can be determined by experimental data from the transient step change in length. Similar experiments for transient step change (stretching and shortening) in length have been performed for ovarian ligament smooth muscle of female rabbits by Meiss [21]. The typical time responses of a transient step change in length are shown in Figure 4.6. The cross-bridges of smooth muscle initially rearranged to the new length of muscle tissue after a transient step change (20% of  $L_r$  shortening) in approximately 3 – 4 seconds (refer to the cyclic rings in Figure 4.6). The initial recovery time of airway smooth muscle (Figure 2.5) and ovarian ligament smooth muscle (Figure 4.6) is similar. In this work, Meiss's data (Figure 4.6) will be used since the time scale reading is more accurate than Gunst's data (Figure 2.5) [38]. When comparing smooth muscles (Figure 4.6) and cardiac muscle (Figure 4.4), the response time of smooth muscle is roughly 60 times slower than that of cardiac muscles. The transient length step experiments required to evaluate the constant parameters ( $\alpha_i$  and  $A_i$ ) from equation (4.20) are fitted with Meiss's data. Figure 4.7 shows that the response of equation (4.20) with  $a = 0.35$ ,  $\alpha_1 = 1.2 \text{ s}^{-1}$ ,  $\alpha_2 = 8 \text{ s}^{-1}$ ,  $\alpha_3 = 48 \text{ s}^{-1}$ ,  $A_1 = 2.5$ ,  $A_2 = 10$  and  $A_3 = 40$ . After comparison with Figure 4.6, Figure 4.7 shows a good representation of Meiss's data (Figure 4.6) [21]. These values of constant parameters are used to represent the airway smooth muscle in this work. More details about the constant parameter  $A_i$  will be discussed in Chapter 6.

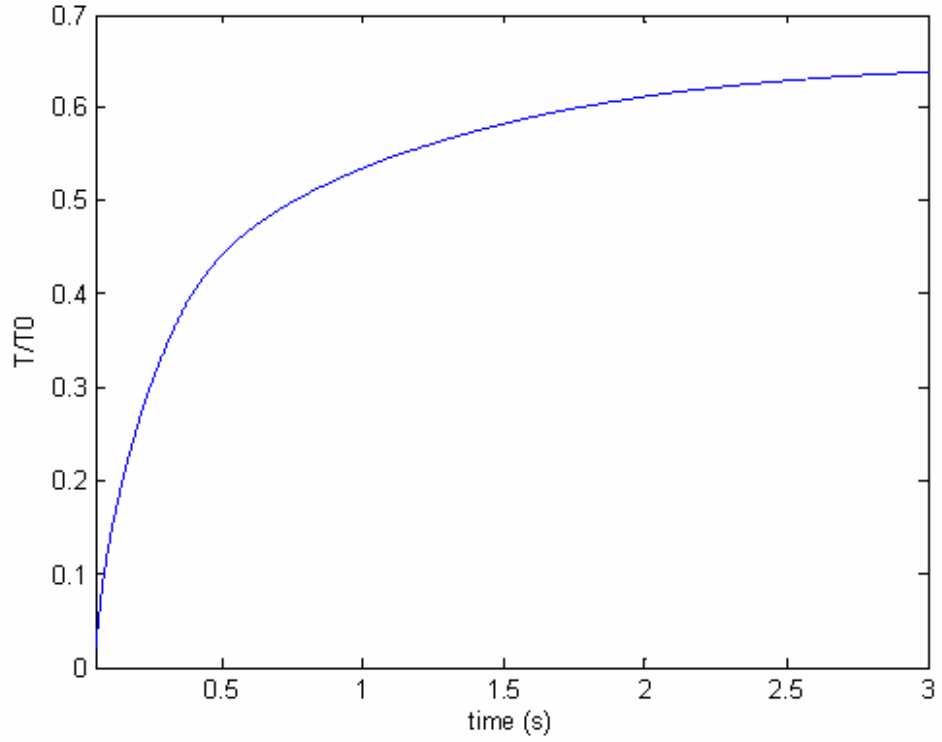


**Figure 4.7** Meiss's data is simulated by the fading memory model after using equation (4.15), the force is recovery by a transient step shortening in length, with values of constant parameter  $a = 0.35$ ,  $\alpha_1 = 1.2 \text{ s}^{-1}$ ,  $\alpha_2 = 8 \text{ s}^{-1}$ ,  $\alpha_3 = 48 \text{ s}^{-1}$ ,  $A_1 = 2.5$ ,  $A_2 = 10$  and  $A_3 = 40$ .

### 4.3.2 Finite Duration Length Step

Any real transient step change takes a finite time duration. Thus, the case is considered when the muscle tissue takes a finite time duration ( $\Delta t$ ) for the length change ( $\Delta \lambda$ ). The velocity of shortening is then given by:

$$\dot{\lambda} = \begin{cases} 0 & t < 0 \\ \frac{\Delta \lambda}{\Delta t} & 0 < t < \Delta t \\ 0 & t > \Delta t \end{cases} \quad (4.22)$$

Substituting equation (4.22) to equation (4.12) gives:

$$\frac{\frac{T}{T_0} - 1}{\frac{T}{T_0} + a} = \sum_{i=1}^3 A_i \int_0^{\Delta t} \exp[-\alpha_i(t-\tau)] \frac{\Delta\lambda}{\Delta t} d\tau = \frac{\Delta\lambda}{\Delta t} \sum_{i=1}^3 A_i \frac{[\exp(\alpha_i \Delta t) - 1]}{\alpha_i} \exp(-\alpha_i t) \quad (4.23)$$

The initial response ( $\frac{T_1}{T_0}$ , the initial decrease in force) for different finite time durations

( $\Delta t$ ) can be calculated by taking  $t = \Delta t$  in equation (4.23):

$$\frac{\frac{T_1}{T_0} - 1}{\frac{T_1}{T_0} + a} = \frac{\Delta\lambda}{\Delta t} \sum_{i=1}^3 A_i \frac{[1 - \exp(-\alpha_i \Delta t)]}{\alpha_i} \quad (4.24)$$

### 4.3.3 Development of a Modified Fading Memory Model for Longitudinal Oscillation

The fading memory model for a length oscillation can simulate the longitudinal vibration experiments conducted in this research. A contracted muscle is placed under an isometric condition and a mechanical length sinusoidal perturbation is imposed without calcium level change. Consider a perturbation of length ratio  $\lambda$  that has an amplitude,  $\Delta\lambda$ , about a mean length of  $\lambda = 1$  and frequency  $\omega$ . This can be written:

$$\lambda = 1 + \Delta\lambda \cdot \exp(j\omega \cdot t) \quad (4.25)$$

where  $j = \sqrt{-1}$ . The velocity of the length change is:

$$\dot{\lambda}(\tau) = \frac{d\lambda(\tau)}{d\tau} = \Delta\lambda \cdot j\omega \cdot \exp(j\omega\tau) \quad (4.26)$$

Substituting equation (4.26) to equation (4.12) to gives:

$$\frac{\frac{T}{T_0} - 1}{\frac{T}{T_0} + a} = \sum_{i=1}^3 A_i \int_{-\infty}^t \exp[-\alpha_i(t-\tau)] \Delta\lambda \cdot j\omega \cdot \exp(j\omega\tau) d\tau \quad (4.27)$$

Rewriting equation (4.27) one obtains:

$$\frac{\frac{T}{T_0} - 1}{\frac{T}{T_0} + a} = \Delta\lambda \cdot j\omega \sum_{i=1}^3 A_i \exp(-\alpha_i t) \int_{-\infty}^t \exp[(\alpha_i + j\omega)\tau] d\tau \quad (4.28)$$

Integrating equation (4.28) gives:

$$\frac{\frac{T}{T_0} - 1}{\frac{T}{T_0} + a} = \Delta\lambda \cdot j\omega \sum_{i=1}^3 A_i \exp(-\alpha_i t) \left[ \frac{\exp[(\alpha_i + j\omega)\tau]}{\alpha_i + j\omega} \right]_{-\infty}^t \quad (4.29)$$

Simplifying equation (4.29) gives:

$$\frac{\frac{T}{T_0} - 1}{\frac{T}{T_0} + a} = \Delta\lambda \cdot j\omega \sum_{i=1}^3 A_i \frac{\exp(j\omega \cdot t)}{\alpha_i + j\omega} \quad (4.30)$$

Finally, the equation that describes the response of the muscle tissue to longitudinal oscillations is given by:

$$\frac{T}{T_0} = \frac{1+Q \cdot a}{1-Q}, \text{ where } Q = \Delta\lambda \cdot j\omega \sum_{i=1}^3 A_i \frac{\exp(j\omega \cdot t)}{\alpha_i + j\omega} \quad (4.31)$$

## 4.4 Finite Element Model

The fading memory model only describes the cross-bridge mechanics of muscles. This model does not consider the entire properties and behaviours of muscles. However elasticity also plays an important role in muscle behaviours and need to be considered. Furthermore, muscle tissue inertia should be considered when the muscle tissue is excited by an external vibration. For this kind of combined behaviour, FEM is an efficient simulation method.

FEM divides a problem domain into many subdomains, each of which is called a finite element. The interconnected points between these elements are called nodes. After computation, FEM gives a solution for each node. The overall solution is the sum of the nodal solutions. In this section, the FEM model considers a strip of airway smooth muscle tissue under two-dimensional plane stress. Cauchy's first law [95 and 96] is invoked to describe the motion of the two-dimensional plate. The governing equations are then developed by applying Galerkin's method [96-98].

### 4.4.1 Physical Laws for the FEM

The basic FEM model is built on a two-dimensional plane, which is assumed to be homogeneous and isotropic. This plane also obeys Hook's law within the elastic limit. First, the basic theoretical equations for motion are derived. Consider the free body

diagram of the infinitesimal element shown in Figure 4.8. Applying Newton's second law to the element, the summation of forces in the horizontal and vertical axes become:

$$\begin{aligned} \left( \sigma_x + \frac{\partial \sigma_x}{\partial x} dx \right) dy - \sigma_x dy + \left( \tau_{xy} + \frac{\partial \tau_{xy}}{\partial y} dy \right) dx - \tau_{xy} dx + f_x dx dy &= \rho \frac{\partial^2 u}{\partial t^2} dx dy \\ \left( \tau_{xy} + \frac{\partial \tau_{xy}}{\partial x} dx \right) dy - \tau_{xy} dy + \left( \sigma_y + \frac{\partial \sigma_y}{\partial y} dy \right) dx - \sigma_y dx + f_y dx dy &= \rho \frac{\partial^2 v}{\partial t^2} dx dy \end{aligned} \quad (4.32)$$

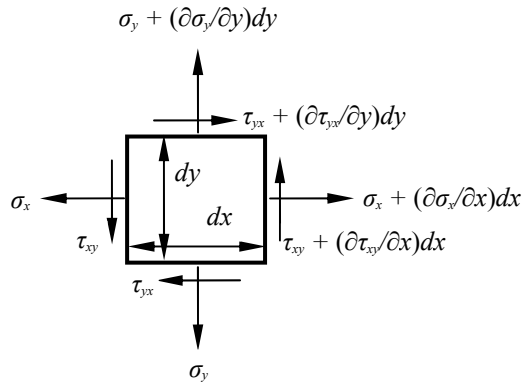


**Figure 4.8** Free body diagram of two-dimensional plane element.

where  $f_x$  and  $f_y$  are body forces per unit volume (assuming unit thickness perpendicular to the plane) in the  $x$  and  $y$  axes and are assumed to be positive when acted along the positive axes.  $u$  and  $v$  are displacements in the horizontal ( $x$  axes) and vertical ( $y$  axes) directions, respectively, and  $\rho$  is the density of the plane (assuming unit thickness perpendicular to the plane). All of the stress components in Figure 4.8 are shown as positive. Simplifying equation (4.32) yields the equations of equilibrium as:

$$\begin{aligned} \frac{\partial \sigma_x}{\partial x} + \frac{\partial \tau_{xy}}{\partial y} + f_x - \rho \cdot \ddot{u} &= 0 \\ \frac{\partial \tau_{xy}}{\partial x} + \frac{\partial \sigma_y}{\partial y} + f_y - \rho \cdot \ddot{v} &= 0 \end{aligned} \quad (4.33)$$

Equation (4.33) is known as Cauchy's first law of motion [95 and 96].

#### 4.4.2 Development of Finite Element Formulae

In order to develop a computing code for the FEM, the following derivation is presented, and more details of the FEM basic principles are introduced in Appendix A.

After applying the weighted residual and integration by parts, equation (4.33) becomes:

$$\int_{\Omega} \rho \begin{bmatrix} w_1 & 0 \\ 0 & w_2 \end{bmatrix} \begin{Bmatrix} \ddot{u} \\ \ddot{v} \end{Bmatrix} d\Omega + \int_{\Omega} \begin{bmatrix} \frac{\partial w_1}{\partial x} & 0 & \frac{\partial w_1}{\partial y} \\ 0 & \frac{\partial w_2}{\partial y} & \frac{\partial w_2}{\partial x} \end{bmatrix} \begin{Bmatrix} \sigma_x \\ \sigma_y \\ \tau_{xy} \end{Bmatrix} d\Omega = \int_{\Omega} \begin{bmatrix} w_1 & 0 \\ 0 & w_2 \end{bmatrix} \begin{Bmatrix} f_x \\ f_y \end{Bmatrix} d\Omega \quad (4.34)$$

$$+ \int_{\Gamma} \begin{bmatrix} w_1 & 0 \\ 0 & w_2 \end{bmatrix} \begin{Bmatrix} \Phi_x \\ \Phi_y \end{Bmatrix} d\Gamma$$

In this work, the problem domain ( $\Omega$ ) is divided using linear triangular elements with the following weighting functions:

$$\begin{aligned} \varphi_1(x, y) &= \frac{1}{2A} [(x_2 y_3 - x_3 y_2) + (y_2 - y_3)x + (x_3 - x_2)y] \\ \varphi_2(x, y) &= \frac{1}{2A} [(x_3 y_1 - x_1 y_3) + (y_3 - y_1)x + (x_1 - x_3)y] \\ \varphi_3(x, y) &= \frac{1}{2A} [(x_1 y_2 - x_2 y_1) + (y_1 - y_2)x + (x_2 - x_1)y] \end{aligned} \quad (4.35)$$

where  $A$  is the area of the triangular element, and  $x_i$  and  $y_i$  are the  $i^{\text{th}}$  node of each triangular element. Each element has three nodes ( $i = 1, 2, 3$ ), and each node has two degrees of freedom (DOF). Galerkin's method uses the weighting functions as basis functions in an FEM formulation.

The first integral on the left-hand-side in equation (4.34) describes the mass inertia, and the accelerations  $\ddot{u}$  and  $\ddot{v}$  can be interpolated using the weighting functions:

$$\begin{aligned}\ddot{u} &= \varphi_1 \cdot \ddot{u}_1 + \varphi_2 \cdot \ddot{u}_2 + \varphi_3 \cdot \ddot{u}_3 \\ \ddot{v} &= \varphi_1 \cdot \ddot{v}_1 + \varphi_2 \cdot \ddot{v}_2 + \varphi_3 \cdot \ddot{v}_3\end{aligned}\tag{4.36}$$

where  $\ddot{u}_i$  and  $\ddot{v}_i$  ( $i = 1, 2, 3$ ) are the nodal accelerations in the  $x$  and  $y$  directions, respectively. In matrix form, these accelerations can also be expressed as:

$$\begin{Bmatrix} \ddot{u} \\ \ddot{v} \end{Bmatrix} = \begin{bmatrix} \varphi_1 & 0 & \varphi_2 & 0 & \varphi_3 & 0 \\ 0 & \varphi_1 & 0 & \varphi_2 & 0 & \varphi_3 \end{bmatrix} \begin{Bmatrix} \ddot{u}_1 \\ \ddot{v}_1 \\ \ddot{u}_2 \\ \ddot{v}_2 \\ \ddot{u}_3 \\ \ddot{v}_3 \end{Bmatrix} = [N] \{\ddot{d}_e\}\tag{4.37}$$

for each element, where  $\{\ddot{d}_e\}$  is the nodal acceleration vector for an element. Integrating the first integral on the left hand side of equation (4.34) over that element domain gives:

$$\int_{\Omega_e} \rho \begin{bmatrix} w_1 & 0 \\ 0 & w_2 \end{bmatrix} \begin{Bmatrix} \ddot{u} \\ \ddot{v} \end{Bmatrix} d\Omega_e = \int_{\Omega_e} \rho [N]^T [N] d\Omega_e \{\ddot{d}_e\} = [M_e] \{\ddot{d}_e\}\tag{4.38}$$

where  $\Omega_e$  denotes the element domain and  $[M_e]$  is known as the mass matrix for each element. Since the total DOF for each element is six, the size of the mass matrix  $[M_e]$  is  $6 \times 6$  elements. Equation (4.38) is known as the consistent matrix and for linear triangular elements becomes:

$$[M_e] = \frac{\rho A}{12} \begin{bmatrix} 2 & 0 & 1 & 0 & 1 & 0 \\ 0 & 2 & 0 & 1 & 0 & 1 \\ 1 & 0 & 2 & 0 & 1 & 0 \\ 0 & 1 & 0 & 2 & 0 & 1 \\ 1 & 0 & 1 & 0 & 2 & 0 \\ 0 & 1 & 0 & 1 & 0 & 2 \end{bmatrix} \quad (4.39)$$

A technique known as “mass lumping” is sometimes used, in which the mass matrix  $[M_e]$  is replaced by a diagonal matrix having diagonal terms equal to the row sums. This is more convenient for computational purposes [96 and 97]. After using mass lumping, equation (4.39) becomes:

$$[M_e] = \frac{\rho A}{3} [\mathbf{I}] \quad (4.40)$$

where  $[\mathbf{I}]$  is a  $6 \times 6$  identity matrix. Finally, the first integral on the left-hand-side of equation (4.27) becomes:

$$\int_{\Omega_e} \rho \begin{bmatrix} w_1 & 0 \\ 0 & w_2 \end{bmatrix} \begin{Bmatrix} \ddot{u} \\ \ddot{v} \end{Bmatrix} d\Omega_e = \frac{\rho A}{3} [\mathbf{I}] \{\ddot{d}_e\} \quad (4.41)$$

The second integral on the left-hand-side of equation (4.27) describes the elasticity of the material and can be written as:

$$\int_{\Omega_e} \begin{Bmatrix} \frac{\partial w_1}{\partial x} \sigma_x + \frac{\partial w_1}{\partial y} \tau_{xy} \\ \frac{\partial w_2}{\partial x} \tau_{xy} + \frac{\partial w_2}{\partial y} \sigma_x \end{Bmatrix} d\Omega_e = \int_{\Omega_e} \begin{bmatrix} \frac{\partial w_1}{\partial x} & 0 & \frac{\partial w_1}{\partial y} \\ 0 & \frac{\partial w_2}{\partial y} & \frac{\partial w_2}{\partial x} \end{bmatrix} \begin{Bmatrix} \sigma_x \\ \sigma_y \\ \tau_{xy} \end{Bmatrix} d\Omega_e \quad (4.42)$$

To calculate the constitutive equation, the stress–strain relationship must be examined. In this model, the plane stress condition is considered to be valid such that the stress is related to strain through (see Appendix B):

$$\begin{aligned}
 \begin{Bmatrix} \sigma_x \\ \sigma_y \\ \tau_{xy} \end{Bmatrix} &= \frac{E}{1-\nu^2} \begin{bmatrix} 1 & \nu & 0 \\ \nu & 1 & 0 \\ 0 & 0 & \frac{1-\nu}{2} \end{bmatrix} \begin{Bmatrix} \gamma_{11} \\ \gamma_{22} \\ 2\gamma_{12} \end{Bmatrix} = \frac{E}{1-\nu^2} \begin{bmatrix} 1 & \nu & 0 \\ \nu & 1 & 0 \\ 0 & 0 & \frac{1-\nu}{2} \end{bmatrix} \begin{Bmatrix} \gamma_x \\ \gamma_y \\ \gamma_{xy} \end{Bmatrix} \\
 &= [D] \begin{Bmatrix} \gamma_x \\ \gamma_y \\ \gamma_{xy} \end{Bmatrix} = [D] \begin{Bmatrix} \frac{\partial u}{\partial x} \\ \frac{\partial v}{\partial y} \\ \frac{\partial u}{\partial y} + \frac{\partial v}{\partial x} \end{Bmatrix} \tag{4.43}
 \end{aligned}$$

Note that in equation (4.43)  $\gamma_{11} = \gamma_x$ ,  $\gamma_{22} = \gamma_y$  and  $2\gamma_{12} = \gamma_{xy}$ . Here  $\gamma_{12}$  is the tensor shear strain component, whereas  $\gamma_{xy}$  refers to the engineering (or total) shear strain.

Both displacements  $u$  and  $v$  are interpolated using the weighting functions:

$$\begin{aligned}
 u &= \varphi_1 \cdot u_1 + \varphi_2 \cdot u_2 + \varphi_3 \cdot u_3 \\
 v &= \varphi_1 \cdot v_1 + \varphi_2 \cdot v_2 + \varphi_3 \cdot v_3
 \end{aligned} \tag{4.44}$$

where  $v_i$  ( $i = 1, 2, 3$ ) are the nodal displacements in the  $x$  and  $y$  directions, respectively. In matrix form, these displacements can be expressed as:

$$\begin{Bmatrix} u \\ v \end{Bmatrix} = \begin{bmatrix} \varphi_1 & 0 & \varphi_2 & 0 & \varphi_3 & 0 \\ 0 & \varphi_1 & 0 & \varphi_2 & 0 & \varphi_3 \end{bmatrix} \begin{Bmatrix} u_1 \\ v_1 \\ u_2 \\ v_2 \\ u_3 \\ v_3 \end{Bmatrix} = [N]\{d_e\} \quad (4.45)$$

where  $\{d_e\}$  is the nodal displacement vector for each element. Use of this expression for the strains yields:

$$\begin{Bmatrix} \frac{\partial u}{\partial x} \\ \frac{\partial v}{\partial y} \\ \frac{\partial u}{\partial y} + \frac{\partial v}{\partial x} \end{Bmatrix} = \begin{bmatrix} \frac{\partial \varphi_1}{\partial x} & 0 & \frac{\partial \varphi_2}{\partial x} & 0 & \frac{\partial \varphi_3}{\partial x} & 0 \\ 0 & \frac{\partial \varphi_1}{\partial y} & 0 & \frac{\partial \varphi_2}{\partial y} & 0 & \frac{\partial \varphi_3}{\partial y} \\ \frac{\partial \varphi_1}{\partial y} & \frac{\partial \varphi_1}{\partial x} & \frac{\partial \varphi_2}{\partial y} & \frac{\partial \varphi_2}{\partial x} & \frac{\partial \varphi_3}{\partial y} & \frac{\partial \varphi_3}{\partial x} \end{bmatrix} \{d_e\} = [B]\{d_e\} \quad (4.46)$$

Integrating the second integral on the left hand side of equation (4.34) over the element domain gives:

$$\int_{\Omega_e} \begin{bmatrix} \frac{\partial w_1}{\partial x} & 0 & \frac{\partial w_1}{\partial y} \\ 0 & \frac{\partial w_2}{\partial y} & \frac{\partial w_2}{\partial x} \end{bmatrix} \begin{Bmatrix} \sigma_x \\ \sigma_y \\ \tau_{xy} \end{Bmatrix} d\Omega_e = \int_{\Omega_e} [B]^T [D][B] d\Omega_e \{d_e\} = [K_e]\{\ddot{d}_e\} \quad (4.47)$$

where  $[K_e]$  is known as the stiffness matrix for each element. Evaluation of the linear shape function of the triangular element provides

$$[B] = \frac{1}{2A} \begin{bmatrix} (y_2 - y_3) & 0 & (y_3 - y_1) & 0 & (y_1 - y_2) & 0 \\ 0 & (x_3 - x_2) & 0 & (x_1 - x_3) & 0 & (x_2 - x_1) \\ (x_3 - x_2) & (y_2 - y_3) & (x_1 - x_3) & (y_3 - y_1) & (x_2 - x_1) & (y_1 - y_2) \end{bmatrix} \quad (4.48)$$

Since both  $[B]$  and  $[D]$  are constant matrices independent of  $x$  and  $y$ ,  $[K_e]$  can also be written as:

$$[K_e] = \int_{\Omega_e} [B]^T [D][B] d\Omega_e = [B]^T [D][B]A \quad (4.49)$$

The size of the matrix  $[K_e]$  is the same as the number of DOF for the element (in this case,  $6 \times 6$  elements). A unit thickness is assumed for the plane stress condition, so the solution is independent of the direction of the thickness.

The two right-hand-side terms in equation (4.34) are force vectors. The first term is due to body forces ( $f$ ) and the second term is due to tractions ( $\Phi$ ). The body force term is a domain integral, and so the same computations that were performed on the stiffness matrix  $[K_e]$  can be performed on this term. In the element domain this term yields:

$$\{F_e\} = \int_{\Omega_e} \begin{bmatrix} w_1 & 0 \\ 0 & w_2 \end{bmatrix} \begin{Bmatrix} f_x \\ f_y \end{Bmatrix} d\Omega_e = \int_{\Omega_e} [N]^T \begin{Bmatrix} f_x \\ f_y \end{Bmatrix} d\Omega_e \quad (4.50)$$

where the body force is constrained on each node on the  $x$  and  $y$  directions. The traction term in equation (4.34) is a boundary integral (Figure 4.9), and this traction can weight on nodal values in an element as follows:

$$\{\Phi_e\} = \int_{\Gamma_e} \begin{bmatrix} w_1 & 0 \\ 0 & w_2 \end{bmatrix} \begin{Bmatrix} \Phi_x \\ \Phi_y \end{Bmatrix} d\Gamma_e = \int_{s_i}^{s_j} \begin{bmatrix} \frac{s_j - s}{s_j - s_i} & 0 \\ 0 & \frac{s_j - s}{s_j - s_i} \\ \frac{s - s_i}{s_j - s_i} & 0 \\ 0 & \frac{s - s_i}{s_j - s_i} \end{bmatrix} \begin{Bmatrix} \Phi_x \\ \Phi_y \end{Bmatrix} ds \quad (4.51)$$

where  $s_i$  and  $s_j$  are the coordinate values along the temporary boundary axis  $s$  and  $i$  and  $j$  are the two nodes on the element boundary where the traction is described. For free standing boundary conditions, there is no traction (i.e.  $\Phi_x = \Phi_y = 0$ ).

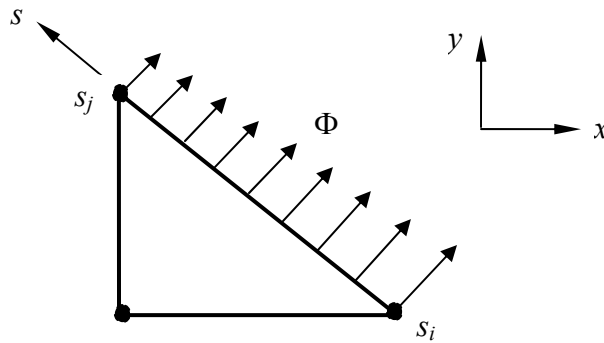


**Figure 4.9** Boundary traction in an element.

Combining equation (4.38), (4.47), (4.50) and (4.51) gives the final equation for each element in the domain:

$$[M_e] \{\ddot{d}_e\} + [K_e] \{d_e\} = \{F_e\} + \{\Phi_e\} \quad (4.52)$$

### 4.4.3 Assembly of Finite Element Equations

To calculate the overall deformation, each element stiffness matrix must be assembled into a global stiffness matrix. Each element has the same element stiffness matrix as that given in equation (4.40), (4.49), (4.50) and (4.51), since each element is the same unit size, and is interpolated by the same basis functions. After assembly, the global matrix is symmetric and will be sparse if there are a large number of elements. If the solution at global node  $i$ , is known, the  $i^{\text{th}}$  equation can be removed and can be replaced with a known value of  $u_i$ . This equation is then uncoupled from other equations and can be removed from the computation. The size of the system is then reduced. The system that needs to be solved is only as big as the number of unknown values of  $u$ . The global system can then be expressed as:

$$[M]\{\ddot{d}\} + [K]\{d\} = \{F\} \quad (4.53)$$

where  $[M]$  is the system mass matrix,  $[K]$  is the system stiffness matrix,  $\{F\}$  is the total force on the system boundary (which includes the body force and the boundary traction) and  $\{\ddot{d}\}$  and  $\{d\}$  are the system acceleration and displacement vectors, respectively.

In this work, the mass of muscle tissue is constant during the excitation, but the stiffness  $[K]$  of the muscle tissue varies with both time and oscillating frequency. Thus, equation (4.53) will be modified as:

$$[M]\{\ddot{d}\} + [K(t, f)]\{d\} = \{F\} \quad (4.54)$$

In general, the form of  $[K(t, f)]$  is nonlinear and cannot be calculated analytically. To determine  $[K(t, f)]$ , experimentally obtained data (from Chapter 3) needs to be used, as will be discussed in Chapter 6.

#### 4.4.4 Longitudinal Vibration

A strip of smooth muscle tissue excited in the longitudinal direction is showed in Figure 4.10. There are total of 80 elements and 63 nodes in the FEM. One end of the tissue is fixed, but the other end of tissue is oscillated in the longitudinal direction by a sine wave with amplitude  $A_a$  and frequency  $\omega$ :

$$d = A_a \sin(\omega \cdot t) \quad (4.55)$$

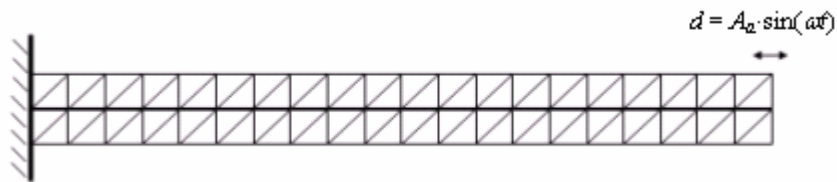


**Figure 4.10** A strip of smooth muscle tissue is excited with a vibration in the longitudinal direction.

The FEM model is programmed using the central difference scheme for the time integration [96]. The central difference technique is conditionally stable and so the time step size should be less than the critical time step size [97] defined as:

$$\Delta t < \Delta t_{crit} = \frac{1}{2\lambda_{max}} \quad (4.56)$$

where  $\lambda_{max}$  is the largest eigenvalue (oscillatory noise) in the matrix  $[A]$ :

$$[A] = [M]^{-1}[K] \quad (4.57)$$

#### 4.4.5 Transverse Vibration

A strip of smooth muscle tissue is simulated using the FEM for excitations in the transverse direction shown in Figure 4.11. There are total 80 elements and 63 nodes in the FEM. Both ends of the tissue are fixed boundaries, the middle of tissue is oscillated in the transverse direction by a sine wave with amplitude  $A_a$  and frequency  $\omega$ .

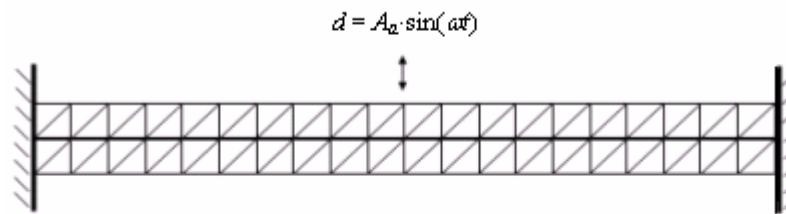


**Figure 4.11** A strip of smooth muscle tissue is excited with a vibration in the transverse direction

As same as the longitudinal vibration, the FEM model is programmed using the central difference scheme for the time integration. The time step size can be determined by equation (4.56).

The results from both these FEM simulation will be given in the next chapter alongside the equivalent experimental results for comparison.

## **Chapter 5**

### **Experimental & Numerical Results**

#### **5.1 Introduction**

The conceptual idea of this work is to systematically determine the response of contracted airway smooth muscle to different external dynamic excitations. These excitations are specified in terms of frequencies, amplitudes and time durations. The muscle stiffness is considered to be the main parameter which reflects the degree of relaxation for the contracted muscle. To achieve this goal, this work is split into an experimental (see Chapter 3) and numerical part (see Chapter 4). The main results from these two chapters will be presented in this chapter.

#### **5.2 Airway Smooth Muscle Tissue Properties**

Relaxed muscles and contracted muscles have different stiffnesses. For contracted muscles, the stiffness varies at different levels of contraction. In this research, the original stiffness is defined to reflect the fully contracted airway smooth muscle property without any external excitation (see section 3.3.2 in Chapter 3). This value will be used for an initial estimate in the numerical model. For the eleven smooth muscle

tissues tested in Chapter 3, an average value of the original stiffness is determined. The original Young's modulus of elasticity,  $E$ , is then calculated from:

$$E = \frac{l \cdot K}{A} \quad (5.1)$$

where  $E$  is the original Young's modulus of muscle,  $l$  is the muscle tissue length,  $K$  is the muscle original stiffness (the ratio of force change to the length change from the measurements,  $K = \Delta F/\Delta l$ ), and  $A$  is the cross-sectional area of muscle tissue obtained from the following equation:

$$A = \frac{m}{\rho \cdot l} \quad (5.2)$$

where  $m$  is the mass and  $\rho$  is the mass density of the muscle tissue. In this work,  $\rho$  is taken to be  $0.001 \text{ g/mm}^3$  [22, 99 and 100], and the physical parameters for the eleven tissue elements tested in Chapter 3 are summarized in Table 5.1.

**Table 5.1 Measure properties of original tissue**

	Tissue mass $m$ (g)	Tissue length $l$ (mm)	Tissue cross-sectional area $A$ (mm <sup>2</sup> )	Tissue stiffness $K$ (mN/mm)	Tissue modulus $E$ (MPa)
1	0.042	18.9	2.228	120.686	1.024
2	0.050	18.9	2.661	138.983	0.987
3	0.050	16.7	2.982	179.101	1.003
4	0.046	18.8	2.452	129.258	0.991
5	0.039	16.5	2.346	119.689	0.842
6	0.042	18.9	2.238	105.747	0.893
7	0.049	16.3	3.031	189.836	1.021
8	0.051	18.1	2.829	154.252	0.987
9	0.045	15.7	2.834	158.690	0.879
10	0.047	18.5	2.551	153.081	1.110
11	0.040	16.1	2.503	153.451	0.987
Average value	0.046	17.6	2.605	145.707	0.975
Standard deviation	0.004	1.3	0.285	25.757	0.076
95% confidence interval	$\pm 0.002$	$\pm 0.8$	$\pm 0.168$	$\pm 15.221$	$\pm 0.045$

### 5.3 Experimental Results

The results from both longitudinal and transverse vibrations are presented in this section. The data relating to the stiffness was acquired and converted using the equations in section 3.5 of Chapter 3.

### 5.3.1 Longitudinal Vibration

In this part of the investigation, contracted airway smooth muscle tissues were excited in the longitudinal direction. First, oscillations were introduced at various frequencies and amplitudes, while the duration of vibration was kept at 1 second. The range of vibration frequencies was from 5 to 75 Hz and the amplitudes of vibration were from 1.2% to 6.0% of the reference length (Appendix C). The variation in stiffness as a function of amplitude and frequency was then calculated. For statistical analysis, the measurements of the eleven pig's airway smooth muscle tissues were averaged for each frequency and amplitude response and are summarized in Table 5.2 (dynamic stiffness,  $K_d$ ) and 5.3 (static stiffness,  $K_s$ ).

**Table 5.2 Average of eleven tissues dynamic stiffness ( $K_d$ ) with 95% confidence interval to different frequencies and amplitudes.**

Frequency (Hz)	$K_d$ for Different Amplitudes of Vibration				
	1.2% of $L_r$	2.5% of $L_r$	3.8% of $L_r$	4.5% of $L_r$	6.0% of $L_r$
5	0.928±0.015	0.915±0.015	0.905±0.015	0.896±0.018	0.872±0.022
15	0.909±0.019	0.894±0.021	0.881±0.023	0.870±0.019	0.839±0.035
25	0.891±0.015	0.868±0.014	0.858±0.019	0.847±0.026	0.821±0.032
35	0.883±0.020	0.847±0.013	0.835±0.022	0.817±0.023	0.805±0.028
45	0.865±0.025	0.820±0.026	0.796±0.030	0.782±0.025	0.768±0.021
55	0.855±0.022	0.813±0.021	0.789±0.028	0.764±0.020	0.727±0.022
65	0.840±0.018	0.805±0.020	0.776±0.028	0.748±0.038	0.706±0.030
75	0.834±0.016	0.787±0.027	0.761±0.028	0.735±0.033	0.667±0.038

**Table 5.3 Average of eleven tissues static stiffness ( $K_s$ ) with 95% confidence interval to different frequencies and amplitudes.**

Frequency (Hz)	$K_s$ for Different Amplitudes of Vibration				
	1.2% of $L_r$	2.5% of $L_r$	3.8% of $L_r$	4.5% of $L_r$	6.0% of $L_r$
5	0.907±0.014	0.851±0.016	0.788±0.029	0.738±0.044	0.681±0.033
15	0.885±0.016	0.825±0.022	0.744±0.031	0.679±0.036	0.603±0.027
25	0.877±0.023	0.803±0.025	0.725±0.019	0.655±0.034	0.582±0.021
35	0.865±0.022	0.800±0.020	0.708±0.034	0.653±0.040	0.575±0.049
45	0.867±0.015	0.802±0.033	0.705±0.028	0.650±0.036	0.578±0.034
55	0.864±0.016	0.801±0.027	0.699±0.029	0.645±0.029	0.576±0.040
65	0.869±0.014	0.794±0.018	0.704±0.030	0.642±0.031	0.569±0.031
75	0.866±0.015	0.785±0.027	0.694±0.031	0.631±0.032	0.549±0.027

In second part of this set of experimental investigation, oscillations were introduced at various time durations. The muscle tissues were oscillated the frequencies of 5 Hz, 35 Hz and 65 Hz, for a time duration of 1, 2, 3 and 5 seconds respectively, while, the amplitude of these oscillations was maintained at 3.8% of  $L_r$ . Six measurements were taken for each frequency and duration, and the average response is given in Table 5.4 for dynamic stiffness ( $K_d$ ) and Table 5.5 for static stiffness ( $K_s$ ). As with the previous experimental data is listed in Appendix C.

**Table 5.4 Average of six tissues dynamic stiffness ( $K_d$ ) with 95% confidence interval to different frequencies and time durations.**

Frequency (Hz)	$K_d$ for Different Time Durations of Vibration			
	1 sec	2 sec	3 sec	5 sec
5	0.917±0.014	0.868±0.014	0.843±0.015	0.832±0.012
35	0.820±0.021	0.823±0.018	0.823±0.017	0.812±0.012
65	0.768±0.020	0.765±0.023	0.758±0.020	0.740±0.022

**Table 5.5 Average of six tissues static stiffness ( $K_s$ ) with 95% confidence interval to different frequencies and time durations.**

Frequency (Hz)	$K_s$ for Different Time Durations of Vibration			
	1 sec	2 sec	3 sec	5 sec
5	0.842±0.026	0.773±0.017	0.730±0.019	0.705±0.017
35	0.713±0.026	0.708±0.031	0.702±0.026	0.643±0.024
65	0.700±0.024	0.703±0.021	0.702±0.023	0.627±0.025

### 5.3.2 Transverse Vibration

This is a new type of experimentation, and to the best of our knowledge has never been reported in the open literature. For these experiments, the contracted smooth muscle tissues were excited in the transverse direction by an oscillator. Experiments were conducted at various frequencies and amplitudes of excitation. The extent of the tissue transverse fluctuation is the same as the amplitude of oscillation and can be converted to a length change ratio of the tissue (see section 3.4.2 in Chapter 3).

Oscillations were introduced at various frequencies and length change ratios, while the duration of vibration was maintained at between 1 – 2 seconds. The frequencies were changed from 5 to 55 Hz at steps of 10 Hz, with length change ratios of 2.2%, 3.5% and 4.8% of  $L_r$ , respectively (Appendix C). The variation in stiffness as a function of length change ratio and frequency was acquired. For statistical analysis, the measurements of the six pig's airway smooth muscle tissues were averaged for each frequency and length change ratio response and are given in Table 5.6 (dynamic stiffness,  $K_d$ ) and 5.7 (static stiffness,  $K_s$ ).

**Table 5.6 Average of six tissues dynamic stiffness ( $K_d$ ) with 95% confidence interval to different frequencies and length change ratios.**

Frequency (Hz)	$K_d$ for Different Length Change Ratios of Vibration		
	2.2% of $L_r$	3.5% of $L_r$	4.8% of $L_r$
5	0.853±0.014	0.806±0.017	0.725±0.015
15	0.815±0.017	0.758±0.021	0.693±0.024
25	0.796±0.023	0.743±0.021	0.673±0.027
35	0.775±0.022	0.727±0.017	0.642±0.030
45	0.783±0.026	0.702±0.019	0.627±0.032
55	0.790±0.024	0.710±0.024	0.624±0.026

**Table 5.7 Average of six tissues static stiffness ( $K_s$ ) with 95% confidence interval to different frequencies and length change ratios.**

Frequency (Hz)	$K_s$ for Different Length Change Ratios of Vibration		
	2.2% of $L_r$	3.5% of $L_r$	4.8% of $L_r$
5	0.837±0.014	0.762±0.017	0.715±0.018
15	0.813±0.016	0.730±0.021	0.666±0.020
25	0.815±0.021	0.721±0.022	0.670±0.024
35	0.811±0.018	0.720±0.021	0.656±0.023
45	0.808±0.023	0.717±0.025	0.660±0.020
55	0.809±0.018	0.717±0.023	0.647±0.026

## 5.4 Numerical Results

The numerical results presented in this section include the fading memory model and the FEM developed in this work. All the computations in this section were performed by using MATLAB 7.0, and the computer code is listed in Appendix D.

### 5.4.1 Fading Memory Model

Equation (4.24) describes the initial force response of airway smooth muscle for different finite time durations ( $\Delta t$ ) of shortening. The results of force response ( $T_1/T_0$ ) varied with different finite time durations ( $\Delta t$ ) and length shortening ratio ( $\Delta l/l_0$ ) are given in Table 5.8.

**Table 5.8 Results of the initial force response ( $T_1/T_0$ ) to different finite time durations ( $\Delta t$ ) and length shortening ratios ( $\Delta/l_0$ )**

Length shorten ratio ( $\Delta/l_0$ )	$T_1/T_0$ for Different Finite Time Durations of Shortening		
	$\Delta t = 1$ ms	$\Delta t = 20$ ms	$\Delta t = 50$ ms
0.0010	0.934	0.951	0.966
0.0025	0.846	0.885	0.918
0.0050	0.724	0.787	0.846
0.0075	0.624	0.704	0.782
0.0100	0.541	0.632	0.723
0.0125	0.471	0.570	0.671
0.0150	0.412	0.515	0.623
0.0175	0.360	0.466	0.580
0.0200	0.315	0.422	0.540
0.0225	0.275	0.383	0.504
0.0250	0.240	0.348	0.470
0.0275	0.209	0.315	0.439
0.0300	0.180	0.286	0.411
0.0325	0.155	0.259	0.384
0.0350	0.132	0.235	0.359
0.0375	0.111	0.212	0.336
0.0400	0.091	0.191	0.314
0.0425	-	0.171	0.294
0.0450	-	0.153	0.274
0.0475	-	0.136	0.256
0.0500	-	0.120	0.239
0.0525	-	0.105	0.223
0.0550	-	0.091	0.208
0.0575	-	-	0.193
0.0600	-	-	0.180
0.0625	-	-	0.167
0.0650	-	-	0.154
0.0675	-	-	0.142
0.0700	-	-	0.131
0.0725	-	-	0.120
0.0750	-	-	0.110
0.0775	-	-	0.100
0.0800	-	-	0.090

The force responses of longitudinal vibration can be simulated by using equation (4.31). The result of the force response ( $T/T_0$ ) varied with different frequencies (5 to 75 Hz) and amplitudes (1% to 3% of  $L_r$ ) and is given in Table 5.9. The phase degree from equation (4.31) varied with different frequencies (5 to 75 Hz) and amplitudes (1% to 3% of  $L_r$ ) and is given in Table 5.10.

**Table 5.9 Results of the force response ( $T_i/T_0$ ) to different frequencies and amplitudes.**

Frequency (Hz)	$T/T_0$ for Different Amplitudes of Vibration		
	1.0% of $L_r$	2% of $L_r$	3% of $L_r$
5	0.732	0.551	0.427
15	0.584	0.366	0.237
25	0.555	0.332	0.200
35	0.546	0.321	0.188
45	0.542	0.316	0.183
55	0.540	0.314	0.180
65	0.538	0.312	0.179
75	0.538	0.311	0.177

**Table 5.10 Results of the phase degree to different frequencies and amplitudes.**

Frequency (Hz)	Phase Degree for Different Amplitudes of Vibration		
	1.0% of $L_r$	2% of $L_r$	3% of $L_r$
5	-14.083	-15.658	-36.254
15	-10.782	-20.065	30.874
25	-7.322	-13.854	22.311
35	-5.431	-10.343	-16.979
45	-4.293	-8.200	-13.584
55	-3.541	-6.775	-11.280
65	-3.011	-5.766	-9.629
75	-2.617	-5.015	-8.391

#### 5.4.2 Finite Element Model

The parameters used in the FEM model are tissue density  $\rho$  of 0.001 g/mm<sup>3</sup>, length of tissue is 17.6 mm (from Table 5.1), width of tissue is 2.6 mm (from Table 5.1), Poisson's ratio is 0.45 [22] and original elastic modulus  $E$  is 0.975 MPa (from Table

5.1). The time step size ( $\Delta t$ ) is  $2 \times 10^{-5}$  seconds for both longitudinal and transverse vibrations. The governing equation of the FEM is equation (4.54). The FEM can be used to simulate airway smooth muscle tissue is excitation under longitudinal and transverse vibrations. Both dynamic and static stiffness were calculated to allow comparison with the experimental data.

The variation in stiffness as a function of amplitude and frequency was acquired for the longitudinal vibrations to give in Table 5.10 for dynamic stiffness ( $K_d$ ) and 5.11 for static stiffness ( $K_s$ ). The duration of the vibration was kept at 1 second during the computation, and the range of vibration frequencies was from 5 to 75 Hz with amplitudes of vibration from 1.2% to 6.0% of the reference length during the computation.

**Table 5.11 Results of dynamic stiffness ( $K_d$ ) for the longitudinal vibration to different frequencies and amplitudes.**

Frequency (Hz)	$K_d$ for Different Amplitudes of Vibration				
	1.2% of $L_r$	2.5% of $L_r$	3.8% of $L_r$	4.5% of $L_r$	6.0% of $L_r$
5	0.957	0.922	0.892	0.884	0.838
15	0.931	0.897	0.861	0.840	0.759
25	0.921	0.878	0.840	0.808	0.730
35	0.909	0.863	0.819	0.791	0.715
45	0.885	0.849	0.787	0.760	0.702
55	0.867	0.832	0.781	0.751	0.696
65	0.855	0.819	0.769	0.735	0.702
75	0.835	0.815	0.754	0.734	0.685

**Table 5.12 Results of static stiffness ( $K_s$ ) for the longitudinal vibration to different frequencies and amplitudes.**

Frequency (Hz)	$K_s$ for Different Amplitudes of Vibration				
	1.2% of $L_r$	2.5% of $L_r$	3.8% of $L_r$	4.5% of $L_r$	6.0% of $L_r$
5	0.905	0.848	0.791	0.760	0.694
15	0.882	0.811	0.740	0.701	0.619
25	0.875	0.800	0.724	0.683	0.596
35	0.872	0.794	0.717	0.675	0.585
45	0.870	0.791	0.713	0.670	0.580
55	0.869	0.790	0.711	0.668	0.576
65	0.868	0.789	0.709	0.666	0.574
75	0.868	0.788	0.708	0.665	0.573

The FEM results for different durations of longitudinal vibration are given in Table 5.12 (dynamic stiffness,  $K_d$ ) and 5.13 (static stiffness,  $K_s$ ). The muscle tissues were simulated under at frequencies of 5, 35 and 65 Hz for a time duration of 1, 2, 3 and 5 seconds (same as with the experiments). The amplitude of vibration was kept at 3.8% of the tissue length during the computation.

**Table 5.13 Results of dynamic stiffness ( $K_d$ ) for the longitudinal vibration to different frequencies and time durations.**

Frequency (Hz)	$K_d$ for Different Time Durations of Vibration			
	1 sec	2 sec	3 sec	5 sec
5	0.891	0.847	0.834	0.826
35	0.801	0.786	0.779	0.770
65	0.753	0.731	0.720	0.719

**Table 5.14 Results of static stiffness ( $K_s$ ) for the longitudinal vibration to different frequencies and time durations.**

Frequency (Hz)	$K_s$ for Different Time Durations of Vibration			
	1 sec	2 sec	3 sec	5 sec
5	0.790	0.731	0.712	0.706
35	0.717	0.706	0.706	0.705
65	0.709	0.706	0.706	0.706

The FEM results for different frequencies and length change ratios of transverse vibration are given in Table 5.14 for dynamic stiffness ( $K_d$ ) and 5.15 for static stiffness ( $K_s$ ). Similar to the experimentation, muscle tissues were simulated under the oscillated frequencies from 5 to 55 Hz in steps of 10 Hz, with length change ratios of 2.2%, 3.5% and 4.8% of  $L_r$ , respectively. The time duration of vibration was kept at 1 second during the computation.

**Table 5.15 Results of dynamic stiffness ( $K_d$ ) for the transverse vibration to different frequencies and length change ratios.**

Frequency (Hz)	$K_d$ for Different Length Change Ratios of Vibration		
	2.2% of $L_r$	3.5% of $L_r$	4.8% of $L_r$
5	0.865	0.788	0.728
15	0.815	0.745	0.672
25	0.812	0.732	0.658
35	0.817	0.733	0.653
45	0.815	0.742	0.660
55	0.827	0.754	0.654

**Table 5.16 Results of static stiffness ( $K_s$ ) for the transverse vibration to different frequencies and length change ratios.**

Frequency (Hz)	$K_s$ for Different Length Change Ratios of Vibration		
	2.2% of $L_r$	3.5% of $L_r$	4.8% of $L_r$
5	0.839	0.772	0.705
15	0.814	0.737	0.661
25	0.809	0.730	0.651
35	0.807	0.727	0.647
45	0.806	0.726	0.646
55	0.806	0.725	0.645

## **Chapter 6**

### **Discussion**

#### **6.1 Introduction**

All the results on this work are given in the previous chapter; however, this chapter will give some rational and physical explanations to the behaviours observed in both experimental and theoretical investigations.

Although there are several postulations on the mechanics of airway smooth muscles, none of them gives full description of why airway smooth muscle reacts to vibration. This research is an attempt to determine (1) whether airway smooth muscle can be relaxed by vibration and (2) the main variation which affects such a relaxation.

The main contributions from this research are:

1. The introduction of the dynamic and static stiffness parameters to explain the dynamic and static behaviours of airway smooth muscle.
2. Demonstrate that airway smooth muscle can be relaxed by vibration.

3. Determine the specific vibration parameters such as the time duration, amplitude and frequency of oscillation on the amount of muscle relaxation.
4. Develop an FEM model to generalize the effect of vibration to determine the stiffness variation.

Although the objectives of the first three points above are clear, the fourth one needs some clarifications. In normal FEM, an attempt is made to determine the eigenvalues and eigenfunctions of a well defined system. However, in the present work the eigenvalues and eigenfunctions are not available and we are more interested in determining the system stiffness.

## **6.2 Longitudinal Vibration Experiments**

In this set of experimental investigations, two parts of experimentation were conducted. First for a constant time duration of oscillation (1 second), the frequencies and amplitudes of the longitudinal oscillation were varied. The second part of the experiments was to inspect the response of the active smooth muscle stiffness over different time durations with oscillations. In this case, the amplitude of oscillation was kept at 3.8% of reference length  $L_r$ . Two samples of the experimental results for both scenarios are presented in Figure 6.1 (constant time duration) and 6.2 for (different time durations).

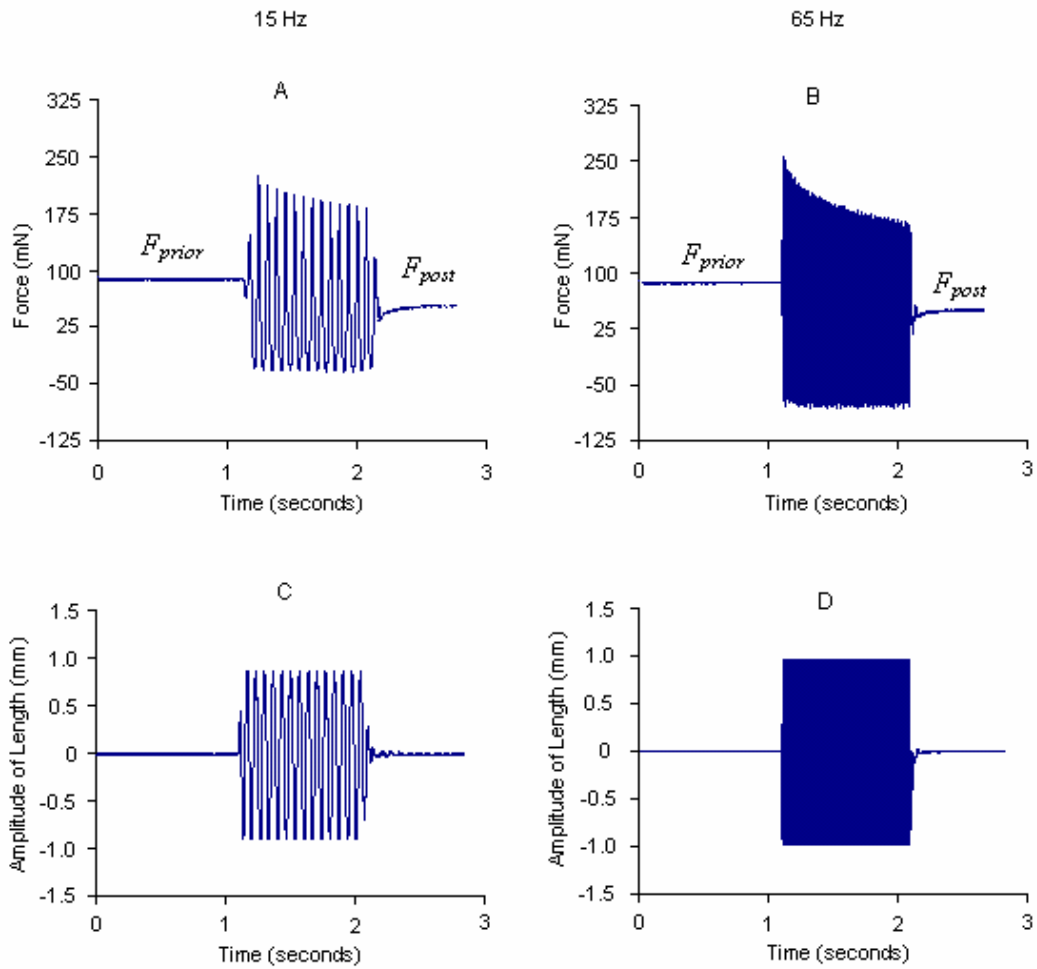


**Figure 6.1** Longitudinal vibrations reduce force and stiffness during isometric contraction. Forces (A and B) and amplitudes of length (C and D) were recorded during isometric contraction. The smooth muscle tissue excited with 15 Hz is shown on the left hand side (A and C), the tissue excited with 65 Hz is shown on the right hand side (B and D). The amplitude of both excitations was 3.8% of the reference length  $L_r$ . Conditions:  $T = 37\text{ }^\circ\text{C}$  and  $\text{pH} = 7.7$

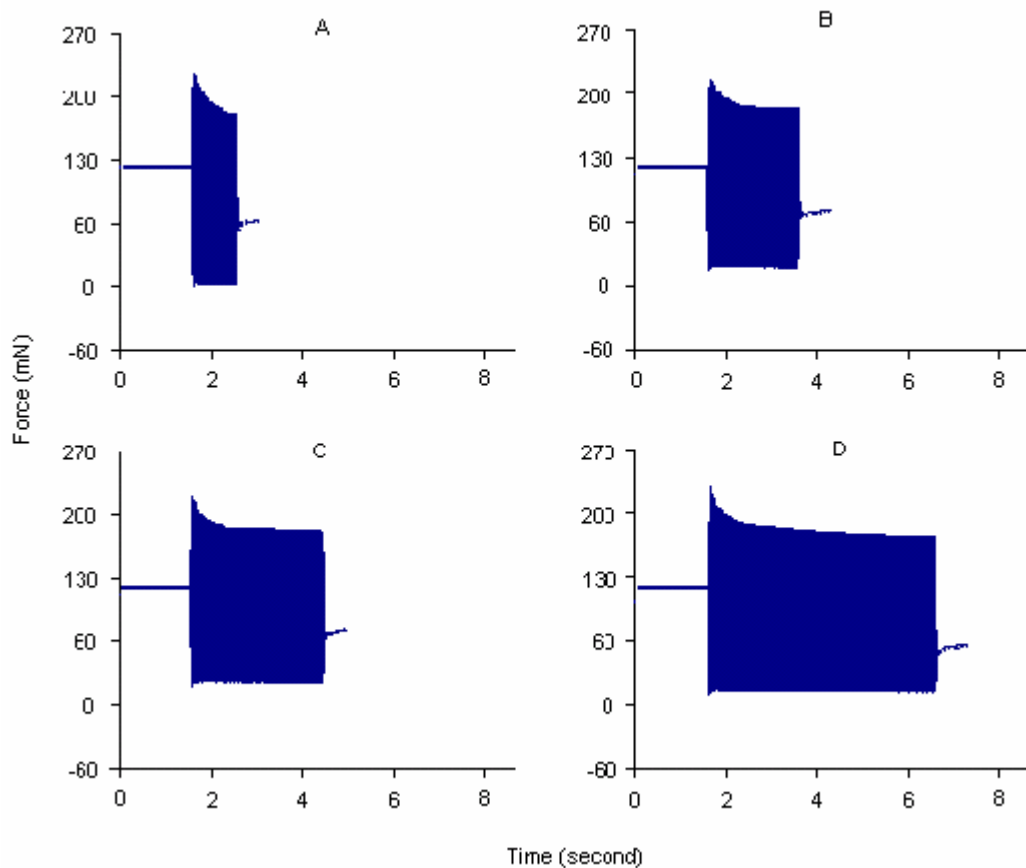


**Figure 6.2** Longitudinal vibrations reduce force during isometric contraction under different durations of vibration: 1 second (A), 2 seconds (B), 3 seconds (C) and 5 seconds (D). All of the vibrations are at a frequency of 35 Hz and with amplitude of the vibration of 3.8% of  $L_r$ .

### 6.2.1 Constant Time Duration of Vibration

In Figure 6.1 with the amplitude of vibration at 3.8% of the reference length  $L_r$ , the muscle tissues were excited at 15 and 65 Hz respectively. After vibration, the measured force (post force,  $F_{post}$ ) was lower than the force before the vibration was applied (prior force,  $F_{prior}$ ). The effect of this force reduction indicates that the muscle is relaxed. This may be attributed to that the external vibration that change the physical position between and myosin filaments and this position change could physically disrupt the attachment of cross-bridges.

On the vibration time scale, the decreasing force response to successive length cycles is seen to be an exponential decline (i.e. the peaks of the sinusoidal wave could be fitted by a single exponential function). The force reduction occurs only temporary and then the lower force ( $F_{post}$ ) gradually returns to the original level force ( $F_{prior}$ ) when the vibration is stopped. This could be explained by the fact that the stimulation of smooth muscle contraction is unaltered during the experiment. The dynamic stiffness ( $K_d$ ) varies with different frequencies for various amplitudes (in percentage of the reference length  $L_r$ ) and the results are shown in Figure 6.3 using data from Table 5.2. Similarly, Figure 6.4 displays the static stiffness ( $K_s$ ) as it varies with different frequencies and amplitudes using data from Table 5.3.

In general, from Figure 6.3 and 6.4, it can be seen that the applied vibrations reduce the stiffness of contracted airway smooth muscle. Figure 6.3 shows that as the frequency increases the dynamic stiffness ( $K_d$ ) continuously decreases, while as the frequency increases the static stiffness ( $K_s$ ) (Figure 6.4) decreases exponentially to about 25 Hz, when it becomes constant. Both Figure 6.3 and 6.4 indicate that increasing the amplitude of vibration results in a decrease in the muscle stiffness. Furthermore, it can be seen that the muscle dynamic stiffness can be reduced to approximately one third and the static stiffness to three fifths of the relaxed state.

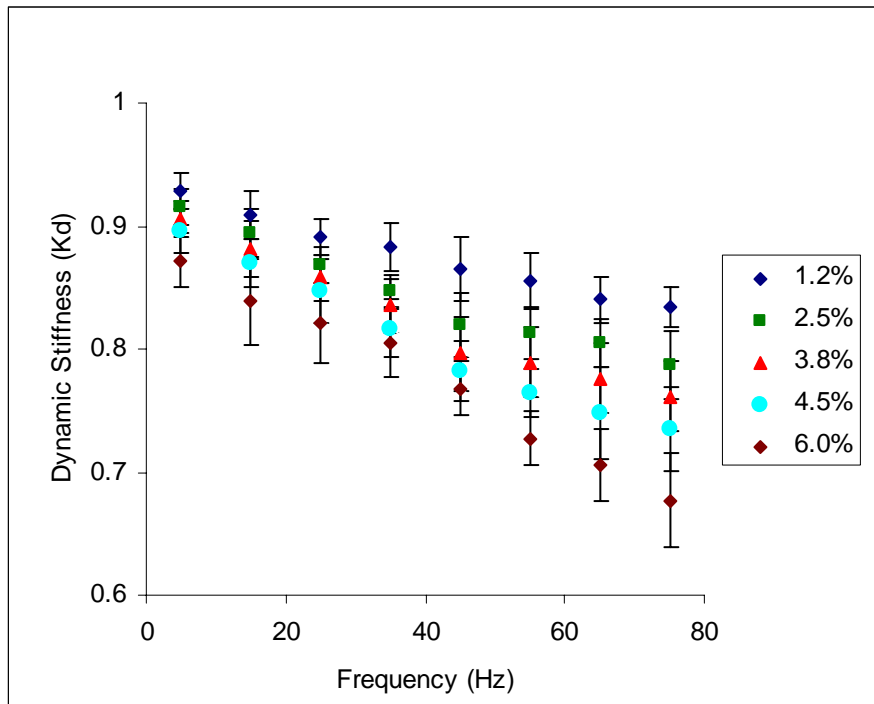


**Figure 6.3** Dynamic stiffness versus vibration frequencies, mean values  $\pm$  95% confidence interval ( $n = 11$ )

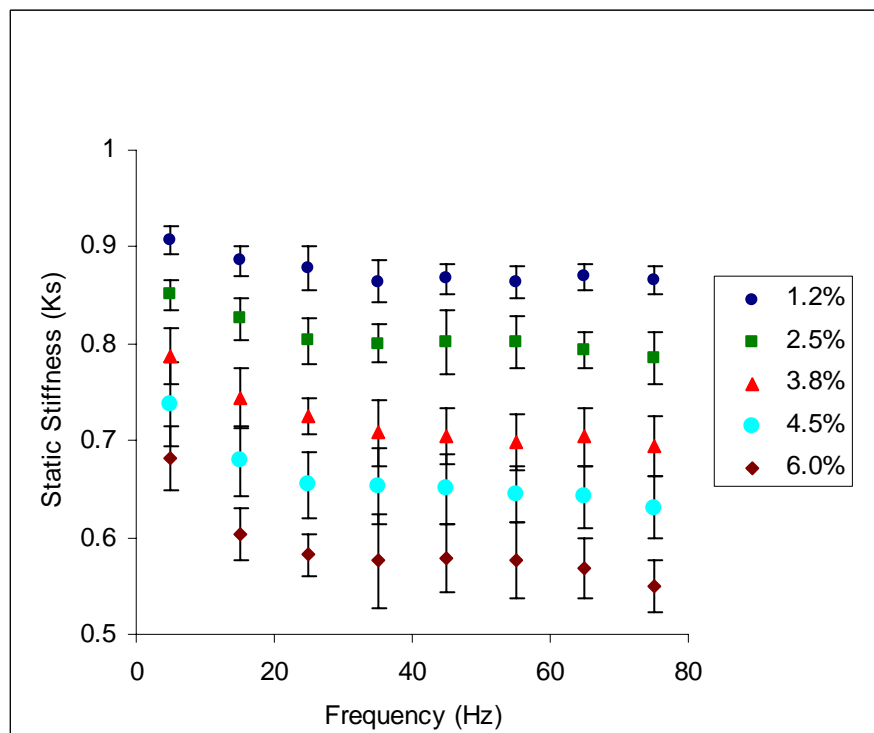


**Figure 6.4** Static stiffness versus vibration frequencies, mean values  $\pm$  95% confidence interval ( $n = 11$ )

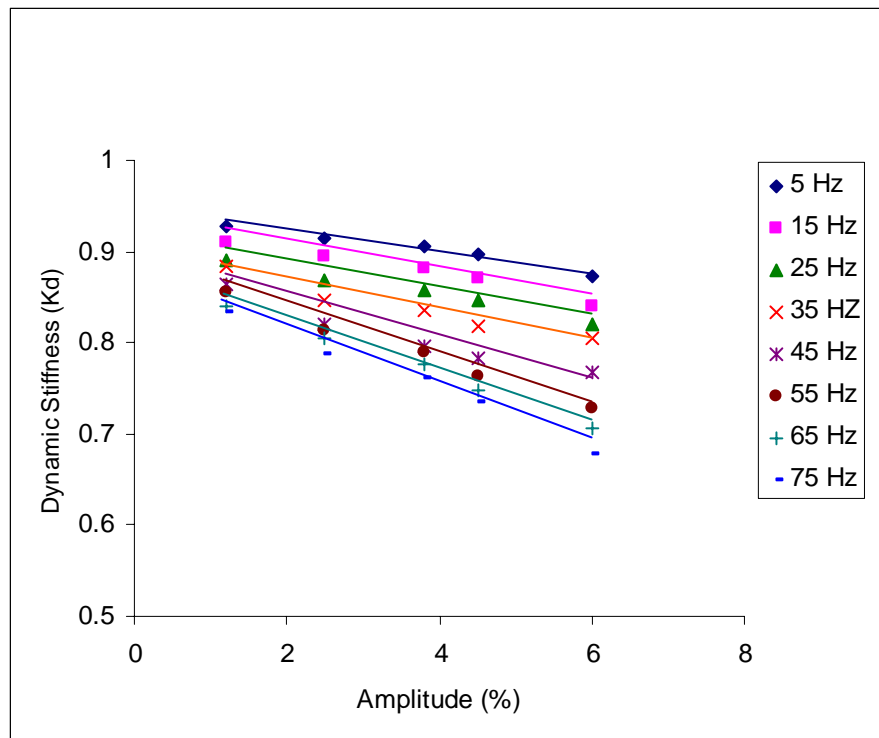
The dynamic stiffness describes the instantaneous effect of muscle stiffness during the episode of the oscillation. This dynamic behaviour reflects the active contractile mechanism, viscoelastic properties and inertia of tissue mass. However, the static stiffness does not deal with changes that occur in the episode of oscillation, and only represents the consequent effects of the episode. Therefore, the static stiffness is natural to reflect the net variation in muscle contractile mechanism after vibration has been applied. Figure 6.4 shows the static stiffness for oscillations, which indicates that the amplitude is the main factor in determining the stiffness change. While the static stiffness is also dependent on the frequency of vibration, this dependence is only at lower frequencies. The reason for these results is determined by the cross-bridge dynamic property, a hypothetical expansion which is discussed in following section.

If a smooth muscle tissue is stimulated in isometric contraction, the myosin-actin cycling begins and the number of interactive cross-bridges increases. Meanwhile, the phosphorylation and the rate of ATP consumption increase abruptly [32 and 48]. The cross-bridges then approach a steady state level called the latch state. In the latch state, the rate of cross-bridge cycling has decreased to its smallest value, and the active force has increased to its maximum attainable value. This value of the active force is depended on the force-length characteristic of the muscle (see Figure 2.2 and 2.4). Comparing the active force development, the phosphorylation and rate of ATP consumption decrease and are maintained at a lower level in the latch state. When oscillating the length of the tissue, the latch state is broken and the myosin-actin cycling increases again. This oscillation does not affect the phosphorylation level. However, the attached dephosphorylation cross-bridge (latch bridge **AM**) and the attached phosphorylation cross-bridge (**AMp**) numbers reduce, and the detached dephosphorylation cross-bridge (**M**) and the detached phosphorylation cross-bridge

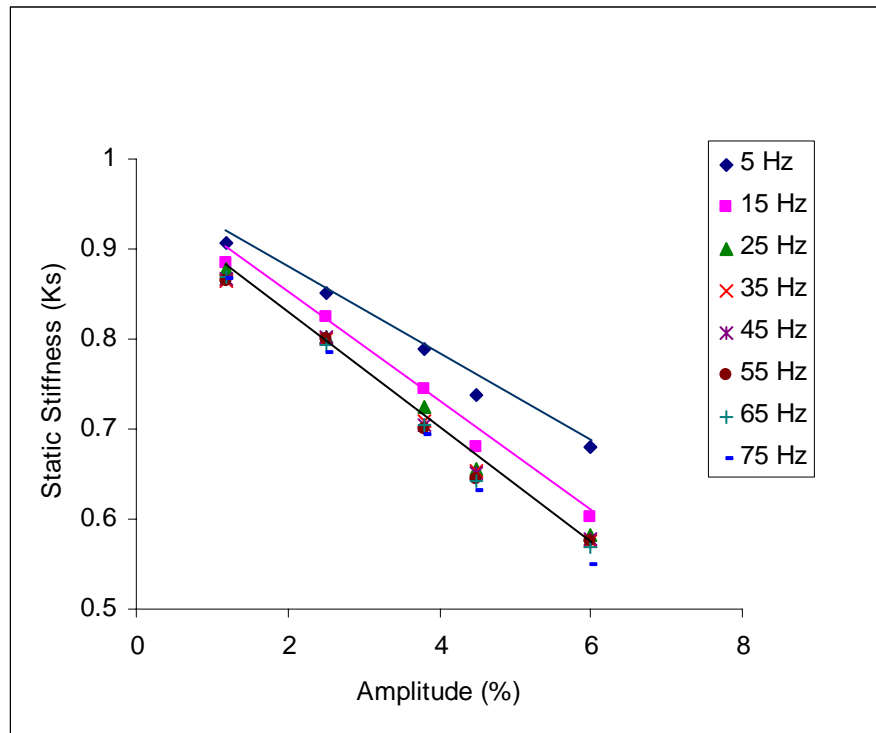
(**Mp**) numbers increase [63 and 101] (see Figure 2.15). This means that the total number of cross-bridge attachments is decreasing. This decrease depends on the amplitude of the oscillation. The larger amplitude causes a greater decrease in cross-bridge attachment. At the same time, the rate of ATP consumption is increasing, which indicates that the cross-bridges are more active (increase in cross-bridge cycling rate) in adapting to a new length. This myosin-actin cycling rate can be regarded as the recovery time, for which higher cycling rate results in a shorter recovery. This cycling rate is determined by the muscle shortening velocity and length. The amplitude of oscillation determines the number of disrupted cross-bridges, and if the frequency is less than the cycling rate, the disrupted cross-bridges receive some time to recover. However, if the frequency is beyond the myosin-actin cycling rate, these disrupted cross-bridges never recover. This is why, for given amplitudes, the force changes are almost the same at higher frequency ranges (above 25 Hz, see Figure 6.4). In this case, the reduction of stiffness (or force) is only determined by the amplitude of vibration. Mijailovich [63] used the four-state latch-bridge model integrated with Huxley's sliding filament model [20] to simulate the smooth muscle tissue as subjected to an external oscillation within the frequency range of 0.01 to 10 Hz. The results show that the contracted force decreases with both increasing amplitude and frequency of oscillation, but the force decrease is diminished when the frequency is greater than 5 Hz. They explained that the **AMp** and **AM** cross-bridges have enough time to adapt to a new length at low frequencies but not at higher frequencies. Our data confirm their simulation.

Figure 6.5 and 6.6 show the effect of the amplitude of external excitations on the dynamic and stiffness respectively. It is clearly indicated that the amplitude of vibration has significant influence on both static and dynamic stiffness. Both figures show a decrease in muscle stiffness with increasing amplitude of vibrations. They also indicate

that this relationship is almost linear. For the dynamic stiffness (Figure 6.5), the gradient becomes steeper for higher frequencies. However, for the static stiffness (Figure 6.6), the result can be approximated by three different straight line segments (upper, middle and lower line) for 5, 15 and 25 Hz and above, respectively. As indicated by the lower line, there is insignificant effect for frequencies above 25 Hz. Also, it can be seen that the gradient of the lower line also is steeper than the other two lines.



**Figure 6.5 Dynamic stiffness versus amplitude of vibration.**



**Figure 6.6** Static stiffness versus amplitude of vibration.

### 6.2.2 Different Time Durations of Vibration

Figure 6.2 shows four different time durations: 1 second (A), 2 seconds (B), 3 seconds (C) and 5 seconds (D); the frequency of vibrations was 35 Hz, and the amplitude was 3.8% of the reference length. It is clearly indicated that the force changes are most significant in the first second. After this initial rapid decrease in force, the forces remain almost constant except for a duration of 5 seconds. Where, there is a slight reduction in the force after the initial rapid change.

The dynamic stiffness ( $K_d$ ) varies with different time durations for various frequencies and are shown in Figure 6.7 using data from Table 5.4. The static stiffness ( $K_s$ ) varies with different time durations and frequencies and is shown in Figure 6.8 using data from Table 5.5. Generally, both stiffness (excluding 5 Hz) seem to remain constant for vibration times of up to 3 seconds, showing only a slight decrease at 5 seconds. For the

latter, the stiffness decreases with increasing vibration times, but this decrease is at a diminishing rate. For dynamic stiffness calculation, the stiffness reductions are also dependent on the frequency. The reduction increases with increasing frequency (Figure 6.7). However, for the static stiffness calculation, the reductions are almost the same for 35 and 65 Hz, and the smaller reduction is for 5 Hz (Figure 6.8). These results are similar to the results given in Figure 6.3 and 6.4.

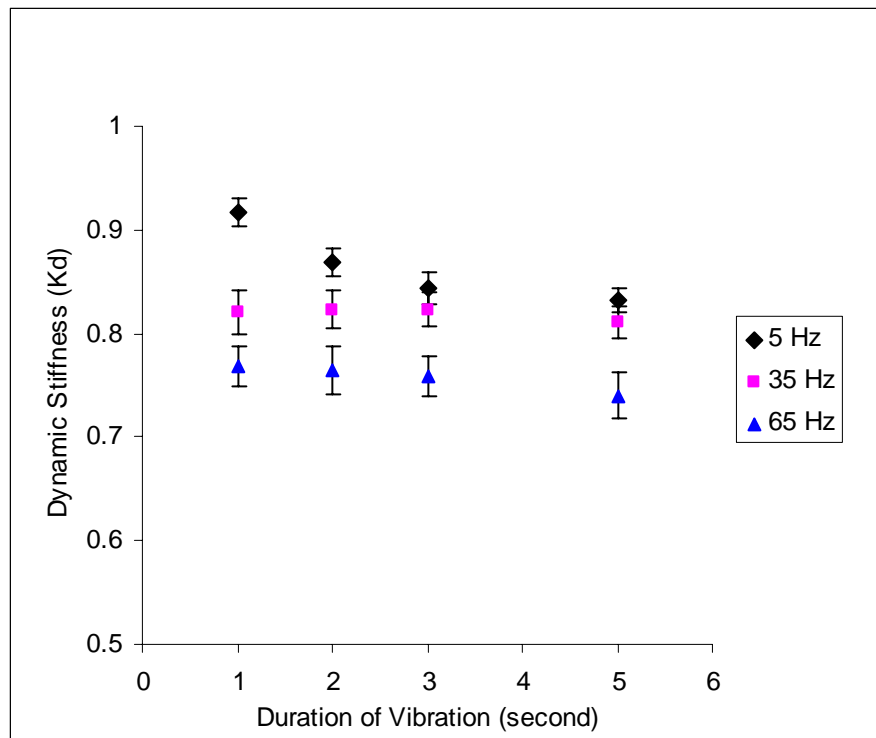


**Figure 6.7** Dynamic stiffness versus durations of vibration, mean values  $\pm$  95% confidence interval ( $n = 6$ ), the amplitude is 3.8% of  $L_r$

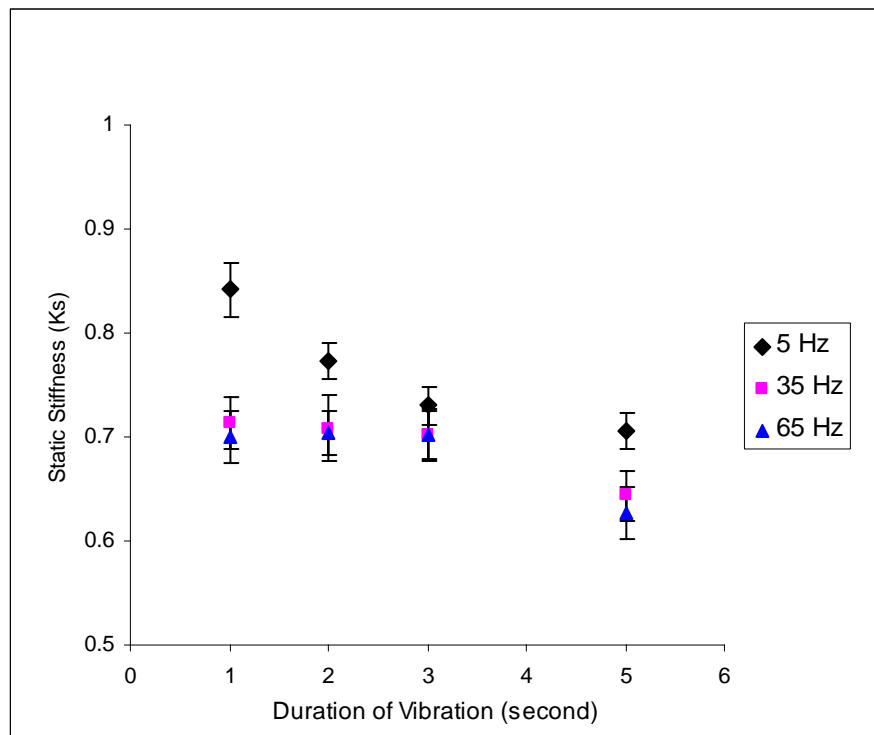


**Figure 6.8** Static stiffness versus durations of vibration, mean values  $\pm$  95% confidence interval ( $n = 6$ ), the amplitude is 3.8% of  $L_r$

### 6.3 Oscillation Cycles Affect Cross-Bridges

One oscillation cycle can be divided into two phases: a stretching phase to lengthen the muscle tissue and shortening phase to shorten the tissue. Figure 6.1 and 6.2 show that the exponential decline in peak force during a vibration episode only occurs in the stretching phase (top part). The peak forces in the shortening phase remain at a constant level (bottom part). This phenomenon may be explained on the basis of cross-bridge mechanisms which are discussed briefly below.

During the stretching cycle oscillations, the individual cross-bridges detach when the stretching forces were larger than the cross-bridge attaching forces. These stretching forces also partly act against the elasticity of actin, myosin and cross-bridges, cell membranes and connective tissues. The population of attached cross-bridges therefore

became smaller. This lesser population of attached cross-bridges results in a reduction in force and stiffness. In the mean time, the detached cross-bridges reattach to the actin again, but this reattachment was not complete since the oscillation was continued. The lesser population of attached cross-bridges was evident in the next stretching cycle. Thus, it was less able to cause individual cross-bridges to become overstressed and fewer cross-bridges were broken during this cycle. The number of broken cross-bridges still increases in the following cycles. However, each subsequent cycle becomes less effective in breaking cross-bridges until a steady state is reached. As the result, the top peak forces display an exponential decline. Obviously, the rate of reattachment is inversely proportional to the frequency of oscillation in a lower range, but is not affected at high frequencies. The process time from the beginning to a reached steady state is also inversely related to the frequency of oscillation; lower frequencies lead to a longer process time. One second of process time is shown in Figure 6.2 for 35 Hz. This why in this work, the results show no effect at higher frequencies but a notable effect at lower frequencies (e.g. 5 Hz) for different time durations of vibration (see Figure 6.7 and 6.8). Increasing the vibration amplitude at this point would lead to a higher rate of detachment and a lower steady-state force response (see Figure 6.4).

Each shortening cycle is regarded as a quick release with a length step (see Figure 2.5), and the muscle force fell abruptly to very low levels (at times with negative values) during the shortening cycles. This low level force was determined by the amplitudes and frequencies of vibration. The amplitude is the extent of the shortening needed to determine the extent of the initial fall in the force. However, the frequency reflects the time of shortening needed to determine the inertial force of tissue mass and the rate of cross-bridge reattachment. Higher frequencies create greater inertial forces on the tissue, and the rate of cross-bridge reattachment is inversely proportional to the frequency of

oscillation. The negative peak forces indicated the very high inertia and lower rate of reattachment during the experiments. These cases mostly occurred at very high frequencies. Thus, for a given amplitude and frequency, the bottom peak forces in the shortening phase were almost at the same level.

The fading memory model enhances the above explanation for the shortening phase. Figure 6.9 shows the results from Table 5.8 during which the muscle tissue initial force response varies for different shortening lengths and times (see section 4.3.2 in Chapter 4). The muscle length is suddenly changed to a new fixed length and a part of the attached cross-bridges are disrupted. These disrupted cross-bridges immediately start to reattach to the actin. The rate of reattachment is dependent on the rate of cross-bridge cycling and time. In contrast, the rate of cross-bridge cycling is dependent on the biophysical event, such as the shortening velocity and length. Figure 6.9 could be explained in that under the same length shortening, the shortening time causes a higher shortening velocity. This higher shortening velocity results in a faster cross-bridge cycling rate which causes a higher rate of reattachment. However, short shortening time does not give a sufficient time for the cross-bridge reattachment. The inverse process is performed at a longer shortening time. Based on this, the rate of cross-bridge cycling and duration of time are contradictory. Figure 6.9 indicates that the time duration of shortening is a more important fact of in determining the force reduction rather than the rate of cross-bridge cycling. As a result, a short time duration causes a larger degree of force reduction.

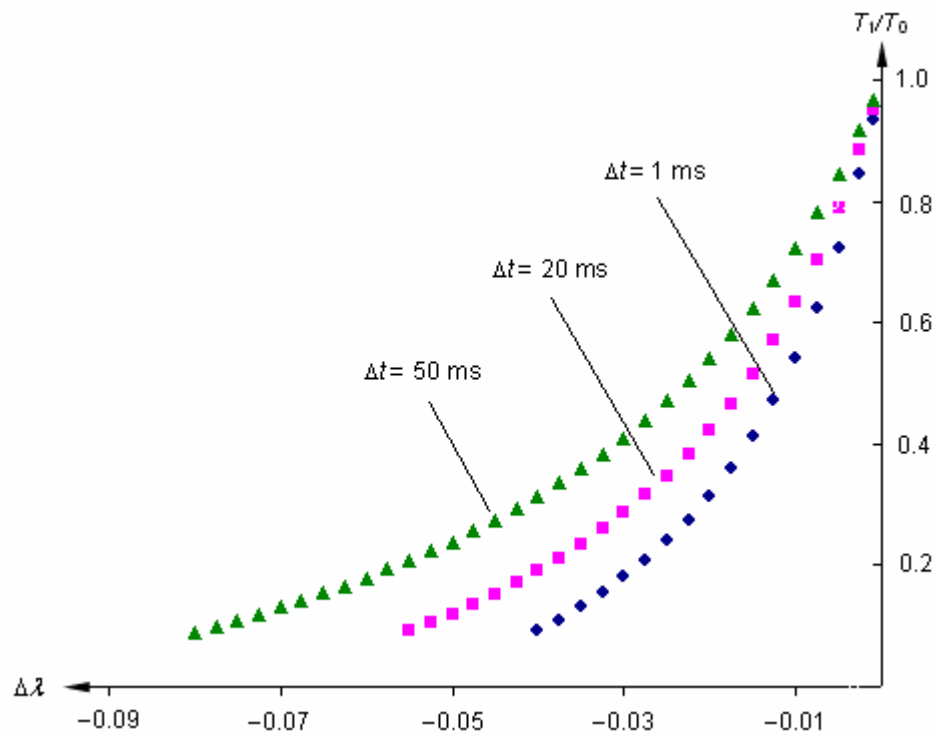


**Figure 6.9** Effects of the initial force response ( $T_1/T_0$ ) to different shortening times ( $\Delta t$ ) and length shortening ratios ( $\Delta\lambda$ ).

The cross-bridge contractile mechanism plays an important role in the oscillation cycles. However, non-cross-bridge mechanisms (connective tissues, cell membranes etc.) also play a role in regulating the effects of length oscillations on smooth muscle contractility. Mijailovich et al. [88] uniaxially oscillated lung tissue in the passive state and found that the elastance of fibrous networks slightly increases with an increasing frequency of oscillation and decreases with an increasing amplitude of oscillation. In contrast, the hysteresivity of fibrous networks decreases with an increasing frequency of oscillation and increases with an increasing amplitude of oscillation. Therefore, contractile and non-contractile components of smooth muscles also possess viscoelastic characteristics which may affect the mechanical response of airway smooth muscle to length oscillations.

## 6.4 Empirical Equation of the Stiffness for the Finite Element Model

The governing equation of the FEM is derived in Chapter 4 (see equation (4.54)) and the stiffness  $[K(t, f)]$  can be experimentally determined from the experimental data. After summarizing section 6.2 and 6.3, the stiffness  $[K(t, f)]$  in equation (4.54) can be proposed as:

$$[K(t, f)] = \exp\left(\frac{\sqrt{f}}{a}t\right) \cdot k_1[K] + k_2[K] \quad (6.1)$$

where  $f$  is the frequency of oscillation,  $t$  is the time duration of oscillation,  $a$  is a constant ( $a = 1.8$ ),  $[K]$  is original contracted stiffness (before vibration, see Table 5.1) and  $k_1$  and  $k_2$  are coefficients determined by:

$$\begin{aligned} k_1 + k_2 &= 1 \\ k_2 &= -0.62A_a + 0.94 \end{aligned} \quad (6.2)$$

We assume the coefficient  $k_2$  is linear with the amplitude of vibration ( $A_a$ , in percent) from the lower slope line in Figure 6.6. The first term on the right side of equation (6.1) represents the reduction in stiffness causing by the external oscillation. This term involves both frequency ( $f$ ) and time ( $t$ ) variables. The second term at the right side of equation (6.1) expresses the remaining stiffness caused by the vibration. Equation (6.1) reflects the muscle active stiffness as a function of frequency and duration time. Equation (6.1) also shows that the airway smooth muscle material is nonlinear, and such as closed form-solutions (e.g. beam model) were disregarded in this research.

As discussed in section 6.3, the cross-bridge mechanism has different working behaviours in the stretching and shortening phase. To match these different behaviours, two different methods for computation were used in the FEM model. For each stretching phase, the computation uses the same equation as equation (6.1). However, the equation used for each shortening phase is:

$$[M]\{\ddot{d}\} + k_2[K]\{d\} = \{F\} \quad (6.3)$$

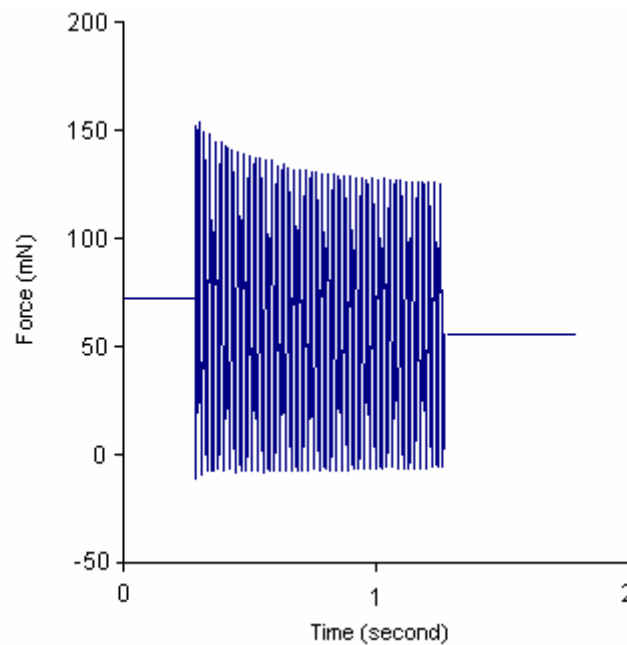


**Figure 6.10** FEM model simulates the longitudinal vibration with frequency 45 Hz and amplitude 3.8%.

We assume that the muscle force falls abruptly to the minimum force ( $T_1$ ) during each shortening phase. Thus, the stiffness for each shortening phase can be approximately considered as the remaining stiffness, which is more closely related the real event. The result of the FEM model for a tissue oscillated at a frequency 45 Hz, amplitude 3.8% of the length and the time duration is 1 second is shown in Figure 6.10. Compared to

Figure 6.1, the FEM model provides a good simulation for airway smooth muscle tissue excited under external vibrations.

## **6.5 Comparison of Experimental and Numerical Results for the Longitudinal Vibration**

Figure 6.11 show dynamic stiffness ( $K_d$ ) for both experimental (top) and FEM (bottom) results, with various frequencies and amplitudes. The general tendencies of both results are same. As the frequency increases the dynamic stiffness continuously decreases. Clearly, the data for an amplitude of 1.2% and 3.8 % is more closed matched between the experiment and FEM compared to the amplitude of 6.0%. This may be attributed to two factors: the uncertainty and viscoelasticity of tissue may have more affect for larger amplitudes of oscillation. Figure 6.12 show static stiffness for both experimental (top) and FEM (bottom) results. Since the static stiffness only reflects the net variation in muscle contractile mechanism, both the experimental and FEM data is close.

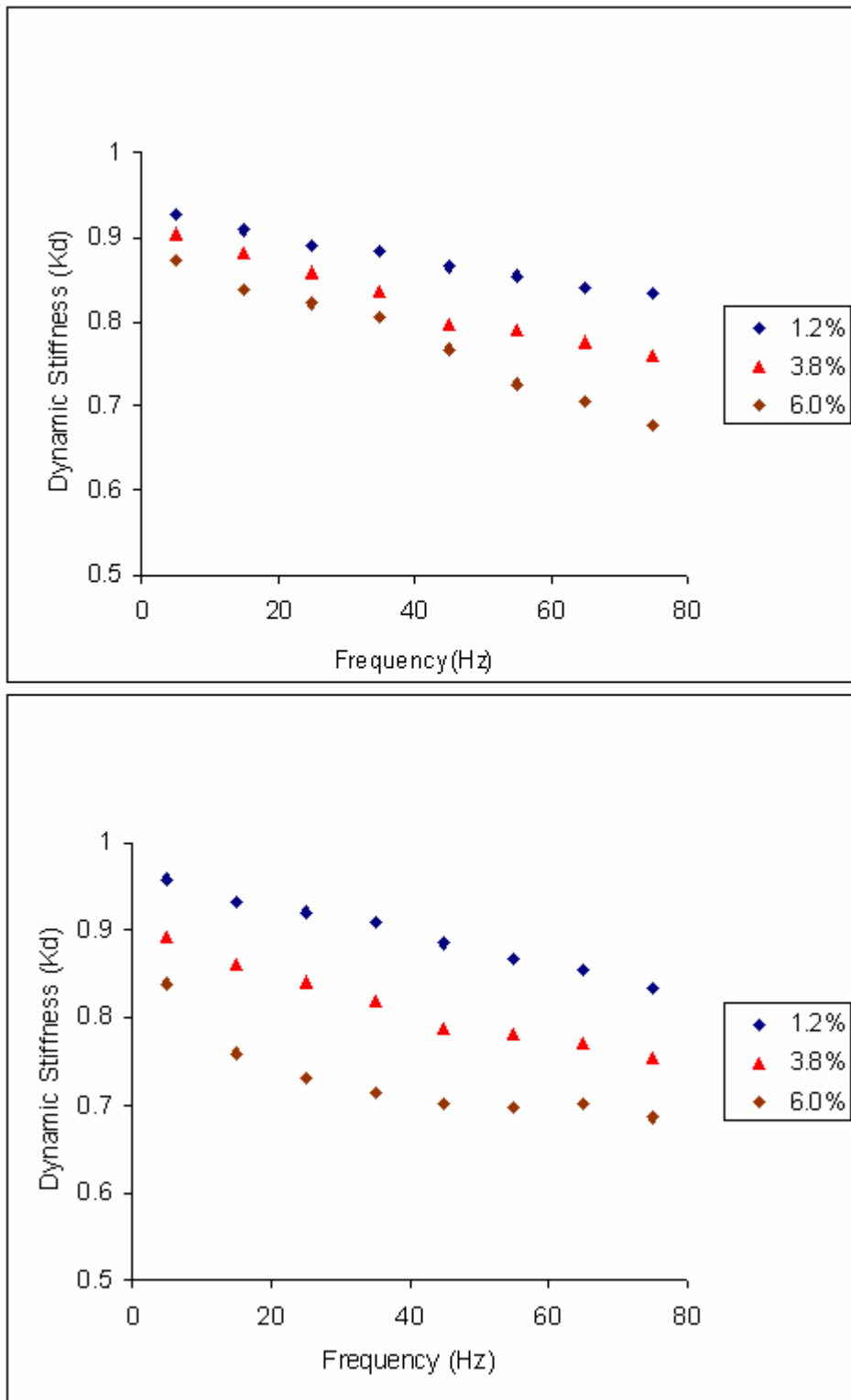


**Figure 6.11 Experimental (top) and FEM (bottom) dynamic stiffness versus frequencies for the longitudinal vibration.**

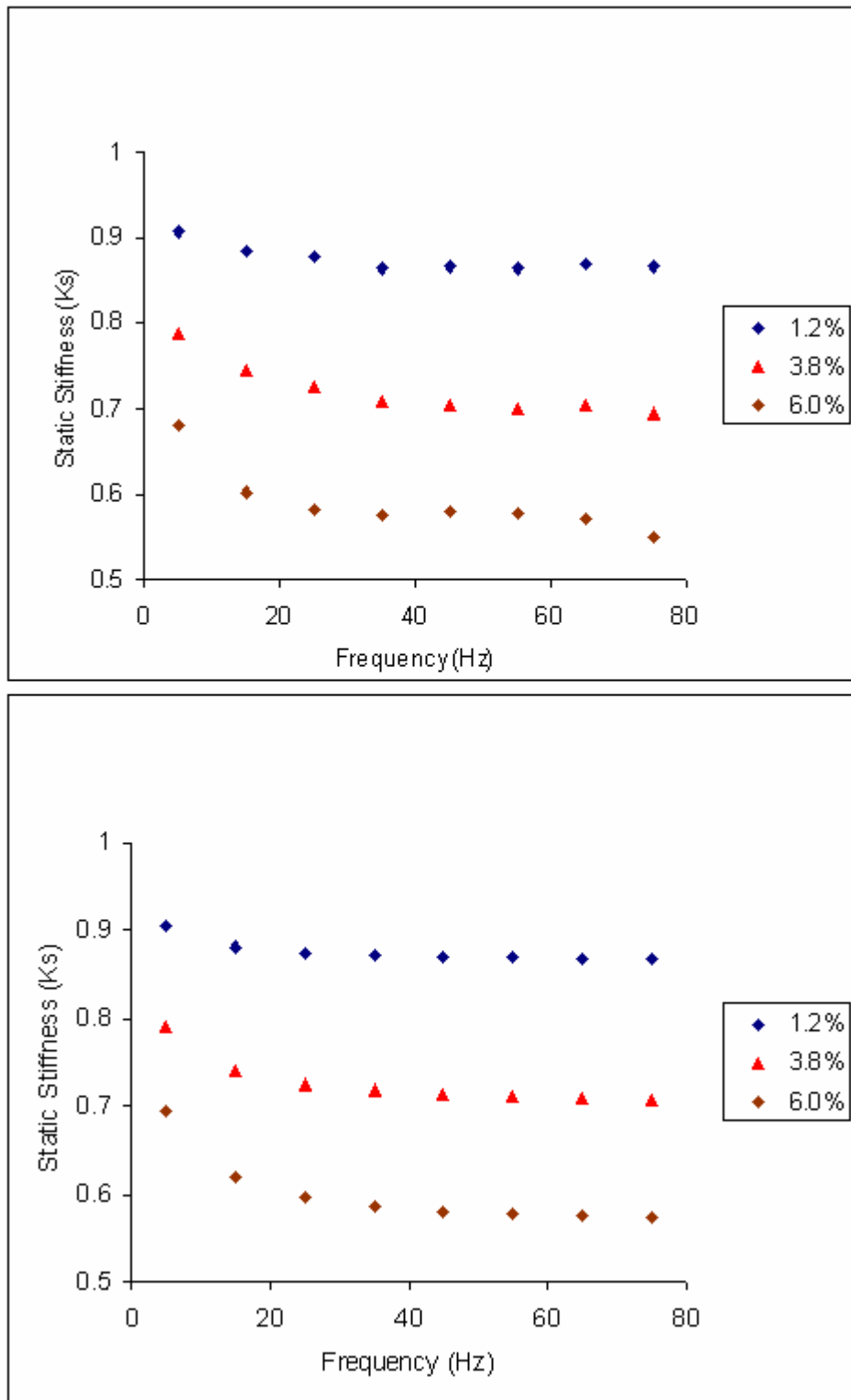


**Figure 6.12** Experimental (top) and FEM (bottom) static stiffness versus frequencies for the longitudinal vibration.

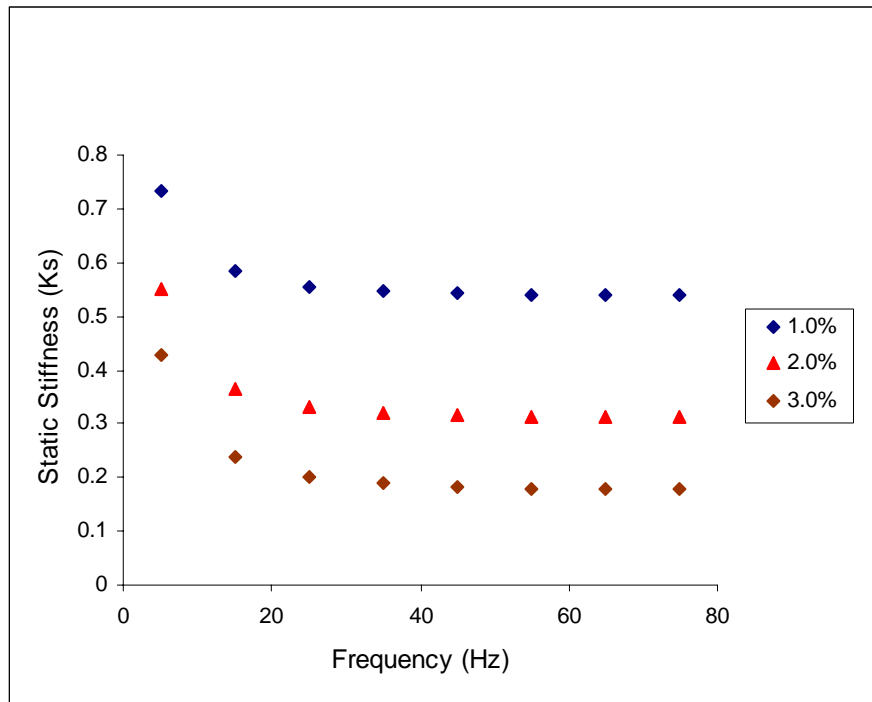


**Figure 6.13 Stiffness from the fading memory model versus frequencies for the longitudinal vibration.**

The fading memory model can simulate the experiment of longitudinal vibration in this research (see section 4.3.3 in Chapter 4) and the results were given in Table 5.9 (Chapter 5). Since the fading memory only considers the cross-bridge kinetics and does not involve the tissue inertia and viscoelasticity, the force response ( $T/T_0$ ) can be regarded as the static stiffness. The results of this model are shown in Figure 6.13. The general tendency of the results indicates that the stiffness decreases exponentially with increasing frequency until 25 Hz where almost no variation is obtained after that. Figure 6.13 also shows that the stiffness decreases as the amplitude of vibration increase. These characteristics are identical to those of Figure 6.12. As mentioned before, the fading memory model can not quantitatively simulate biophysical events, but can still qualitatively interpret certain biophysical processes.

The comparison of different time durations between the experiments and FEM are shown in Figure 6.14 (dynamic stiffness) and 6.15 (static stiffness). Both figures indicate good agreement between the experimental and FEM data.

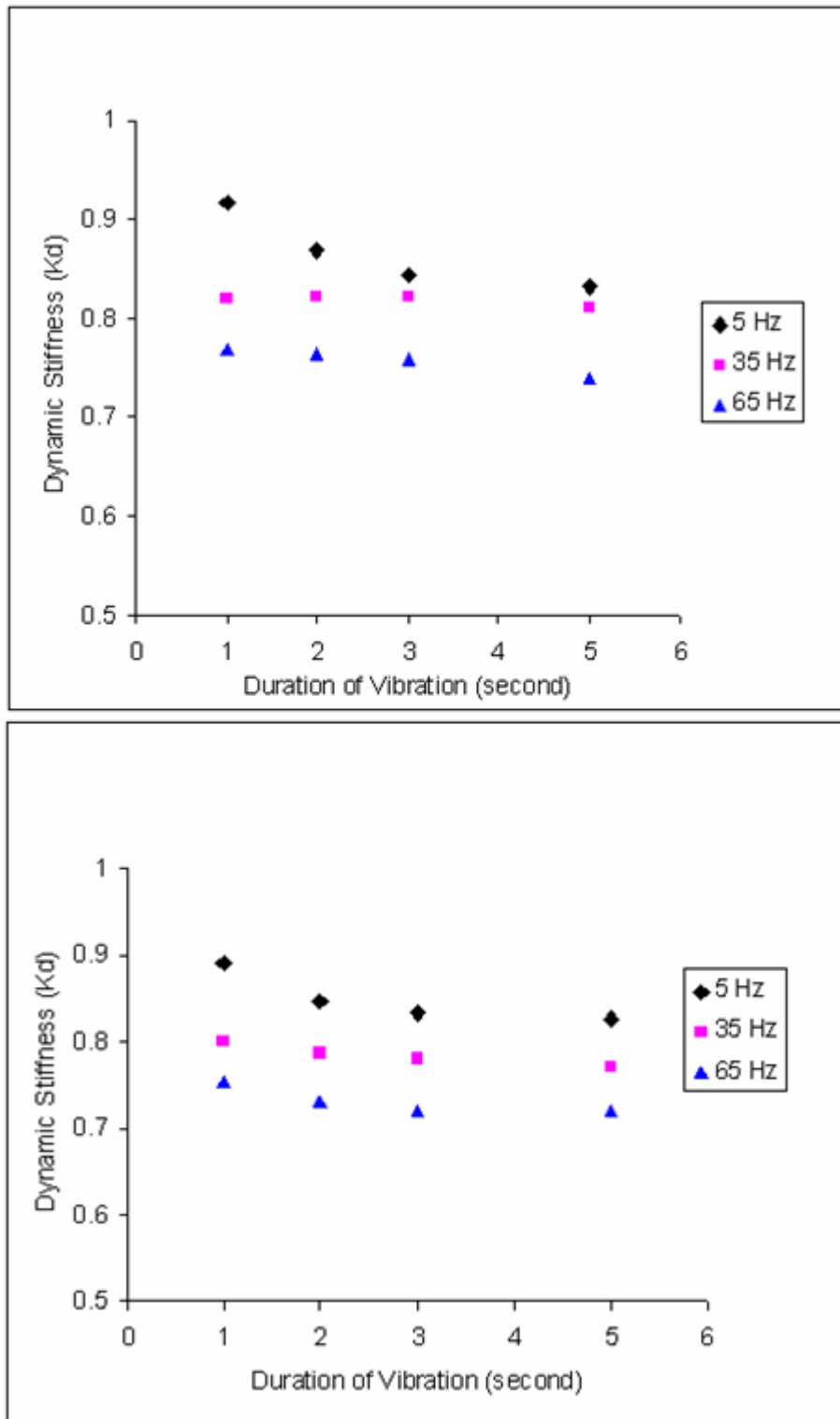


**Figure 6.14** Experimental (top) and FEM (bottom) dynamic stiffness versus durations for the longitudinal vibration.

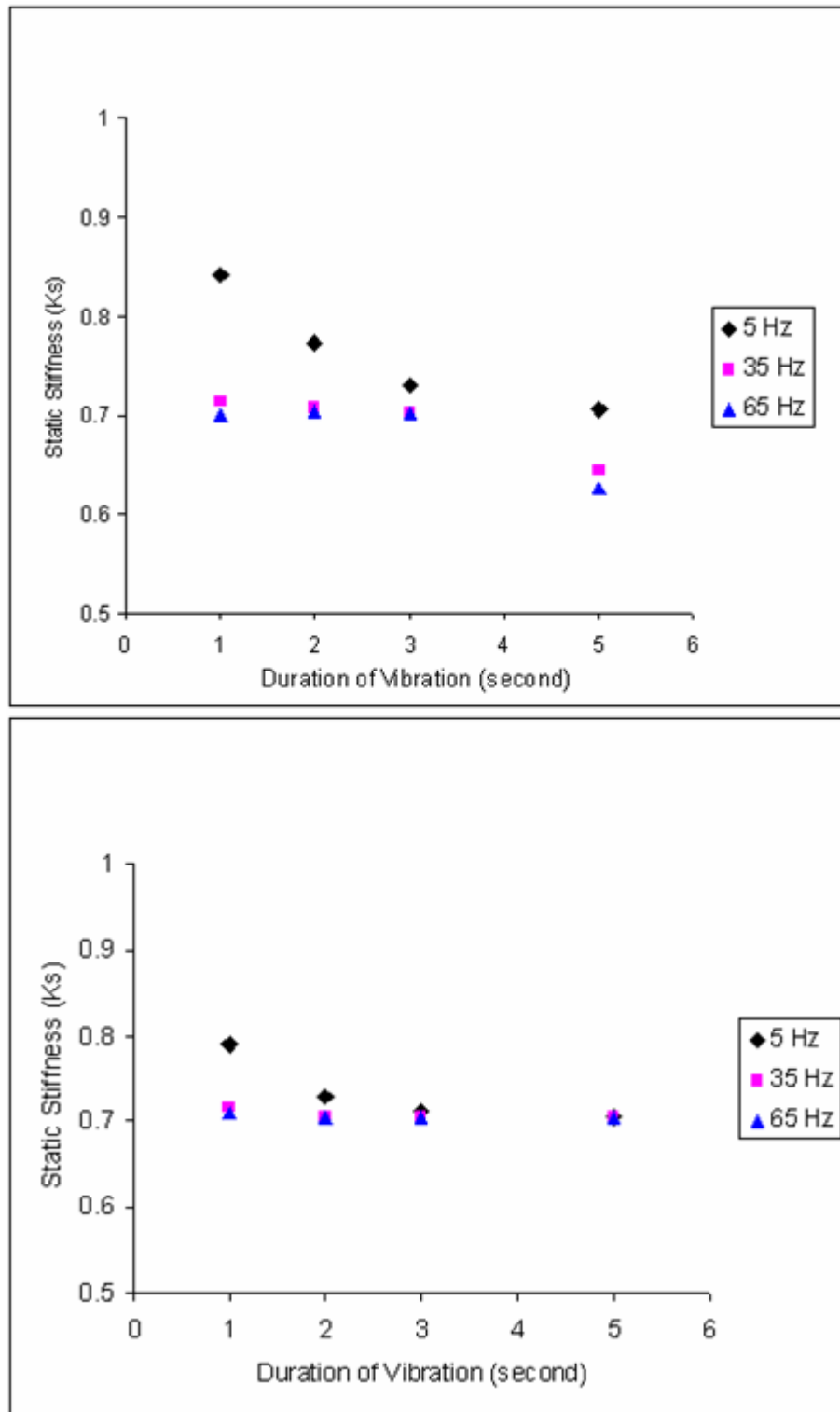


**Figure 6.15** Experimental (top) and FEM (bottom) static stiffness versus durations for the longitudinal vibration.

## 6.6 Compare Experimental and FEM Results for the Transverse Vibration

Typical results of experiments for the transverse vibration are shown in Figure 6.16. This figure shows the experimental results when the length change ratio of vibration was 4.8% of the reference length ( $L_r$ ). The left hand side of the figure (A and C) shows that muscle tissue excited at 5 Hz, and the right hand side of the figure (B and D) shows that the muscle tissue excited at 25 Hz, for a duration of between 1 – 2 seconds. From Figure 6.16, it is clearly indicated that the muscle tissue force after vibration (post force  $F_{post}$ ) was lower than the force before vibration (prior force  $F_{prior}$ ). This force reduction indicates that the disrupted cross-bridge linkage during the vibration is the same as for the longitudinal vibration.

The difference between the longitudinal and mechanical transverse vibration is that, for the former vibration, the frequency and amplitude exactly reflect the tissue length change frequency and ratio, and for the latter, the muscle tissue is lengthened twice during one frequency cycle (see Figure 3.9 in Chapter 3). This means that the tissue length change frequency was twice that of the vibration frequency. This phenomenon is shown in Figure 6.16A and 6.16C. Also, the frequency  $f$  in equation (6.1) is double the frequency of the oscillation in the FEM computation for the transverse vibration.

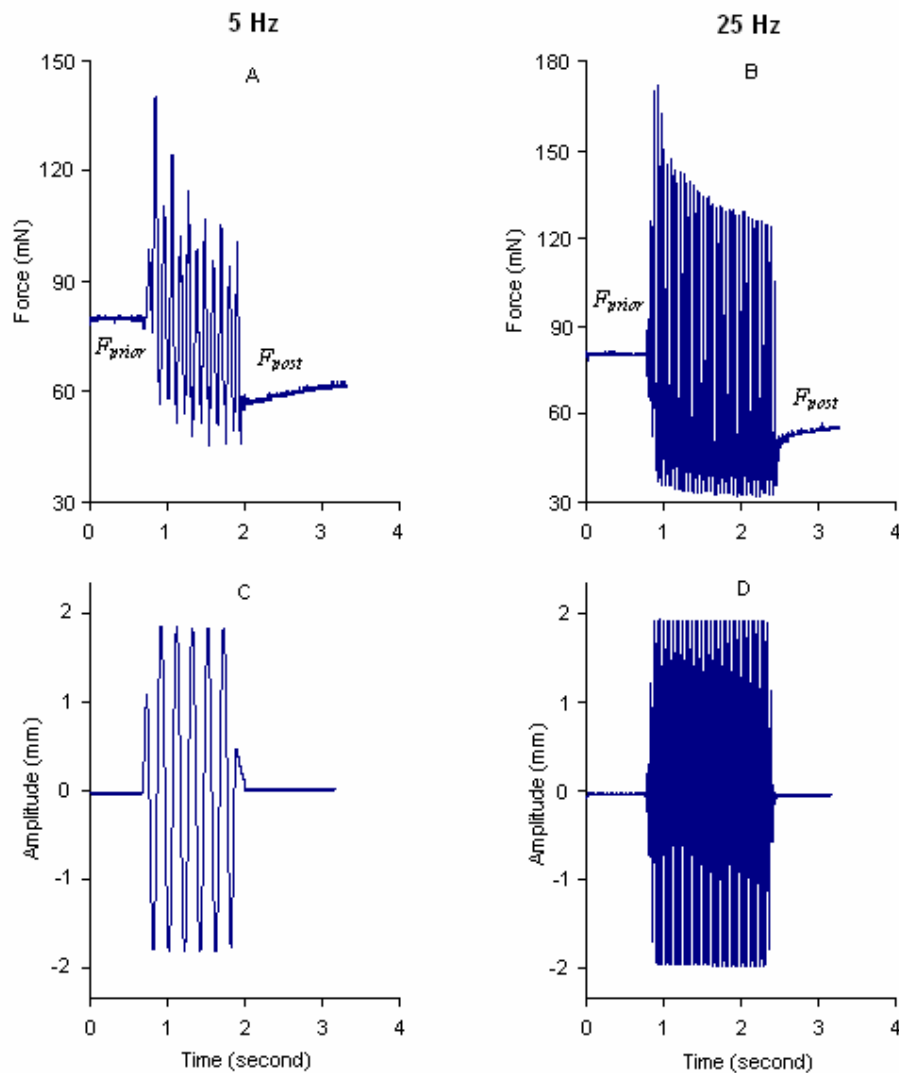


**Figure 6.16** Mechanical transverse vibrations reduce force and stiffness during isometric contraction. Forces (A and B) and amplitudes of oscillation (C and D) were recorded duration isometric contraction. The smooth muscle tissue excited with 5 Hz is shown on the left hand side (A and C), the tissue excited with 25 Hz is shown on the right hand side (B and D). The length change ratio of both excitations was 4.8% of the reference length  $L_r$ .

On the time scale, the decreasing force response to successive length cycles is seen to be an exponential decline in the peaks of oscillation. This decline could be fitted by a single exponential function, to give a similar result to the longitudinal vibration. It is believed that the disrupted actin-myosin linkage was also temporarily disrupted during the experiments, and the lower force ( $F_{post}$ ) gradually returned to the original level force ( $F_{prior}$ ) after the vibration was stopped. This is attributed to the fact that the concentration of stimulus was kept constant during the experiment.

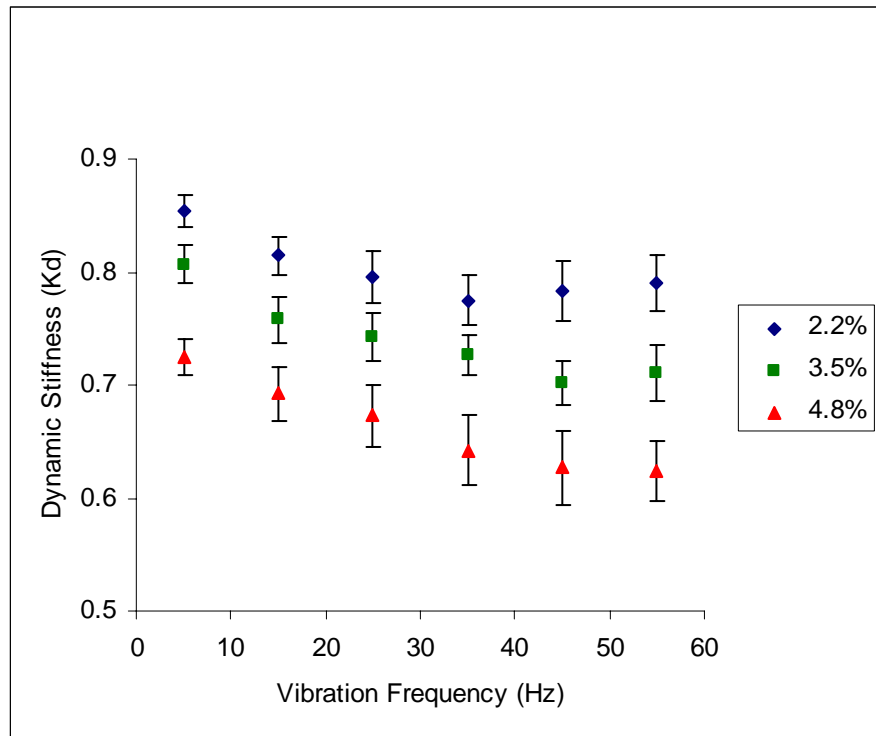


**Figure 6.17** Experimental dynamic stiffness versus vibration frequencies, mean values  $\pm$  95% confidence interval ( $n = 6$ ).

The experimental dynamic stiffness ( $K_d$ ) variations with frequency and length change ratio (in percentage of the reference length  $L_r$ ) are shown in Figure 6.17. From the figure, the general tendency of the dynamic stiffness ( $K_d$ ) is a pronounced decrease in stiffness with increasing frequency at less than 40 Hz. However, for frequencies above 40 Hz, the stiffness increases with increasing frequency. This trend is slightly different from the longitudinal vibration (see Figure 6.3), where the stiffness decreases with increasing frequency for all measured frequencies. This may be attributed to the fact that the vibration in two different directions (longitudinal and transverse) causes different inertial responses, an explanation verified by the FEM model. The dynamic stiffness of FEM is shown Figure 6.18, and can be seen to match the experimental data quite well. This confirms that the two different oscillating directions (longitudinal and transverse) cause different inertial responses at different frequencies for the dynamic stiffness calculation.

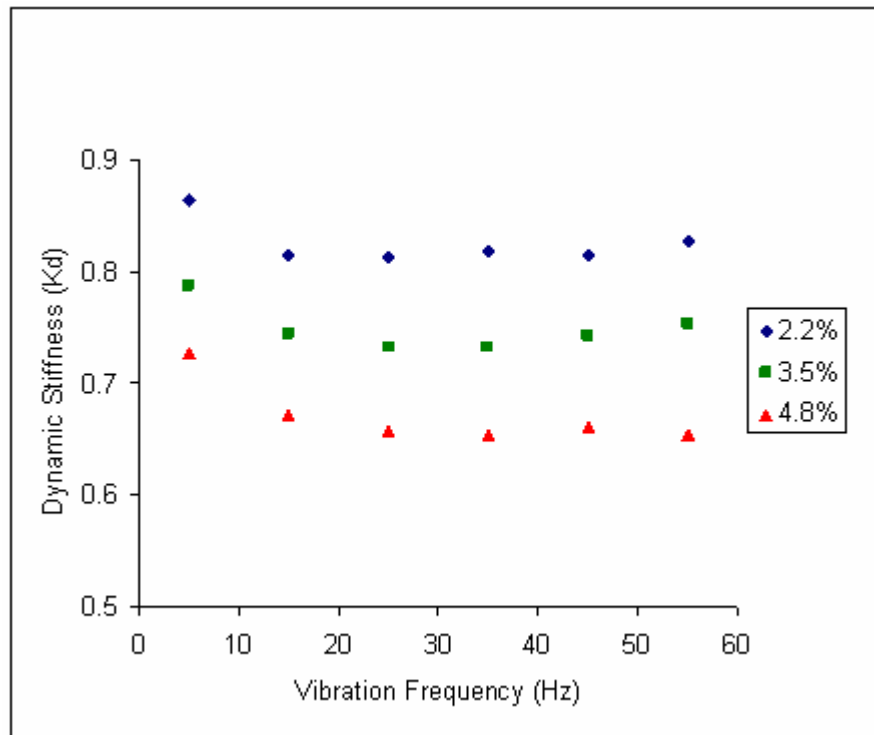


**Figure 6.18 FEM dynamic stiffness versus vibration frequencies.**

The experimental static stiffness variations with frequency and length change ratio (in percentage of the reference length  $L_r$ ) are shown in Figure 6.19. The stiffness ( $K_s$ ) almost maintains the same values for different frequencies except at a frequency of 5 Hz; the latter has smaller reduction than the others. This is slightly different from the longitudinal vibration (see Figure 6.4), and may be attributed to the fact that the tissue is lengthened twice during one frequency cycle. The static stiffness of FEM for the transverse vibration is shown Figure 6.20. Both Figure 6.19 and 6.20 indicate that the experimental and FEM data are identical.

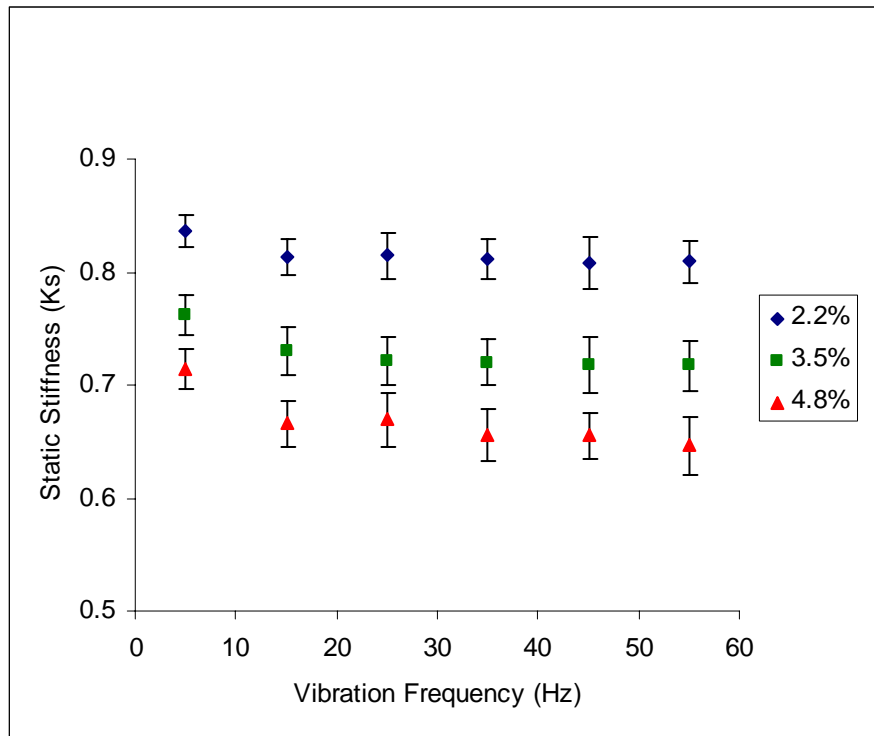


**Figure 6.19** Experimental static stiffness versus vibration frequencies, mean values  $\pm$  95% confidence interval ( $n = 6$ ).

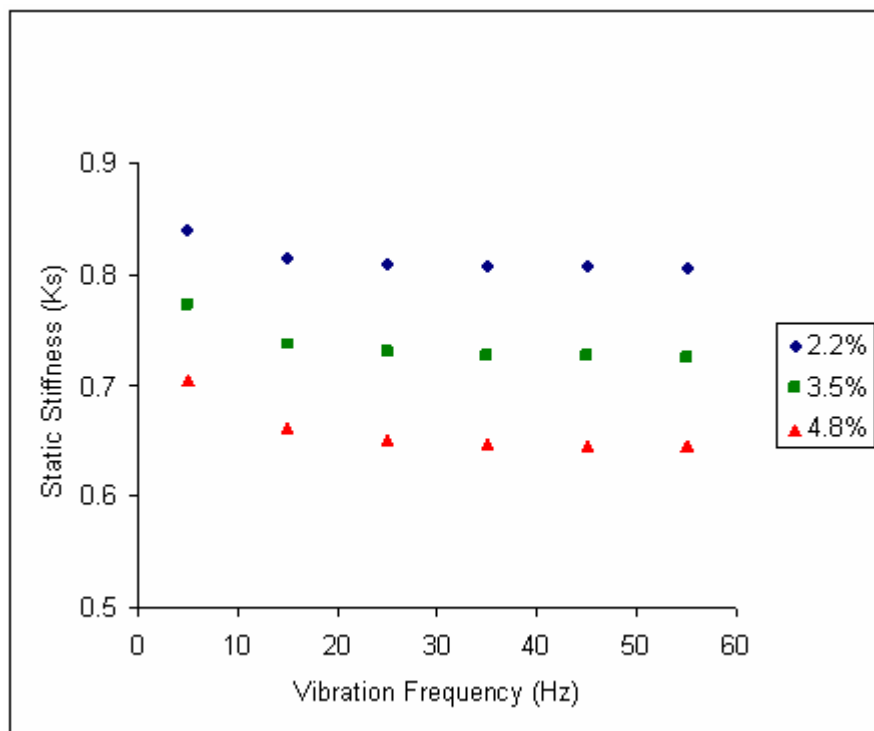


**Figure 6.20** FEM static stiffness versus vibration frequencies.

For experiments of the transverse vibration, both the dynamic and static stiffness versus the tissue length change ratios are shown in Figure 6.21 (dynamic stiffness) and Figure 6.22 (static stiffness). Both figures show a decrease in muscle stiffness with increasing tissue length change ratio, and this relationship is almost linear. These results are in a good agreement with the results of the longitudinal vibration (comparing Figure 6.21, 6.5 and Figure 6.22, 6.6).

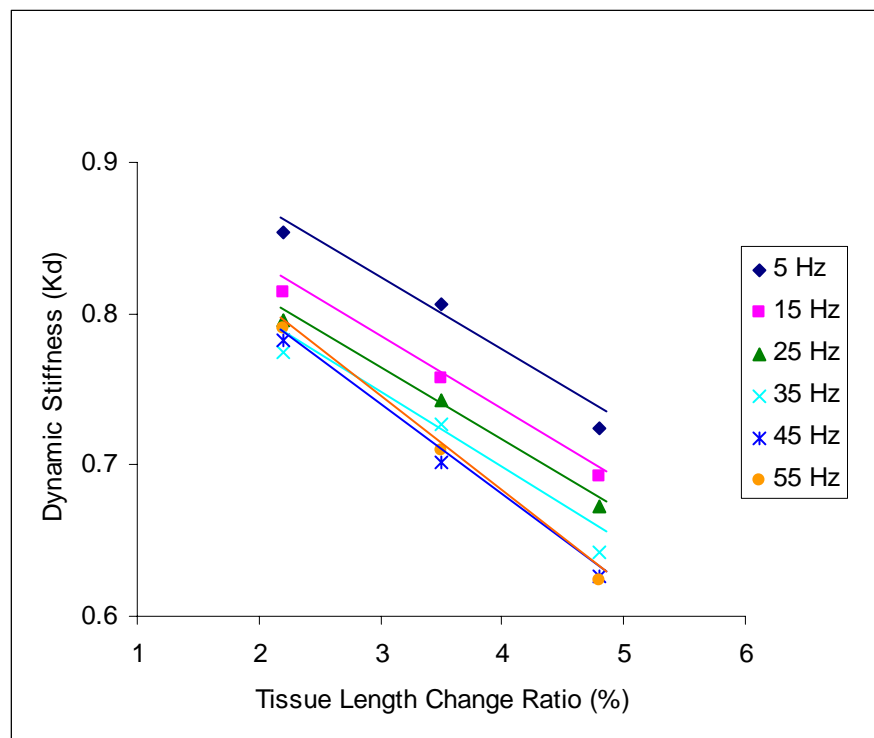


**Figure 6.21** Experimental dynamic stiffness versus tissue length change ratio.

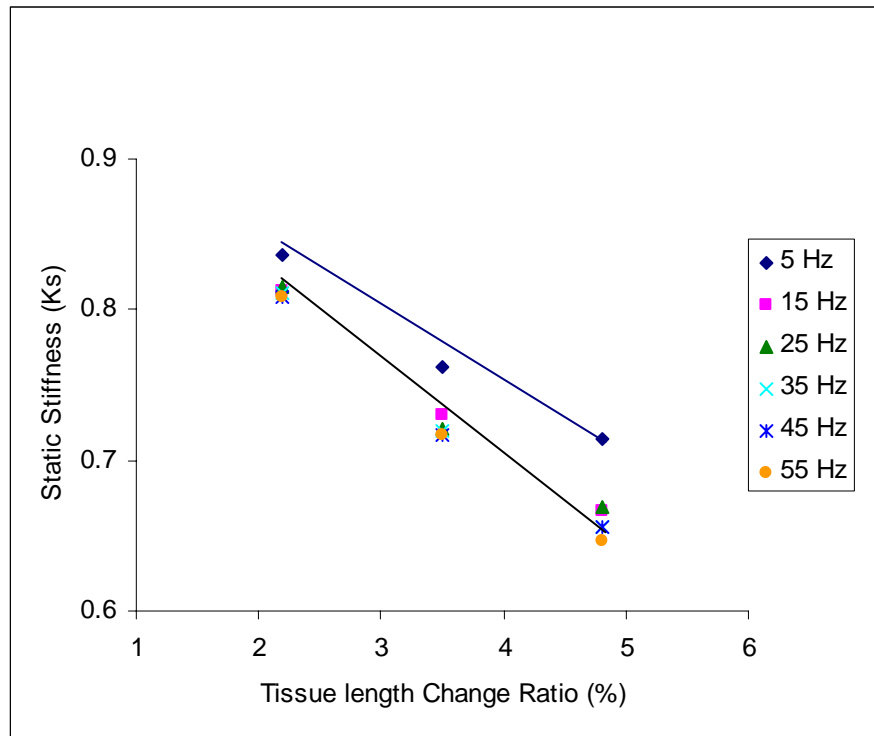


**Figure 6.22** Experimental static stiffness versus tissue length change ratio.

Figure 6.21 shows that the dynamic stiffness ( $K_d$ ) change has a linear relation with an increasing gradient for higher frequencies. However, for the static stiffness ( $K_s$ ) changes (Figure 6.22), the figure can be approximated with two straight lines of different slopes. The upper line displays the stiffness reduction at 5 Hz, while the lower line represents the stiffness reduction for all other frequencies, which shows that the stiffness changes only relate to the amplitude of vibration and not to the frequency. The gradient of the lower slope line is also steeper than that of the upper slope line.

## 6.7 Hysteresivity and Cross-Bridge Cycling Rates

The muscle force during the length oscillation at the longest and shortest lengths of the oscillation cycles were computed in terms of the length-force loops as shown in Figure 6.23. The experimental data is from the transverse vibration with 5 Hz and length change ratio of 2.2%. The area formed by the loop is called the hysteresivity [28], and

has a different physical meaning with regards to viscoelastic tissues. Fredberg [23] defined the hysteresivity ( $\eta$ ) to reflect the rate of turnover of cross-bridges or the cross-bridge cycling rate. This cross-bridge cycling rate is attributable in part to a direct mechanical effect at the level of the cyclic interaction of myosin and actin [20]. Figure 6.23 indicates that the rate of interaction of myosin-actin at the beginning of the cycle is greater than at the end of the cycle during the oscillation. This means that the cross-bridge cycling rate is higher at the beginning of oscillation and then decreases with the oscillation. Fredberg [102] described hysteresivity ( $\eta$ ) as follows:

$$\eta = \tan \varphi \quad \text{and} \quad \varphi = \sin^{-1}(4A/\Delta F \Delta l) \quad (6.4)$$

where  $A$  is the area of the loop,  $\Delta F$  is the peak-to-peak force excursion,  $\Delta l$  is the peak-to-peak length excursion, and  $\varphi$  is the phase lag between the length and force. Here, equation (4.31) is used to calculate the phase-frequency relationship. This phase can be considered as the hysteresivity ( $\eta$ ) of the muscle, and the results are shown in Figure 6.24.

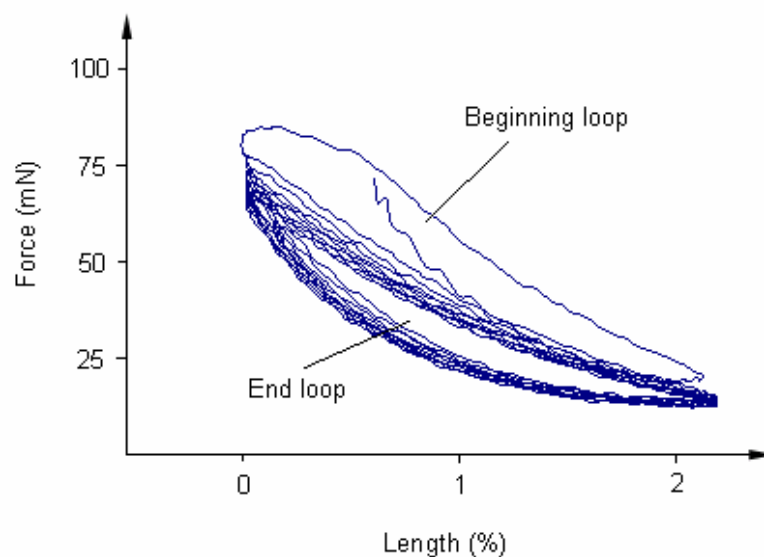


**Figure 6.23** Length-force loops during the oscillation for 5 Hz and 2.2% of  $L_r$ .

Generally, the tendency of the phase-frequency relationship is to decrease in phase with increasing frequency (negative values of phase mean that the phase is time lagging). The phase also increases with an increase in the amplitude of oscillation. This means that the hysteresivity increases with increasing amplitudes of oscillation. This result is identical to the results obtained by Shen [28] and Fredberg [23].

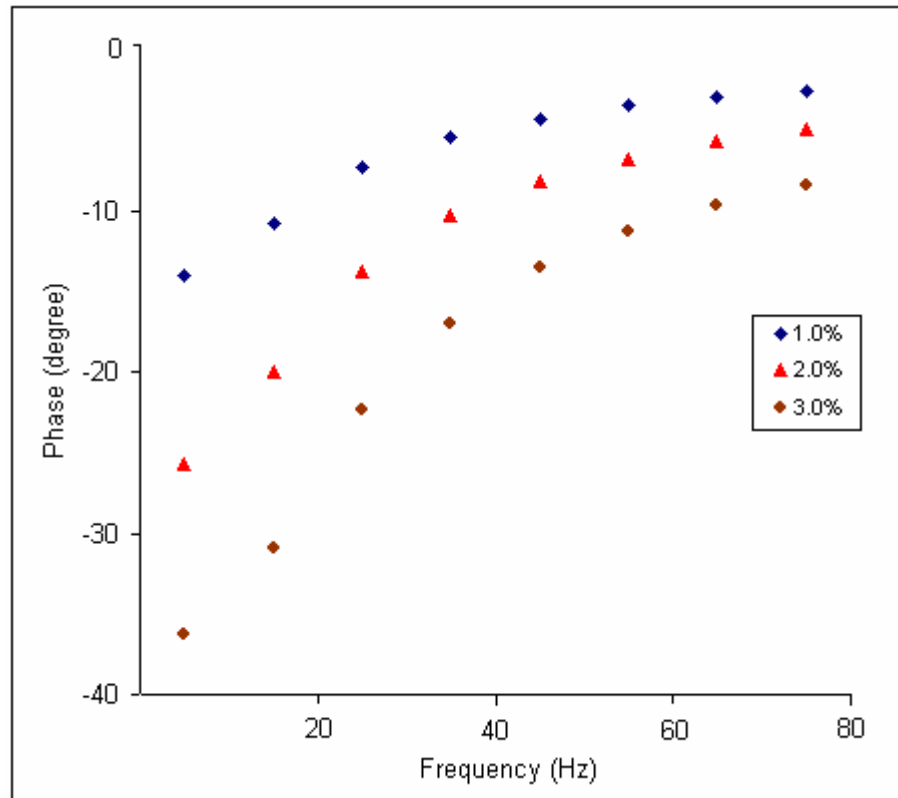


Figure 6.24 Phase-frequency relationship for the fading memory model.

## 6.8 Constants $A_i$ for the Fading Memory Model

The fading memory model simulates a transient step change in length, and the results are shown in Figure 4.4. The force immediately after the step is called  $T_1$  (see Figure 4.4), which is the minimum force that can be reached at  $t = 0$ . The equation used to calculate this minimum force is equation (4.21), which is repeated here for convenience:

$$\frac{\frac{T_1}{T_0} - 1}{\frac{T_1}{T_0} + a} = \Delta\lambda \sum_{i=1}^3 A_i \quad (6.5)$$

The force  $T_1$  is regarded as the active force and is determined by the number of cross-bridge attachments. The three dimensionless constants ( $A_i$ ) in equation (6.5) are determined from experimental results. From equation (6.5), larger  $A_i$  values determine a lower minimum force ( $T_1$ ).

As mentioned in section 4.3.2, any real transient step change takes a finite time duration and creates inertial forces. This inertial force is dependent on the finite time, and a short finite time creates a greater inertial force. However, long finite times can not be considered transient. Thus, the real value of  $T_1$  is very difficult to obtain from experiments. The experimental  $T_1$  value is combined with the inertial force and may be the viscoelastic force of the connective tissue. The second contributing factor to the inaccuracies in  $T_1$  is the smooth muscle uncertainties. The experimental results could be different even for the same muscle tissue at different testing times. Summarily, the values of these three constants ( $A_i$ ) are determined qualitatively rather than quantitatively.

## 6.9 Uncertainties of Airway Smooth Muscle Tissue

An important characteristic of airway smooth muscle is the lack of structurally identifiable “sarcomere” (i.e. the actin and myosin filaments within the smooth muscle myofibrils are randomly distributed unlike its uniform distribution within skeletal and cardiac muscle fibres). On the other hand, the orientation of myofibrils in airway

smooth muscle determines the direction of contraction in the airways, which may contribute to the degree of airway narrowing and function. It has long been known that the arrangement of airway smooth muscle bundles varies according to location within the airway tree. In the trachea, smooth muscle is arranged transversely at right angles to the long axis of the airway. In the periphery of the lung, smooth muscle is said to be arranged in a helical fashion [103]. Ebina *et al.* [104] reported that airway smooth muscle bundles are arranged at an angle of  $30^\circ$  to the long axis of the bronchi by using three-dimensional reconstruction of intraparenchymal airways. Lei *et al.* [105], however, found that the orientation of myofibrils in airway smooth muscle varied in all airway generations from  $-20^\circ$  to  $20^\circ$  relative to the transverse axis (Figure 6.25).

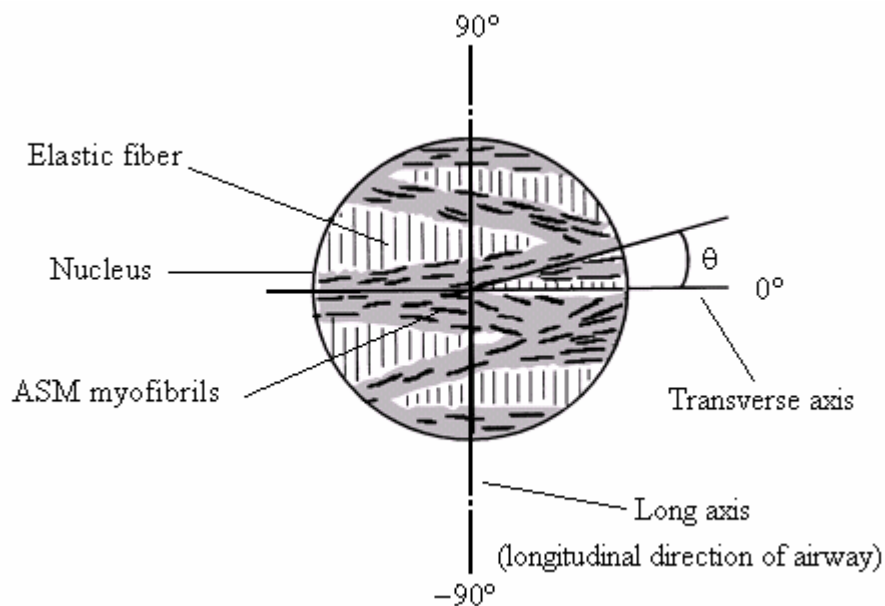


**Figure 6.25** Illustration of method used to calculate angle of orientation of airway smooth muscle ( $\theta$ ). Specimen was aligned with long axis of (ASM) airway vertical, and  $\theta$  was measured relative to transverse axis [105].

During the experiments in this research, airway smooth muscle tissues were cut in two different directions: along the long axis; and along the transverse axis (see Figure 6.26). After the same stimulation, it was found that the long axial cutting approach produced

less or no generated force, but the transverse axial cutting approach did produce a generated force. This generated force, however, varied even if samples were taken from the same trachea and of the same size. This finding proves that smooth muscle is arranged transversely rather than longitudinally. Also this transverse arrangement is not uniform as the result is identical to Lei's findings [105]. The above characteristics of airway smooth muscles determine that the capacities of generated force and shortening are not a unique function of tissue size and location. The experiments showed that the degree of stiffness reduction was proportionally related to the level of generated force. This finding could be explained by an increase in stiffness at high force levels of compliant structures in series with the contractile elements. This would cause a larger portion of the imposed length oscillations to be transmitted to the contractile machinery and thus result in a greater detachment of cross-bridges.

Some authors [36, 38, 106-112] have reported that the uncertainties of smooth muscle depend on the histories of muscle loading, length and activation. These variations can occur over the course of days, hours, and even seconds. As a result, the length-force relationship of airway smooth muscle is highly unstable. In contrast, striated muscle possesses a structurally stable and well-defined contractile apparatus, which represents a stable length-force relationship that was elicited by the classical methods [113]. Although shifting of the length-force curve is known to occur in striated muscle, this occurs only under unphysiological conditions and takes long period of time (hours or days) [114 and 115]. The shifting of the length-force curve in smooth muscle can occur over a much shorter period of time (minutes or seconds) [37] (see Figure 6.27). This phenomenon occurred in the experiments, conducted in this work as the isometric force varied at different times within the same tissue and length.

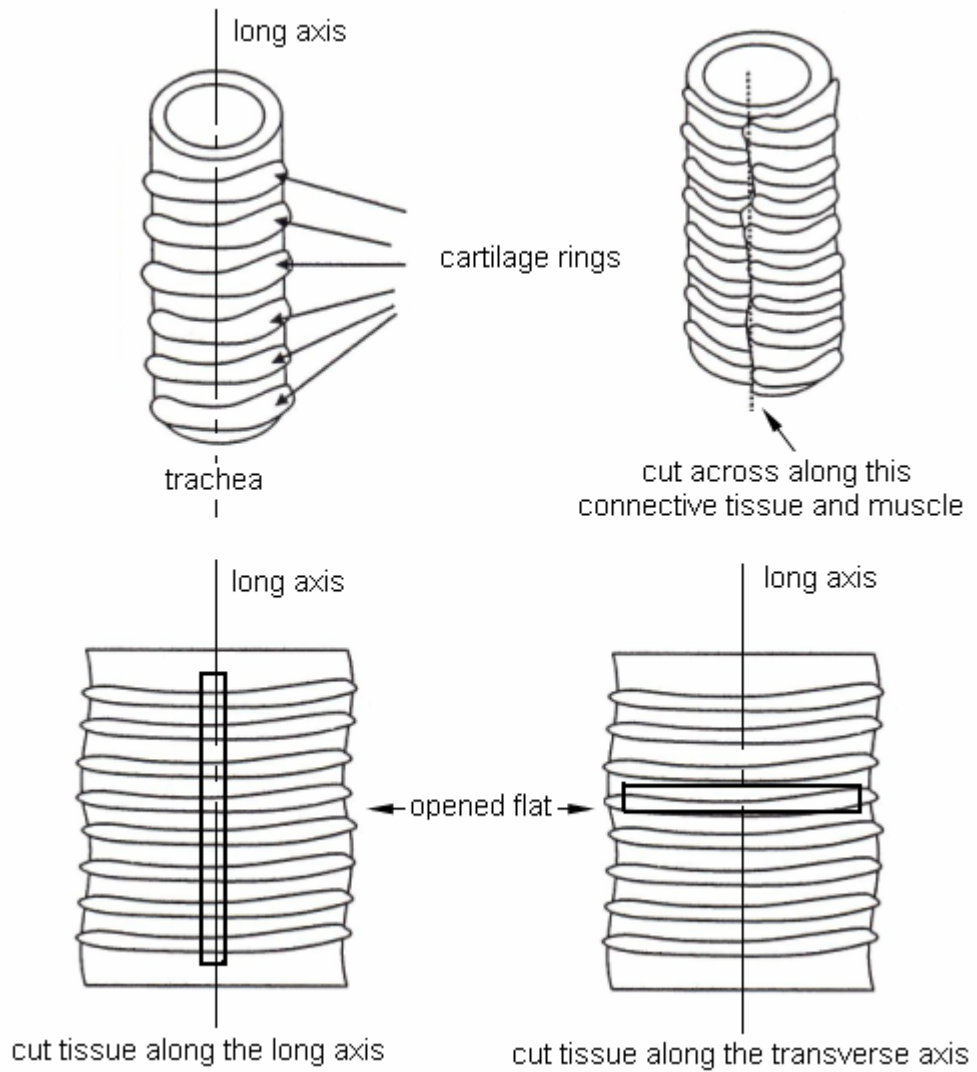


**Figure 6.26** Cutting the tissue along the long axis and transverse axis.

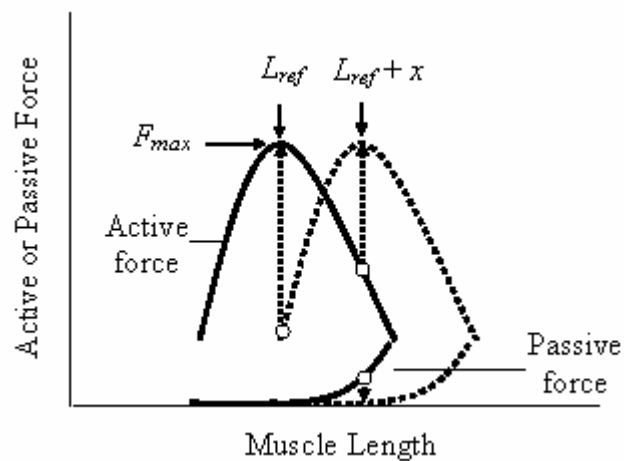


**Figure 6.27** Schematic illustrations of muscle adaptation and resulting shifts in both the active and passive length-force curve. This indicates the reference length for smooth muscle is very unstable [37].

All these uncertainties could be attributed to the history of loading and the state of activation [36, 38, 106-112], as well as the orientation of myofibrils within the tissue [103-105], and stress time relaxation of the viscoelastic elements within the tissue [41 and 116]. The effect of these uncertainties can affect the experimental results, which results in the confidence intervals overlapping in Figure 6.3 and 6.4.

## **6.10 Other Conditions Affecting the Muscle Response**

The temperature is one of the factors that affects the muscle response. To avoid this factor influencing the experimental data, the temperature of the tissue bath was controlled at 37 °C during the experiments. The reduced forces in the smooth muscle during vibrations were temporary and gradually recovered after the vibration was stopped and the time rate of this recovery was found to be temperature dependent [25]. Ljung [25] reported that the time required to reach half the original force level after cessation of vibrations was approximately 3 seconds at 25 °C compared with approximately 30 seconds at 5 °C. Lower temperatures affect ionic fluxes in the airway smooth muscle membrane, mainly reducing the activity of the sodium ( $\text{Na}^+$ ) and potassium ( $\text{K}^+$ ) pumps and the membrane potential of airway smooth muscle cells [117-120]. As a result, the lower temperatures reduce the ability of the smooth muscle to contract.

Potassium ( $\text{K}^+$ ) is the other factor that influences a smooth muscle's contraction ability, as evidenced by different researchers using different ingredients of saline solution (i.e. different concentrations of potassium chloride (KCl)). Some experiments [94 and 121] have proved that a saline solution with a high concentration of KCl can produce transient rises in cytoplasmic free calcium ( $\text{Ca}^{2+}$ ) concentration and therefore boost

muscle contracted force. The reason is that KCl plays a significant role in intracellular  $\text{Ca}^{2+}$  release in smooth muscle [83 and 122]. High concentrations of KCl increase the membrane potential of smooth muscle cells as a function of  $\text{K}^+$  depolarization, which triggers a greater release of  $\text{Ca}^{2+}$  into the cells to increase contraction. This  $\text{K}^+$  depolarization also affects the response of vibration. High KCl concentrations inhibited the effect of vibrations, as found by Ljung and Sivertsson [25]. However, this factor is not considered in this research since the concentration of the saline solution was constant.

During the experiments, some muscle tissue showed a significant reduction in the force, especially for a 5 second duration at 65 Hz. After excitation, these tissues did not fully recover to the original force level ( $F_0 \pm 10\%$ ), and were considered to be degraded. These data was then excluded from the results. The findings in the experiments also showed that the time rate of recovery for 5 seconds of excitation was more than other excitation times (sometimes > 30 seconds). The fatigue level of tissue is dependent on the duration, frequency and amplitude of vibrations and this is why the peak force slightly continues to decline after the initial rapid change for 5 seconds of excitation (Figure 6.2). There is also a slightly greater reduction in the stiffness for 5 seconds of excitation in Figure 6.7 and 6.8. The reason for this is that when *in vitro* muscle tissue is isolated from its matrix, its metabolic environment is different from the living organism. This isolated smooth muscle tissue is very fragile in the artificial environment. From this point of view, it does not necessarily mean that greater a reduction in stiffness (or force) is caused by the prolonged vibration time. The greater reduction in stiffness (or force) could be caused by the declined tissue reactivity. In this *in vitro* test, we can only conclude that the active force is temporarily reduced during the vibration. Whether a specific period of vibration can permanently sustain a relaxation of contracted smooth

muscle? Can not be answered by this work and requires *in vitro* testing. This is left as a future investigation.

## **Chapter 7**

### **Conclusions & Future Applications**

#### **7.1 Conclusions**

The results of this research are considered as the foundation for future airway smooth muscle research. These results could contribute to the study of relieving asthma by alternative means other than the traditional medical medications. The experiments in this work have been designed to investigate the responses of smooth muscle under external vibration and the developed FEM model can simulate these external excitations. The fading memory model also qualitatively describes the cross-bridge kinetics. The results obtained from this work leads to the following conclusions:

1. The stiffness of active airway smooth muscle can be physically reduced using external vibrations.
2. The two proposed stiffness parameters are believed to better describe the behaviour of tissues due to external excitations. The dynamic stiffness reflects the instantaneous effect of various dynamic components such as the viscoelastic and inertia forces, while the static stiffness reflects the effects of the vibration.

3. It is clearly indicated that the amplitude of oscillation is the main contributor to the stiffness reductions.
4. The effects of longitudinal and transverse vibration are same for the static stiffness and only slightly different for the dynamic stiffness. This may be attributed to the fact that the vibration in two different directions (longitudinal and transverse) causes different inertial responses for the dynamic stiffness.
5. The frequency of vibration affects the cross-bridge cycling rate, which is reflected at frequencies lower than 25 Hz. This effect is present in the static stiffness.

## **7.2 Future Applications**

Some researchers report that the pressure waves can easily conduct into the lung system and provide the system resonant response [123-126]. Other researchers have suggested that pressure waves can improve lung function [127-130]. Airway smooth muscle tissues could be excited using acoustic (sound) waves, which avoids any contact with the excitation point and reflects a possible type of *in vivo* excitation. In principle, direct contact excitation to smooth muscle is impossible to apply *in vivo*. However, pressure wave oscillation is a feasible and more acceptable method, and for this reason it could be hypothesized that acoustic oscillation may produce the same result as mechanical vibrations.

A possible acoustic vibration setup proposed for future application is shown in Figure 7.1. An acoustic pressure chamber is constructed which consists of a speaker, a Perspex tube and a base. A tissue bath can be set in the chamber. The speaker and Perspex tube are then joined to become a top part, which can be easily removed for muscle tissue

loading. The speaker can generate acoustic waves, which are controlled by a computer. To maintain a certain pressure in the chamber, there is a rubber sealing ring between the top part and the base, which is coated silicon sealant. All of the transducer cables and the aerating tube can be inserted into the base of the apparatus through a rubber wire seal. A pressure transducer sensor can be placed in the chamber to measure the acoustic pressure. A strip of smooth muscle could then be mounted on two hooks, one of which is fixed, while the other is connected to a force transducer. The length adjuster can be set on the force transducer side for the tissue reference length adjustment. This setup could be used to investigate the response of airway smooth muscle tissue under acoustic wave excitation.

To provide more accurate FEM results, the properties of muscle will be extended to viscoelasticity in future. The FEM can also be developed to simulate a circular tube to model the contracted airway behaviours under external vibrations.

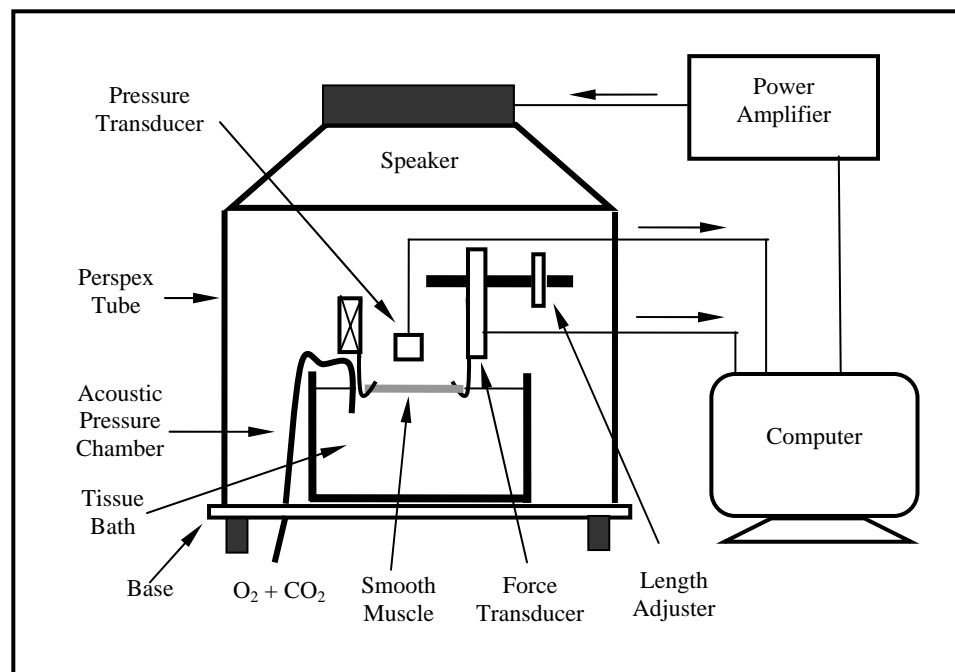


**Figure 7.1** A proposal of acoustic vibration setup for future application.

## References

1. Guyton, A. C. and Hall, J. E., 2000, *Textbook of Medical Physiology*, W. B. Saunders Co., Philadelphia
2. Ganong, W. F., 2001, *Review of Medical Physiology*, McGraw-Hill, New York
3. Weibel, E. R., 1963, *Morphometry of the Human Lung*. Academic Press, New York
4. Marieb, E. N., 1998, *Human Anatomy Physiology*, Benjamin/Cummings Science Publishing, California
5. Kamm, R. D., 1999, Airway wall mechanics, *Annual Review of Biomedical Engineering*, **01**, 47-72
6. Du, Y. and Al-Jumaily, A.M., 2004, Tracheal smooth muscle response to vibrations, *Proceedings of ASME International Mechanical Engineering Congress & Exposition*, **IMECE2004-59095**, Anaheim, California, November 13-19, 2004
7. Tortora, G. J. and Grabowski, S. R., 2000, *Principle of Anatomy and Physiology*, John Wiley & Sons Inc., New York
8. *Asthma*, WWW Document (<http://www.m-w.com/dictionary/asthma>), Accessed on 09 June 2004
9. Blanc, F-X., Coirault, C., Salmeron, S, Chemla, D. and Lecarpentier, Y., 2003, Mechanics and crossbridge kinetics of tracheal smooth muscle in two inbred strains, *European Respiratory Journal*, **22**, 227-234
10. Fredberg, J. J., 2004, Bronchospasm and its biophysical basis in airway smooth muscle, WWW Document (<http://respiratory-research.com/content/5/1/2>), Accessed on 10 May 2005
11. Hirst, S. J., Walker, T. R. and Chilvers, E. R., 2000, Phenotypic diversity and molecular mechanisms of airway smooth muscle proliferation in asthma, *European Respiratory Journal*, **16**, 159-177

12. James, A. and Carroll, N. 2000, Airway smooth muscle in health and disease; methods of measurement and relation of function, *European Respiratory Journal*, **15**, 782-789
13. Amrani, Y. and Panettieri, R. A., 2003, Airway smooth muscle: contraction and beyond, *The International Journal of Biochemistry & Cell Biology*, **35**, 272-276
14. Chung, K.F., 2000, Airway smooth muscle cell: contributing to and regulating airway mucosal inflammation, *European Respiratory Journal*, **15**, 961-968
15. Martin, J. G., Duguet, A. and Eidelman, D. H., 2000, The contribution of airway smooth muscle to airway narrowing and airway hyperresponsiveness in disease, *European Respiratory Journal*, **16**, 349-354
16. Wynsberghe, D. V., Noback, C. R. and Carola, R., 1995, *Human Anatomy and Physiology*, McGraw-Hill Inc, New York
17. Au, P. M. and Al-Jumaily, A.M., 2002, Asthma relief and airway mechanics “a literature review”, *Transworld Research Network, Advanc*, **TRN/SV/3**, 479-495
18. *Muscle Tissue*, WWW Document (<http://www.uoguelph.ca/zoology/devobio/210labs/muscle1.html>), Accessed on 16 September 2005
19. Fung, Y. C., 1993, *Biomechanics: Mechanical Properties of Living Tissues*, Springer-Verlag Inc., New York
20. Huxley, A. F., 1957, Muscle structure and theories of contraction, *Progress in Biophysics and Biophysical Chemistry*, **7**, 255-318
21. Meiss, R. A., 1982, Transient responses and continuous behavior of active smooth muscle during controlled stretches, *American Journal of Physiology – Lung Cellular and Molecular Physiology*, **242**, L146-L158
22. Dhanaraj, N., Pidaparti, R. M. and Meiss, R. A., 2002, Smooth muscle tissue response to applied vibration following extreme isotonic shortening, *Proceedings of ASME International Mechanical Engineering Congress & Exposition*, **IMECE2002-33600**, New Orleans, Louisiana, November 17-22, 2002
23. Fredberg, J. J., Inouye, D. S., Miller, B., Nathan, M., Jafari, S., Raboudi, S. H., Butler, J. P. and Shore, S. A., 1997, Airway smooth muscle, tidal stretches, and dynamically determined contractile states, *American Journal of Respiratory and Critical Care Medicine*, **156**, 1752-1759
24. Ljung, B. and Sivertsson, R., 1972, The inhibitory effect of vibrations on tension development in vascular smooth muscle, *Acta Physiologica Scandinavica*, **85**(3), 428-430

25. Ljung, B. and Sivertsson, R., 1975, Vibration-induced inhibition of vascular smooth muscle contraction, *Blood Vessels*, **12**(1), 38-52
26. Meiss, R. A., 1991, An analysis of length-dependent active stiffness in smooth muscle strips, *Regulation of Smooth Muscle Contraction*, 425-434
27. Meiss, R. A. and Pidaparti, R. M., 2004, Mechanical state of airway smooth muscle at very short lengths, *Journal of Applied Physiology*, **96**, 655-667
28. Shen, X., Wu, M. F., Tepper, R. S. and Gunst, S. J., 1997, Mechanical for the mechanical response of airway smooth muscle to length oscillation, *Journal of Applied Physiology*, **83**(3) , 731-738
29. Sivertsson, R. and Ljung, B., 1976, Vibration-induced changes in vascular tone, *Acta Chirurgicala Scandinavica. Supplementum*, **465**, 20-22
30. Sjoqvist, A. and Ljung, B., 1980, Dissociation of electrical and mechanical activity caused by vibrations in the spontaneously active smooth muscle of the rat portal vein, *Acta Physiologica Scandinavica*, **110**, 381-384
31. Bioengineering Notes, PDF Document ([http://www.esc.auckland.ac.nz/teaching/Engsci441SC/electrophysiol/Nash\\_electrophys2003.pdf](http://www.esc.auckland.ac.nz/teaching/Engsci441SC/electrophysiol/Nash_electrophys2003.pdf)) Accessed on 20 March 2005
32. Hai, C.M. and Murphy, R. A., 1988, Regulation of shortening velocity by cross-bridge phosphorylation in smooth muscle, *American Journal of Physiology – Lung Cellular and Molecular Physiology*, **255**, L86-L94
33. Kargacin, G. J., Cooke, P. H., Abramson, S. B. and Fay, F. S., 1989, Periodic organization of the contractile apparatus in smooth muscle revealed by the motion of dense bodies in single cells, *The Journal of Cell Biology*, **108**, 1465-1475
34. Lambert, R. K., Pare, P. D. and Seow, C. Y., 2004, Mathematical description of geometric and kinematic aspects of smooth muscle plasticity and some related morphometrics, *Journal of Applied Physiology*, **96**, 469-476
35. Lecarpentier, F., Blanc, F. X., Salmeron, S., Pourny, J. C., Chemla, D. and Coirault, C., 2002, Myosin cross-bridge kinetics in airway smooth muscle: a comparative study of humans, rats, and rabbits, *American Journal of Physiology – Lung Cellular and Molecular Physiology*, **282**, L83-L90
36. Seow, C. Y., 2000, Response of arterial smooth muscle to length perturbation, *Journal of Applied Physiology*, **89** , 2065-2070
37. Bai, T, R. *et al.*, 2004, On the terminology for describing the length-force relationship and its changes in airway smooth muscle, *Journal of Applied Physiology*, **97** 2029-2034
38. Gunst, S. J., Meiss, R. A., Wu, M.F. and Rowe, M., 1995, Mechanisms for the mechanical plasticity of tracheal smooth muscle, *American Journal of Physiology – Cell Physiology*, **268**, C1267-C1276

39. Hill, A. V., 1938, The heat of shortening and the dynamic constants of muscle, *Proceedings of the Royal Society London B*, **126**, 136-195
40. Hill A. V., 1970, *First and Last Experiments in Muscle Mechanics*, Cambridge University Press, Cambridge
41. Stephens, N. L., Li, W., Jiang, H., Unruh, H. and Ma, X., 2003, The biophysics of asthmatic airway smooth muscle, *Respiratory Physiology & Neurobiology*, **137**, 125-140
42. Gunst, S. J. and Tang, D. D., 2000, The contractile apparatus and mechanical properties of airway smooth muscle, *European Respiratory Journal*, **15**, 600-616
43. Meiss, R. A. and Pidaparti, R. M., 2004, Active and passive components in the length-dependent stiffness of tracheal smooth muscle during isotonic shortening, *Journal of Applied Physiology*, **98**, 234-241
44. Meiss, R. A., 1999, Influence of intercellular tissue connections on airway muscle mechanics, *Journal of Applied Physiology*, **86**(1), 5-15
45. Pidaparti, R. M., Liu, Y. and Meiss, R. A., 1997, A viscoelastic material model to represent smooth muscle shortening, *Bio-Medical Materials and Engineering*, **7**, 171-177
46. Murphy, R. A., 1994, What is special about smooth muscle? The significance of covalent crossbridge regulation, *The FASEB Journal*, **8**, 311-318
47. Mitchell, R. W., Seow, C. Y., Burdyga, T., Maass-Moreno, R., Pratusевич, V. R., Ragozzino, J. and Ford, L. E., 2001, Relationship between myosin phosphorylation and contractile capability of canine airway smooth muscle, *Journal of Applied Physiology*, **90**, 2460-2465
48. Hai, C.M. and Murphy, R. A., 1988, Cross-bridge phosphorylation and regulation of latch state in smooth muscle, *American Journal of Physiology – Cell Physiology*, **254**, C99-C106
49. Allen, B. G. and Walsh, M. P., 1994, The biochemical basis of the regulation of smooth-muscle contraction, *Trends in Biochemical Sciences*, **19**, 362-368
50. Sieck, G. C., Han, Y.S., Prakash, Y. S. and Jones, K. A., 1998, Cross-bridge cycling kinetics, actomyosin ATPase activity and myosin heavy chain isoforms in skeletal and smooth muscle respiratory muscle, *Comparative Biochemistry and Physiology Part B*, **119**, 435-450
51. Yumura, S. and Uyeda, T. Q. P., 2003, Myosins and cell dynamics in cellular slime model, *International Review of Cytology*, **224**, 173-225
52. Zahalak, G. I., 1981, A distribution-moment approximation for kinetic theories of muscle contraction, *Mathematical Biosciences*, **55**, 89-114

53. Tozeren, A., 1985, Constitutive equations of skeletal muscle based on cross-bridge mechanism, *Biophysical Journal*, **47**, 225-236
54. Mijailovich, S. M., Fredberg, J. J. and Butler, J. P., 1996, On the theory of muscle contraction: filament extensibility and the development of isometric force and stiffness, *Biophysical Journal*, **71**, 1475-1484
55. Huxley, A. F. and Simmons, R. M., 1971, Proposed mechanism of force generation in striated muscle, *Nature*, **233**, 533-538
56. Redaelli, A., Soncini, M. and Montevecchi, F. M., 2001, Myosin cross-bridge mechanics: geometrical determinants for a continuous sliding, *Journal of Biomechanics*, **34**, 1607-1617
57. Iwazumi, T., 1989, Molecular mechanism of muscle contraction, *Physiological Chemistry and Physics and Medical NMR*, **21**, 187-219
58. Noble, M. I. M. and Pollack, G. H., 1977, Molecular mechanism of contraction, *Circulation Research*, **40**(4), 333-341
59. West, J. M., Higuchi, H., Ishijima, A. and Yanagida, T., 1996, Modification of the bi-directional sliding movement of actin filaments along native thick filaments isolated from a clam, *Journal of Muscle Research and Cell Motility*, **17**, 637-646
60. Shadmehr, R. and Wise, S. P., *A Simple Muscle Model*, WWW Document ([http://www.bme.jhu.edu/~reza/book/muscle\\_model/musclemodel.htm](http://www.bme.jhu.edu/~reza/book/muscle_model/musclemodel.htm)), Accessed on 12 November 2005
61. Hunter, P. J., McCulloch, A. D. and Keurs, H. E. D. J., 1998, Modelling the mechanical properties of cardiac muscle, *Progress in Biophysics & Molecular Biology*, **69**, 289-331
62. Yu, S. N., Crago, P. E. and Chiel, H. J., 1997, A nonisometric kinetic model for smooth muscle, *American Journal of Physiology – Cell Physiology*, **272**, C1025-C1039
63. Mijailovich, S. M., Butler, J. P. and Fredberg, J. J., 2000, Perturbed equilibria of myosin binding in airway smooth muscle: bond-length distributions, mechanics, and ATP metabolism, *Biophysical Journal*, **79**, 2667-2681
64. Hai, C.M. and Kim, H. R., 2005, An expanded latch-bridge model of protein kinase C-mediated smooth muscle contraction, *Journal of Applied Physiology*, **98**, 1356-1365
65. Anafi, R. C. and Wilson, T. A., 2002, Empirical model for dynamic force-length behavior of airway smooth muscle, *Journal of Applied Physiology*, **92**, 455-460
66. Bates, J. H. T. and Lauzon, A.M., 2005, Modeling the oscillation dynamics of activated airway smooth muscle strips, *American Journal of Physiology – Lung Cellular and Molecular Physiology*, **289**, L849-L855

67. Fabry, B. and Fredberg, J. J., 2003, Remodeling of the airway smooth muscle cell: are we built of glass?, *Respiratory Physiology & Neurobiology*, **137**, 109-124
68. Laudadio, R. E., Millet, E. J., Fabry, B., An, S. S., Butler, J. P. and Fredberg, J. J., 2005, Rat airway smooth muscle cell during actin modulation: rheology and glassy dynamics, *American Journal of Physiology – Cell Physiology*, **289**, C1388-C1395
69. Raboudi, S. H., Miller, B., Butler, J. P., Shore, S. A. and Fredberg, J. J., 1998, Dynamically determined contractile states of airway smooth muscle, *American Journal of Respiratory and Critical Care Medicine*, **158**, S176-S178
70. Gunst, S. J. and Russell, J. A., 1982, Contractile force of canine tracheal smooth muscle during continuous stretch, *Journal of Applied Physiology: Respiratory Environment Exercise Physiology*, **52**(3), 655-663
71. Shue, G.H. and Brozovich, F. V., 1999, The frequency response of smooth muscle stiffness during  $\text{Ca}^{2+}$ -activated contraction, *Biophysical Journal*, **76**, 2361-2369
72. Rembold, C. M. and Murphy, R. A., 1990, Latch-bridge model in smooth muscle:  $[\text{Ca}^{2+}]_i$  can quantitatively predict stress, *American Journal of Physiology – Cell Physiology*, **259**, C251-C257
73. Ohhashi, T., Azuma, T. and Sakaguchi, M., 1979, Effect of microvibration on activity of ureteral and portal smooth muscles, *American Journal of Physiology – Cell Physiology*, **236**(5), C192-C201
74. Binks, A. P., Bloch-Salisbury, E., Banzett, R. B. and Schwartzstein, R. M., 2001, Oscillation of the lung by chest-wall vibration, *Respiration Physiology*, **126**, 245-249
75. *James Method — Drug Free Asthma Treatment Since 1920*, WWW Document (<http://www.jamesmethod.com>), Accessed on 02 December 2005
76. Homma, I., Obata, T., Sibuya, M. and Uchida, M., 1984, Gate mechanism in breathlessness caused by chest-wall vibration in humans, *Journal of Applied Physiology*, **56**, 8-11
77. Bosco, C., Colli, R., Introiini, E., Cardinale, M., Tsarpela, O., Madella, A. Tihanyi, J. and Viru, A., 1999, Adaptive responses of human skeletal muscle to vibration exposure, *Clinical Physiology*, **19**(2), 183-187
78. Warman, G., Humphries, B. and Purton, J., 2002, The effects of timing and application of vibration on muscular contractions, *Aviation, Space, and Environmental Medicine*, **73**, 119-127
79. Dowell, M. L., Lakser, O. J., Gerthoffer, W. T., Fredberg, J. J., Stelmack, G. L., Halayko, A. J., Solway, J. and Mitchell, R. W., 2005, Latrunculin B increases force fluctuation-induced relengthening of ACh-contracted,

- isotonically shortened canine tracheal smooth muscle, *Journal of Applied Physiology*, **98**, 489-497
80. Kuo, K.H., Herrera, A. M., Wang, L., Pare, P. D., Ford, L. E., Stephens, N. L. and Seow, C. Y., 2003, structure-function correlation in airway smooth muscle adapted to different lengths, *American Journal of Physiology – Cell Physiology*, **285**, C384-C390
  81. Shen, X., Wu, M. F., Tepper, R. S. and Gunst, S. J., 1997, Pharmacological modulation of the mechanical response of airway smooth muscle to length oscillation, *Journal of Applied Physiology*, **83**(3), 739-745
  82. Wang, L.U., Pare, P. D. and Seow, C. Y., 2002, Changes in force-velocity properties of trachealis due to oscillatory strains, *Journal of Applied Physiology*, **92**, 1865-1872
  83. Chan, W.L., Silbertein, J. and Hai, C.M., 2000, Mechanical strain memory in airway smooth muscle, *American Journal of Physiology – Cell Physiology*, **278**, C895-C904
  84. Eyre, P., 1969, The pharmacology of sheep tracheobronchial muscle: a relaxant effect of histamine on the isolated bronchi, *British Journal of Pharmacology*, **36**, 409-417
  85. Kulshrestha, S., Misra, S. S., Sharma, A. L., Sharma, P. and Singhal, D., 1983, Response of the goat trachea to some autonomic drugs, *Indian Journal of Pharmacology*, **15**(2), 107-110
  86. van Lunteren, E. and Moyer, M., 2001, Auxotonic contractile responses of rat tracheal and bronchial airway smooth muscle, *Pulmonary Pharmacology & Therapeutics*, **14**, 443-453
  87. Kreyszig, E., 1993, *Advanced Engineering Mathematics*, John Wiley & Sons, Inc., New York
  88. Mijailovich, S. M., Stamenovic, D., Brown, R., Leith, D. E. and Fredberg, J. J., 1994, Dynamic moduli of rabbit lung tissue and pigeon ligamentum propatagiale undergoing uniaxial cyclic loading, *Journal of Applied Physiology*, **76**(2), 773-782
  89. de Tombe, P. P. and ter Keurs, H. E. D. J., 1990, Force and velocity of sarcomere shortening in trabeculae from rat heart. Effects of temperature, *Circulation Research*, **66**, 1239-1254
  90. de Tombe, P. P. and ter Keurs, H. E. D. J., 1991, Sarcomere dynamics in cat cardiac trabeculae, *Circulation Research*, **68**, 588-596
  91. de Tombe, P. P. and ter Keurs, H. E. D. J., 1992, An internal viscous element limits unloaded velocity of sarcomere shortening in rat myocardium, *The Journal of Physiology*, **454**, 619-642

92. Hancock, W. O., Martyn, D. A. and Huntsman, L. L., 1993, Ca<sup>2+</sup> and segment length dependence of isometric force kinetics in intact ferret cardiac muscle, *Circulation Research*, **73**(4), 603-611
93. Sieck, G. C. and Prakash, Y. S., 1997, Cross-bridge kinetics in respiratory muscles, *European Respiratory Journal*, **10**, 2147-2158
94. Takahashi, K., Yoshimoto, R., Fuchibe, K., Fujishige, A., Mitsui-Saito, M., Hori, M., Ozaki, H., Yamamura, H., Awata, N., Taniguchi, S., Katsuki, M., Tsuchiya, T. and Karaki, H., 2000, Regulation of shortening velocity by calponin in intact contracting smooth muscles, *Biochemical and Biophysical Research Communications*, **279**, 150-157
95. Chung, T. J., 1996, *Applied Continuum Mechanics*, Cambridge University Press, Cambridge
96. Kwon, Y. W. and Bang, H. C., 2000, *The Finite Element Method Using MATLAB*, CRC Press, Boca Raton
97. Hunter, P. J. and Pullan, A., 2001, *FEM/BEM Notes*, Department of Engineering Science/The University of Auckland, Auckland
98. Zienkiewicz, O. C. and Taylor, R. L., 2000, *The Finite Element Method: Volume 1 The Basis*, Butterworth-Heinemann, Oxford
99. Halpern, D. and Grotberg, B., 1992, Fluid-elastic instabilities of liquid-lined flexible tubes, *Journal of Fluid Mechanics*, **244**, 615-632
100. Owen, M. R. and Lewis, M. A., 2001, The mechanics of lung tissue under high-frequency ventilation, *Society for Industrial and Applied Mathematics*, **61**(5), 1731-1761
101. Fredberg, J. J., Inouye, D. S., Mijailovich, S. M. and Butler, J. P., 1999, Perturbed equilibrium of myosin binding in airway smooth muscle and its implication in bronchospasm, *American Journal of Respiratory and Critical Care Medicine*, **159**, 959-967
102. Fredberg, J. J., Bunk, D., Ingenito, E. and Shore, S. A., 1993, Tissue resistance and the contractile state of the lung parenchyma, *Journal of Applied Physiology*, **74**, 1387-1397
103. Miller, W. S., 1937, *The Lung*, Springfield, IL: Thomas
104. Ebina, M., Yaegashi, H., Takahashi, T., Motomiya, M. and Tanemura, M., 1990, Distribution of smooth muscle along the bronchial tree: a morphometric study of ordinary autopsy lungs, *The American Review of Respiratory Disease*, **141**, 1322-1326
105. Lei, M., Ghezzi, H., Chen, M. F. and Eidelman, D. H., 1997, Airway smooth muscle orientation in intraparenchymal airways, *Journal of Applied Physiology*, **82**(1), 70-77

106. Gunst S. J., 1986, Effect of length history on contractile behavior of canine tracheal smooth muscle, *American Journal of Physiology – Cell Physiology*, **250**, C146-C154
107. Gunst S. J., 1989, Effect of muscle length and load on intracellular Ca<sup>2+</sup> in tracheal smooth muscle, *American Journal of Physiology – Cell Physiology*, **256**, C807-C812
108. Gunst S. J., Wu, M. F. and Smith, D. D., 1993, Contraction history modulates isotonic shortening velocity in smooth muscle, *American Journal of Physiology – Cell Physiology*, **265**, C467-C476
109. Pratusевич, V. R., Seow, C. Y. and Ford L. E., 1995, Plasticity in canine airway smooth muscle, *The Journal of General Physiology*, **105**, 73-94
110. Silberstein J. and Hai, C. M., 2002, Dynamics of length-force relations in airway smooth muscle, *Respiratory Physiology & Neurobiology*, **132**, 205-221
111. Stephens, N. L., and, van Niekerk, W., 1977, Isometric and isotonic contractions in airway smooth muscle, *Canadian Journal of physiology and Pharmacology*, **55**, 833-838
112. Wang, L.U., Pare, P. D. and Seow, C. Y., 2001, Selected contribution: effect of chronic passive length change on airway smooth muscle length-tension relationship, *Journal of Applied Physiology*, **90**, 734-740
113. Gordon, A. M., Huxley, A. F. and Julian F. J., 1966, The variation in isometric tension with sarcomere length in vertebrate muscle fibres, *The Journal of Physiology*, **184**, 170-192
114. Farkas, G. A. and Roussos, C., 1983, Diaphragm in emphysematous hamsters: sarcomere adaptability, *Journal of Applied Physiology*, **54**, 1635-1640
115. Jakubiec-Puka A. and Carraro, U., 1991, Remodelling of contractile apparatus of striated muscle stimulated electronically in a shortened position, *Journal of Anatomy*, **178**, 83-100
116. Maksym, G. N., Kearney, R. E. and Bates, J. H., 1998, Nonparametric block-structured modelling of lung tissue strip mechanics, *Annals of Biomedical Engineering*, **26**, 242-252
117. Chen, W. Y., 1989, Effect of Na<sup>+</sup> pump suppression on reactivity of rat trachealis to cooling, *Clinical and Experimental Pharmacology and Physiology*, **16**, 375-381
118. Gonzalez, O. and Santacana, G. E., 2000, Effect of the airway epithelium on the contraction of rat isolated trachea under conditions of low temperature, *Respiration*, **67**, 439-443

119. Hall, I. P., 2000, Second messengers, ion channels and pharmacology of airway smooth muscle, *European Respiratory Journal*, **15**, 1120-1127
120. Souhrada, M. and Souhrada, J. F., 1981, The direct effect of temperature on airway smooth muscle, *Respiration Physiology*, **44**, 311-323
121. Wang, H.L., Zhang, X.H. and Chang, T.H., 2002, Effects of tetrandrine on smooth muscle contraction induced by mediators in pulmonary hypertension, *Acta Physiologica Scandinavica*, **23**(12), 1114-1120
122. Munro, D. D. and Wendt, I. R., 1994, Effect of cyclopiazonic acid on  $[Ca^{2+}]_i$  and contraction in rat urinary bladder smooth muscle, *Cell Calcium*, **15**, 369-380
123. Al-Jumail, A.M. and Du, Y., 2002, Obstruction identification in a compliant tube with application to airway passages, *Journal of Vibration and Control*, **8**, 643-657
124. Du, Y., 2001, Dynamic Characteristics of constricted-tube system as applied to the upper airway with an obstruction, *Master Thesis*, Auckland University of Technology
125. Grimal, Q., Watzky, A. and Naili, S., 2002, A one-dimensional model for the propagation of transient pressure waves through the lung, *Journal of Biomechanics*, **35**, 1081-1089
126. Fredberg, J. J., Sidell, R. S., Wohl, M. E. and DeJong, R. G., 1978, Canine pulmonary input impedance measured by transient force oscillations, *Journal of Biomechanical Engineering*, **100**, 67-71
127. Al-Jumail, A.M., Au, P. M., Du, Y., Hermawan, V. and Manilal, P., 2004, Asthma: acoustic identification and vibration relief, *Australian Asthma Conference, The Asthma Foundation of Australia*, Melbourne, Australia, February 23-25, 2004
128. Chang, H. K., 1984, Mechanisms of gas transport during ventilation by high-frequency oscillation, *Journal of Applied Physiology*, **56**(3) 553-563
129. Manilal, P. I., 2004, The effect of pressure oscillations on neonatal breathing, *Master Thesis*, Auckland University of Technology
130. Miyamoto, Y., Saito, K. and Mikami, T., 1979, Factors affecting frequency dependence of resistance observed in healthy lungs, *Japanese Journal of Physiology*, **29**(6), 789-803
131. Humphrey, J. D., 2002, *Cardiovascular Solid Mechanics Cells, Tissues, and Organs*, Springer-Verlag N.Y. Inc. New York